EXPERIMENTAL AND ANALYTICAL ESTIMATION OF DAMPING IN BEAMS AND PLATES WITH DAMPING TREATMENTS

By

Wanbo Liu

Submitted to the graduate degree program in
Aerospace Engineering and the Graduate
Faculty of the University of Kansas School of
Engineering in Partial Fulfillment of the
Requirements for the Degree of
Doctor of Philosophy

Committee:

_____
Dr Mark Ewing, Chairperson

_____
Dr Karan Surana

_____
Dr Richard Hale

_____
Dr Saeed Farokhi

_____
Dr Ronald Barrett-Gonzalez

Date defended
11-24-2008

The Dissertation Committee for Wanbo Liu certifies
that this is the approved version of the following dissertation:

EXPERIMENTAL AND ANALYTICAL ESTIMATION OF DAMPING IN BEAMS AND PLATES WITH DAMPING TREATMENTS

Committee:

_____
Dr Mark Ewing, Chairperson

_____
Dr Karan Surana

_____
Dr Richard Hale

_____
Dr Saeed Farokhi

_____
Dr Ronald Barrett-Gonzalez

Date approved _____

EXPERIMENTAL AND ANALYTICAL ESTIMATION OF DAMPING IN BEAMS AND PLATES WITH DAMPING TREATMENTS

By

Wanbo Liu

November 2008

Abstract

The research presented in this dissertation is devoted to the problem of damping estimation in engineering structures, especially beams and plates with passive damping treatments. In structural design and/or optimization, knowledge about damping is essential. However, due to the complexity of the dynamic interaction of system components, the determination of damping, by either analysis or experiments, has never been straightforward. In this research, currently-used methods are reviewed and gaps are identified first. Then both analytical and experimental studies on the damping estimation are conducted and possibilities of improvement are explored.

Various passive damping treatments using ViscoElastic Materials (VEMs) are designed, manufactured and then added to aluminum and composite beams and plates. Experiments on these damped structures are conducted. Currently used experimental methods, namely, the free-decay method, the modal curve-fitting method and the Power Input Method (PIM), are used to process the experimental data and investigate the damping characteristics. Especially, 1) experimental procedures of the power input method are carefully identified and investigated; 2) the power input method is applied to non-uniformly damped structures; 3) the

power input method is applied in an extended frequency range (from 0 to 5000 Hz) to meet emerging needs of the transportation industries.

A new analytical power input method is proposed for evaluating the loss factor of built-up structures, based on the finite element model with assigned properties of the constituents. Finite Element (FE) models of beams and plates with various damping configurations are developed so a frequency response solution suffices to provide mobility and energy results needed by the new analytical power input method. The analytical power input method is evaluated by comparison with the commonly used Modal Strain Energy (MSE) method. Instead of making an approximate correction of the constant material properties, this analytical power input method directly takes into account the frequency-dependent material properties of the viscoelastic material using the MSC/NASTRAN direct frequency response solution. Features of each method are compared and summarized. Especially, 1) the complex frequency-dependency of viscoelastic materials used in constrained layer damping is modeled using MSC Patran/NASTRAN; 2) a new procedure of estimating loss factors is presented, using the concept of the power input method.

Particle damping is also investigated. A fluid analogy is proposed and applied to composite beams and metallic plates. Results show that the fluid analogy can effectively estimate peak damping frequencies and peak damping levels.

Both experimental and analytical loss factor results for various engineering structures are presented and discussed.

Acknowledgements

The author would like first to express his gratitude to his advisor Dr Mark Ewing, whose support and direction made the author's PhD study possible.

The author also would like to thank his other dissertation committee members Dr Richard Hale, Dr Saeed Farokhi, Dr Karan Surana and Dr Ronald Barrett-Gonzalez for their assistance through the development of this dissertation.

The author seriously recognizes the teachings from other professors that have lectured him at the University of Kansas.

The author appreciates all the help from the faculty and staff of the Department of Aerospace Engineering as a whole for their support.

Special thanks go to the author's parents Detian Liu and Ronglan Lu for their support and understanding.

The author never forgets that he is indebted to many other people as well, though the following can in no way include all the helpers on his study: Charles Gabel, Justin Lohrmeyer, Patrick McNamee, Jim Weaver, Ashok Gandhi Pavanasam, Wannok Sio, and Norman Holmskog.

Table of Contents

List of Figures

List of Tables

Nomenclature

c	=	wave speed of glass microspheres
$E_S^{(r)}$	=	system's overall average strain energy from all components of the natural mode *r* for the modal strain energy method
$E_{Si}^{(r)}$	=	average strain energy in material i when the structure deforms at the natural mode *r* for the modal strain energy method
E_D	=	energy dissipated per cycle during period *T*
E_K	=	average kinetic energy
E_S	=	average strain energy
E_{Tot}	=	total mechanical (stored/vibrational) energy
E	=	elastic modulus
$E*$	=	complex elastic modulus
E'	=	real part of elastic modulus
E''	=	imaginary part of elastic modulus
$F_f(t)$	=	force at the driving point
$F_f(\omega)$	=	Fourier transform of $F_f(t)$
f	=	frequency
f_r	=	*r*th modal frequency calculated with the core shear modulus as $G_{2,REF}$ for the modal strain energy method
G_i	=	shear modulus of the elastic layers *i* in sandwich structures
$G_2'(f)$	=	real part of the shear modulus of the viscoelastic layer 2
$G_2''(f)$	=	imaginary part of the shear modulus of the viscoelastic layer 2
$G_{2,REF}$	=	real part of the shear modulus of the viscoelastic layer 2 used in normal modes calculation for the modal strain energy method
g_{REF}	=	reference element damping coefficient used in normal modes calculation for the modal strain energy method
g	=	overall structural damping coefficient
KE	=	max kinetic energy of the sandwich plate
m_i	=	mass of portion *i* for the experimental power input method
PE	=	max potential energy of the sandwich plate
P_D	=	dissipated power, $P_D = (1/T)E_D = [\omega/(2\pi)]E_D$
P_I	=	input power
$R_{F_fV_f}(0)$	=	cross correlation between the driving point force and driving point velocity
$R_{V_iV_i}(0)$	=	auto-correlation of the velocity at point *i*
$S_{F_fF_f}(\omega)$	=	power spectrum density of the driving point force
$S_{F_fV_f}(\omega)$	=	cross power spectrum density between the driving point force and driving point velocity

$S_{V_iV_i}(\omega)$	=	power spectrum density of the velocity at points *i*
SE	=	max strain energy of the sandwich plate
T	=	period of a vibrational cycle
$TR(f)$	=	tabular function representing the real part of the complex moduli
$TI(f)$	=	tabular function representing the imaginary part of the complex moduli
t_i	=	thickness of layer *i* for the sandwich plate
u_i	=	in plane displacement variable in *x* direction for layer *i* of the sandwich plate
V	=	velocity
$V_f(t)$	=	velocity at the driving point
v_i	=	in plane displacement variable in *y* direction for layer *i* of the sandwich plate
v	=	viscosity coefficient
w	=	transverse displacement variable in *z* direction of the sandwich plate
$Y_{ff}(\omega)$	=	mobility (velocity/force) of the driving point
$Y_{if}(\omega)$	=	mobility (velocity/force) between the driving point *f* and the point *i*
$Z(\omega)$	=	impedance (force/velocity)
σ	=	stress
ε	=	strain
η	=	system loss factor
η_i	=	material loss factor for material *i*
η_{VEM}	=	material loss factor for the viscoelastic material
$\eta^{(r)}$	=	system's modal loss factor at the *r*th mode of the modal strain energy method
$\eta^{(r)'}$	=	system's adjusted modal loss factor for the *r*th mode of the modal strain energy method
μ	=	Poisson's ratio
ρ	=	density
ω	=	angular frequency
ω_1	=	lower limit of the frequency band
ω_2	=	upper limit of the frequency band
ω_C	=	center frequency of the frequency band $[\omega_1, \omega_2]$
$\Delta\omega$	=	bandwidth
P, Q	=	differential operators for stress and strain
P, Q	=	polynomials of the Laplace variable s for stress and strain
$[M]$	=	mass matrix
$[B]$	=	damping matrix
$[K]$	=	stiffness matrix
$\overline{\quad}$	=	time average

1. Introduction

Most engineering structures experience vibrational motion. Unwanted vibrations can result in premature structural fatigue and/or failure, and often unpleasant noise. Damping characteristics represent the structure's ability to dissipate vibrational energy, and thus represent the structure's ability to suppress unwanted vibration. Estimation of damping in engineering structures has been a developing science in both analytical and experimental respects.

Generally speaking, the methods to increase damping can be categorized into two categories: passive damping and active damping. Full-scale implementation of active and semi-active damping treatment has been slow due to high costs and complexity. Passive damping as a well-developed technique, in general, is more simple and cost-effective [69].

1.1. Passive Damping

Among passive damping treatments, Constrained Layer Damping (CLD) and Particle Damping (PD) are the two most commonly-used methods.

1.1.1. Constrained Layer Damping

In constrained layer damping, a thin damping layer (usually viscoelastic materials) is added to the structure, and then covered by a constraining layer, as shown in Figure 1.1. When the base structure deforms, the damping layer is loaded in shear. Thus, under dynamic load, the viscoelastic material dissipates energy by disrupting the bonds of its long-chain molecules to convert kinetic energy to thermal energy (heat). An optional segmented spacer can be added in between the base structure and the damping layer to amplify the deformation of the base structure, often for structures with high specific stiffness, e.g., honeycomb

sandwich composites. In this case, the damping treatment is called Stand-Off Constrained Layer Damping (SOCLD). Composite honeycomb sandwich structures do not deform much under external excitation due to their high stiffness. Thus, if constrained layer damping is applied directly on to the surface of such structures, there will be a lack of shear strain energy in the viscoelastic layer. To solve this problem, stand-offs can be added to amplify the deformation. These stand-offs should have high shear stiffness but near-zero bending stiffness.

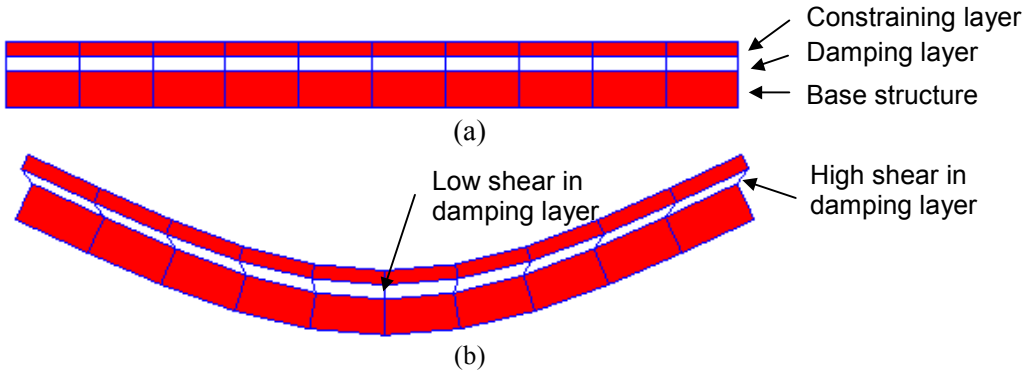

Figure 1.1 Schematic of constrained layer damping treatment. (a) Undeformed structure; (b) deformed structure.

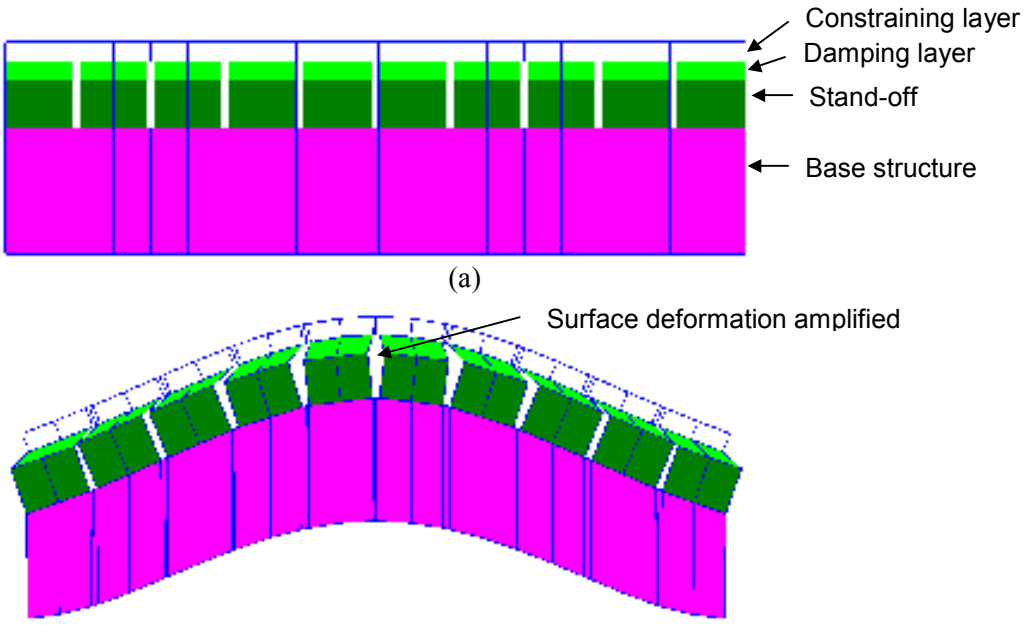

Figure 1.2 Schematic of stand-off constrained layer damping treatment. (a) Undeformed structure; (b) deformed structure.

1.1.2. Particle Damping

In particle damping, the damper is an enclosure or enclosures filled with particles made of a variety of materials (e.g., lead, steel, tungsten, glass, etc.), as shown in Figure 1.3. The energy loss is due to the inter-particle and particle-wall friction and inelastic impact. Unlike constrained layer damping, particle damping can be used over a broad range of temperature due to the intrinsic insensitivity to temperature of its damping materials. On the other hand, the effect of any moisture in the medium may need to be considered if the temperature is below the freezing point or if the particles are easily stuck together due to moisture. The mechanism of particle damping is still not fully understood. It has been found to be closely related to many factors, including particle size, particle density, particle shape, particle surface friction, vibrational direction, packing ratio, vibration amplitude, etc. Once the region to install particles is determined, the only design variables left are the particle type, the cavity depth and the packing ratio.

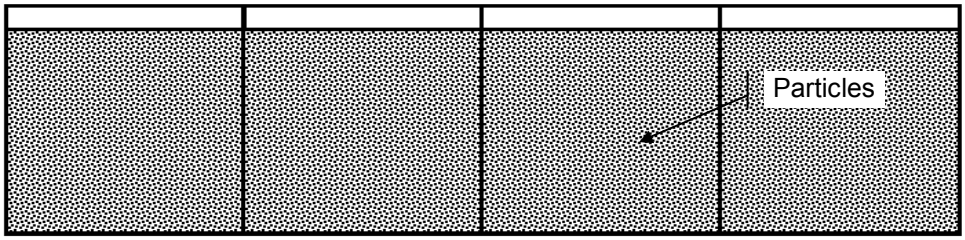

Figure 1.3 Schematic of particle damping treatment.

1.2. Loss Factor

The damping loss factor is widely accepted as one of the major damping indices, and it is used throughout this research. Hence, it is introduced first.

1.2.1. Definition of Loss Factor

The loss factor of a system is defined in energy terms [71] [8] [39] [24]:

$$\eta = \frac{P_D}{\omega E_{Tot}} = \frac{E_D}{2\pi E_{Tot}} \tag{1.1}$$

where P_D is the dissipated power; E_{Tot} is the total mechanical (stored) energy, which is the summation of average strain energy and average kinetic energy, $E_{Tot} = E_S + E_K$; E_D is the energy dissipated per cycle during period T, $P_D = \frac{1}{T} E_D = \frac{\omega}{2\pi} E_D$; ω is the angular frequency.

1.2.2. Loss Factor and Damping Ratio

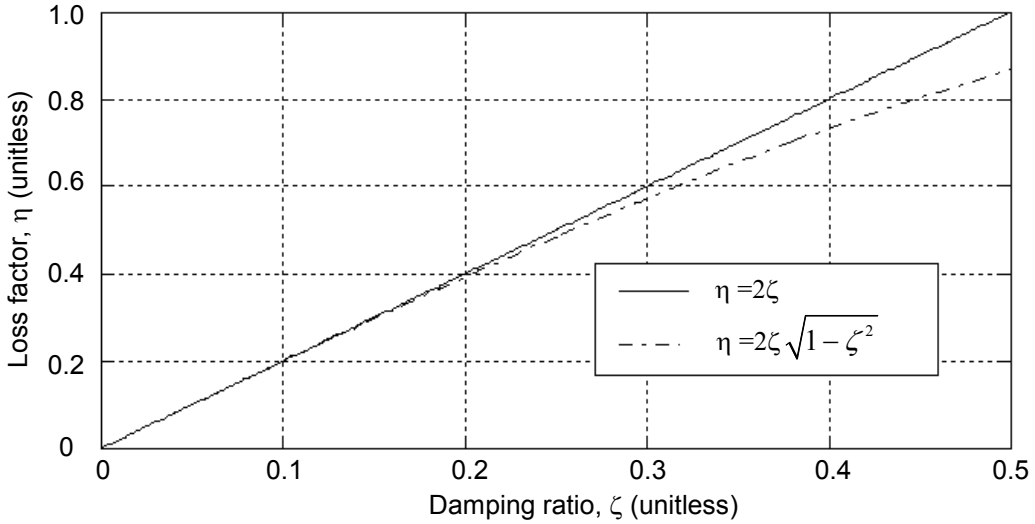

Figure 1.4 Relationship between loss factor η and damping ratio ζ.

In many references (Reference [35], Reference [59] and Section 7 in reference [78]), it is stated that $\eta = 1/Q = 2\zeta$, where ζ is the damping ratio and Q is the quality factor. This is usually accepted as the relationship between loss factor and damping ratio. However, the accuracy is conditional. As pointed out by Nashif, Jones and Henderson (1985) [59] and Graessner and Wong (1992) [36], $Q^{-1} = 2\zeta = \sqrt{1+\eta} - \sqrt{1-\eta}$, so the loss factor is actually

$\eta = 2\zeta\sqrt{1-\zeta^2}$. Thus, $\eta = 2\zeta$ is accurate within 5% for $0 \le \eta \le 0.3$. The comparison is plotted in Figure 1.4.

1.3. Experimental Methods

1.3.1. Commonly-used Experimental Methods

Currently-used experimental methods of damping estimation can be broadly classified into three groups [15] [17] [66], as briefly summarized below.

1) Time-domain free-decay methods. The method is based on the observation of the time history of energy dissipation. In particular the response decay is expected to be exponential when a single mode is excited. In the high frequency ranges, where modal density is high, the time history curve usually shows beating, as shown in Figure 1.5. This causes difficulty fitting a straight line to the log of the decay-rate curve. Loss factors have been shown to vary with measurement points [71]. Also, irregularities in decay history may occur if the excitation frequency does not quite coincide with the natural frequency Section 4.4.2.2 in reference [24]. The free decay method is best suited for lightly damped structures (if a directly-attached excitation is used) in the low and middle frequency range.
2) Frequency-domain modal curve-fitting methods. These methods determine loss factors at each individual natural mode, using frequency response function (FRF) data measured from steady-state response. Modal frequencies are identified at the peak resonance frequencies and modal damping is identified by the "width" of the resonance peak. As an alternative, some techniques attempt to match measured data

with an analytical expression, often called curve-fitting. Difficulty in mode identification arises as modal coupling and damping increases.

3) Power input method. The concept is directly based on the definition of structural energy losses. Thus, there is no theoretical limitation on broad frequency application. The concept of using the power input method to measure structural loss appeared in the late 1970's. However, due to the limitation on measurement instrumentation and computational capabilities, development has been slow. It is not mentioned in the general surveys in Cremer, Heckl and Ungar (1973) [22], Chu and Wang (1980) [19] and Soovere and Drake (1985) [78], but it gradually draws more attention as shown in literature [39], [66], [16], [17] and [18]. Recently the power input method appears as an alternative method in the general survey by Cremer, Heckl and Petersson (2005) [24]. The power input method is proven to have advantages over the other two methods, though understanding of the experimental procedure is still developing. Therefore, this method is given special attention in the current research.

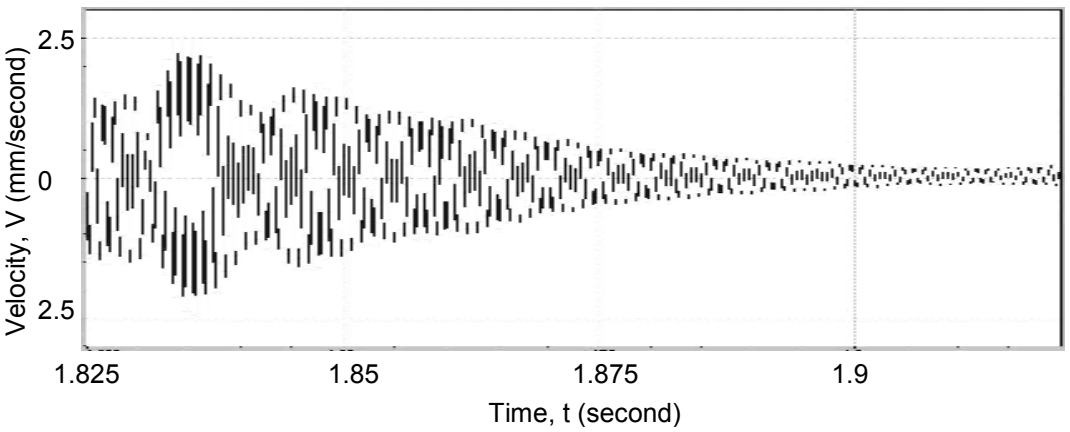

Figure 1.5 Measured free-decay time history of a sandwich honeycomb composite panel at 973 Hz showing multi-modal interferenece.

1.3.2. Basic Principles of Experimental Power Input Method

The concept of the power input method to measure the loss factor is based directly on the equation that defines this quantity, as shown in Equation (1.1) which is restated as:

$$\eta = \frac{P_D}{\omega E_{Tot}} = \frac{E_D}{2\pi E_{Tot}} \tag{1.1}$$

In a practical measurement, the following two steps are usually taken first.

1) As for the numerator, the input power is eventually converted into heat, which cannot be easily measured. However, for a steady-state vibration, the dissipated power of the system P_D equals the input power P_I from the excitation. Thus, if the structure is driven at a single point, the input power can be estimated from the time-averaged product of the force at the driving point $F_f(t)$ and the velocity at the driving point $V_f(t)$: $P_D = P_I = \overline{F_f(t) \cdot V_f(t)}$.

2) As for the denominator, the total mechanical energy E_{Tot} cannot be easily measured either, because it consists of two parts: the average kinetic energy and the average strain energy, where average strain energy is hard to measure directly. So it is replaced with twice the average kinetic energy E_K [9][37][39][40], that is $E_{Tot} = 2E_K = \int_v \rho \overline{V^2(t)}\, dv$.

Now the loss factor in time-averaged terms is [39]:

$$\eta = \frac{\overline{F_f(t) \cdot V_f(t)}}{\omega \int_v \rho \overline{V^2(t)}\, dv} \tag{1.2}$$

Specifically, the input power is:

$$\overline{F_f(t) \cdot V_f(t)} = R_{F_f V_f}(0) = \int_0^\infty \mathrm{Re}\left[S_{F_f V_f}(\omega) \right] d\omega = \int_0^\infty \mathrm{Re}\left[Y_{ff}(\omega) \right] S_{F_f F_f}(\omega)\, d\omega \tag{1.3}$$

and the strain energy is:

$$\int_v \rho \overline{V^2(t)}\, dv = \int_v \rho R_{V_i V_i}(0)\, dv = \int_v \rho \frac{1}{\pi} \int_0^\infty S_{V_i V_i}(\omega)\ d\omega\, dv \tag{1.4}$$

where $R_{F_f V_f}(0)$ is the cross correlation between the driving point force and velocity; $R_{V_i V_i}(0)$ is the auto-correlation of the velocity at point *i*; ρ is the density of the structure; $S_{F_f V_f}(\omega)$ is the cross power spectrum density between the driving point force and velocity; $Y_{ff}(\omega)$ is the mobility (velocity/force) of the driving point; $S_{F_f F_f}(\omega)$ is the power spectrum density of the driving point force and $S_{V_i V_i}(\omega)$ is the power spectrum density of the *i*'th point velocity. However, practically, the kinetic energy can only be represented by the summation of a finite number of measurements, *N*, representing the response over the whole structure: $E_S \cong \sum_{i=1}^{N} m_i \cdot \frac{1}{\pi} \cdot \int_0^\infty S_{V_i V_i}(\omega)\ d\omega$. Similarly, the above discretization is obtained by assuming that the excitation frequency varies from zero to infinity, but practically the excitation frequency can only vary in a finite frequency-band $[\omega_1, \omega_2]$.

Thus, a frequency-band averaged loss factor is defined as

$$\eta(\omega_C, \Delta\omega) = \frac{\int_{\omega_1}^{\omega_2} \mathrm{Re}\left[Y_{ff}(\omega)\right] S_{F_f F_f}(\omega)\ d\omega}{\sum_{i=1}^{N} m_i \int_{\omega_1}^{\omega_2} \omega S_{V_i V_i}(\omega)\ d\omega} \tag{1.5}$$

where ω_C is the center frequency of the frequency-band; $\Delta\omega$ is the bandwidth; ω_1 and ω_2 are the lower and upper limits of the frequency-band. By the mean value theorem for integrals, Equation (1.5) can be rewritten as

$$\eta(\omega_C,\Delta\omega)=\frac{(\omega_2-\omega_1)\,\mathrm{Re}\left[Y_{ff}(\omega')\right]S_{F_fF_f}(\omega')}{\sum_{i=1}^{N}m_i(\omega_2-\omega_1)\cdot\omega_i'S_{V_iV_i}(\omega_i')} \tag{1.6}$$

where ω' and ω_i' are frequencies in $[\omega_1,\omega_2]$. Through simplification,

$$\eta(\omega_C,\Delta\omega)=\frac{\mathrm{Re}\left[Y_{ff}(\omega')\right]S_{F_fF_f}(\omega')}{\sum_{i=1}^{N}m_i\omega_i'S_{V_iV_i}(\omega_i')} \tag{1.7}$$

When $\omega_1,\omega_2\to\omega_C$, i.e., $\Delta\omega\to 0$

$$\lim_{\Delta\omega\to 0}\eta(\omega_C,\Delta\omega)=\frac{\mathrm{Re}\left[Y_{ff}(\omega_C)\right]S_{F_fF_f}(\omega_C)}{\sum_{i=1}^{N}m_i\omega_CS_{V_iV_i}(\omega_C)} \tag{1.8}$$

i.e.,

$$\eta(\omega)=\frac{\mathrm{Re}\left[Y_{ff}(\omega)\right]S_{F_fF_f}(\omega)}{\sum_{i=1}^{N}m_i\omega S_{V_iV_i}(\omega)} \tag{1.9}$$

For linear systems, $S_{V_iV_i}(\omega)=\left|Y_{if}(\omega)\right|^2S_{F_fF_f}(\omega)$, where $Y_{if}(\omega)$ is the mobility between the driving point *f* and the point *i*. Finally the loss factor at a frequency ω becomes [10] [16] [17]

$$\eta(\omega)=\frac{\mathrm{Re}\left[Y_{ff}(\omega)\right]}{\sum_{i=1}^{N}m_i\omega\left|Y_{if}(\omega)\right|^2} \tag{1.10}$$

which is the commonly-used expression of the experimental power input method. Each term in Equation (1.10) can be measured directly using conventional instruments similar to modal analysis.

1.3.3. Current Development of the Experimental Power Input Method

Bies and Hamid (1980) [8] measured the loss factors of a lightly damped steel plate by both the decay method and the power input method. For the power input method measurement, their test setup included: a shaker; a "power flow transducer" (impedance head) to measure input power; and a number of accelerometers to measure response velocities. It was observed that the two experimental methods yielded different results. A suggested reason was given as “the energy distribution among modes of the system during reverberant decay was not in steady-state equilibrium”, attributing the difference to energy dissipation mechanisms. It was also pointed out that a very large number of accurate measurements were required, thus suggesting automated data processing and a new generation of measurement equipment.

Ranky and Clarkson (1983) [71] measured the loss factors of a lightly damped plate using both the decay-rate method and the power input method. An electromagnetic coil/impedance head/accelerometer test setup was used. Six accelerometer positions were used to calculate the energy (which is in disagreement with the suggestion by Bies and Hamid (1980) that many more measurement locations were needed). However, it was concluded in their paper that “there was no significant difference between the results from the two methods as long as the modes in the analysis band had similar loss factors”. It was also concluded that otherwise, the log of the decay-rate record would not be a straight line and thus made it difficult to obtain a constant loss factor.

Jacobsen (1986) [36] tested several structures including a rectangular steel box, an open aluminum shell (moderately damped and heavily damped), a steel plate (moderately damped and heavily damped), a steel cylindrical shell (undamped) and an aluminum beam (lightly damped). A shaker/force transducer/accelerometer test setup was used. The kinetic energy

was estimated by averaging the velocity across 10 to 50 points. By observation of the test results, Jacobsen concluded that for his method of implementation:

1) The power input method was "unsuited for examining heavily damped (η>0.1) or very lightly damped (η<0.001) structures". [It has been shown that heavily damped structures can be estimated using the power input method in the current research.] Possible reasons were given as
    a) An inadequate number of measurement points were used for heavily damped structures.
    b) Minute phase errors in the two measurement channels.
2) The power input method was not good for quick survey measurements because it was time consuming to move and position the accelerometer across many points.
3) The power input method could not be used on structures with complex shapes due to the requirement that the structure under test should "allow a meaningful determination of the local mass-per-point in the discrete spatial averaging".

Plunt (1991) [66] measured a lightly-damped steel plate using both the free-decay method and the power input method. Ten to twenty measurement positions were used. Two test setups were investigated: 1) Hammer/accelerometer; 2) Shaker/impedance head/accelerometer. From the comparison between the free-decay method and the power input method results, it was concluded that the shaker setup agreed better with the free-decay method results. In addition, a damped car floor was measured. The tested frequency range was from 0 to 2000 Hz. Results showed loss factors as high as 0.3 in the medium frequency range. Conclusions included:

1) The power input method could be used for complex built-up structures. It was superior to the free-decay method when modal coupling was strong.

2) Loss factor results could be obtained for a wide range from 0.001 to 0.5.

3) Data acquisition could be very similar to conventional modal analysis measurement.

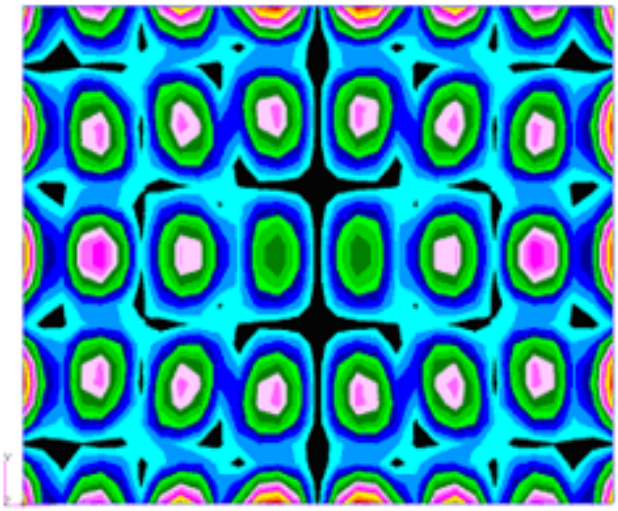

Figure 1.6 The mode shape of Wu, Agren and Sundback's (1997) [89] 0.545×0.460×0.005 m steel plate at 2473 Hz.

Wu, Agren and Sundback (1997) [89] tested several lightly and moderately damped plates using both the decay-rate method and the power input method. A shaker/impedance head/accelerometer setup was used. For the moderately damped plate (described as "highly damped" in [89]), it was observed that in the frequency range from 1600 to 2500 Hz, a systematic difference between the two methods existed. However, it was concluded that "the decay rate and the power input methods are consistent only when damping is light or moderate" and as a result, "for a certain number of driving and measurement points, the decay method should be the first choice when determining a reliable estimate of damping loss factors compared to the power input method." However a further investigation in the current research reveals the true reason: it is because there were not enough measurement points to represent the kinetic energy of the 0.545×0.460×0.005 m steel plate over a frequency range from 0 to 2500 Hz. To check the validity of the discretization, a finite element modal analysis

is carried out. As shown in Figure 1.6, at 2473 Hz, the mode shape of an undamped plate is too complex to be represented by only six measurement points. Thus, it is believed that the difference in damping estimation is because of a lack of discretization, not because of the damping level.

Carfagni and Pierini (1999) [17] tested highly damped steel plates, as well as conducted numerical investigations, which are summarized in a later section. A hammer/accelerometer setup was used. Conclusions included:

1) Manual skills of hammer tapping turned out to have an influence on the test result.
2) The excitation point position affects the test result. Edges and nodal lines should be avoided if possible.
3) The loss factor results converge as the discretization becomes finer.

Carfagni, Citti and Pierini (1998) [18] also used a shaker to replace the hammer excitation so that the measurement problems associated with hammer excitation could be avoided, which is consistent with what Plunt (1991) pointed out.

Renji and Narayan (2002) [72] tested a composite sandwich plate with carbon-fiber-reinforced polymer (CFRP) face sheets and an aluminum honeycomb core using the power input method only. A shaker/impedance head/accelerometer test setup was used. Considering the fact that usually the test was conducted in air, it was pointed out that the loss factors measured were total loss factors that consisted of dissipation loss factors and radiation loss factors. Radiation loss factors were calculated theoretically, and then subtracted from the experimental total loss factors to get dissipation loss factors. It was claimed that "the dissipation loss factors of the composite panel with carbon-fiber-reinforced polymer face sheets are approximately the same as those with aluminum face sheets. No comparative study was presented.

Bloss and Rao (2002) [9] tested a commercial vehicle door using a shaker/force transducer/laser vibrometer setup. The use of a laser vibrometer allowed an automated scan of measurement points without introducing the mass-loading effect in accelerometer measurements. Later, a more thorough investigation was done by Bloss and Rao (2005) [10] to compare the free-decay method and the power input method (as well as numerical investigations, which are summarized in Section 1.4.1). Experiments were conducted on a damped steel plate, using both the free-decay method and the power input method. "Both methods returned similar results but variance between the two existed", as shown in Figure 1.7. It can be seen that questions about the comparison are left to be answered.

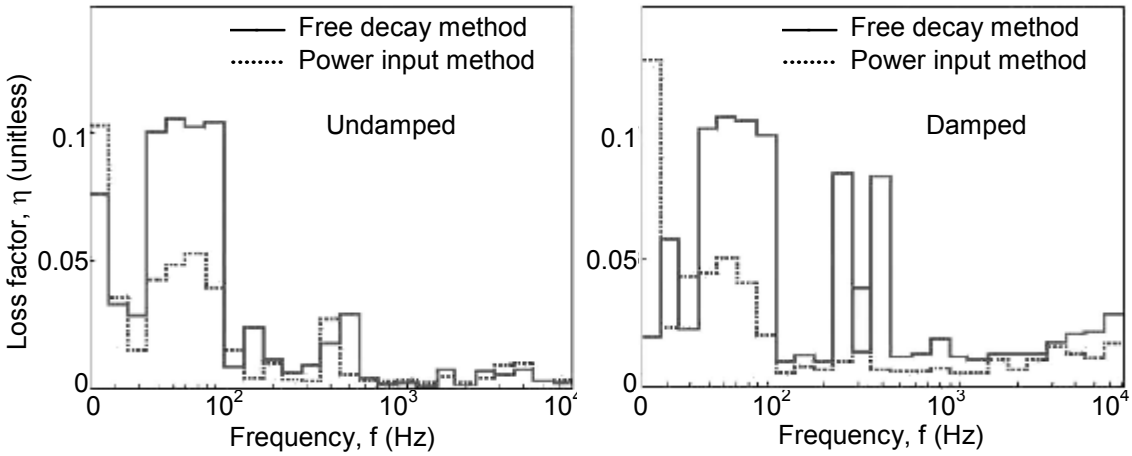

Figure 1.7 Bloss and Rao's (2005) [9] comparison of the decay method and the power input method. (a) Loss factors of the undamped plate; (b) loss factors of the damped plate.

Bolduc (2007) [11] compared a shaker/force transducer/ laser vibrometer setup and hammer/accelerometer setup to measure loss factors. Major conclusions include:

1) The power input method is better for structures with high damping values than the decay rate method.
2) Hammer excitation is difficult to distribute input power in "soft" structures. One way to overcome this is to use a shaker instead.

Based on the above literature survey, it is identified that current needs in experimental methods are:

1) Thorough studies of the experimental power input method, e.g., excitation configuration study, discretization convergence study, etc.
2) Comparison of the experimental power input method results with analytical ones.
3) Damping estimation in an extended frequency range (from 0 to 5000Hz) to meet emerging needs of the transportation industries [67].
4) Application of the power input method to investigate structures with particle damping and non-uniformly damped structures, e.g., partially-covered constrained layer damping panels.

1.4. Analytical Methods

1.4.1. Analytical Methods for Viscoelastic Damping

There has been a need for analytical damping estimation, as reflected in the statement by Zhu, Crocker and Rao (1989) [92] that "because of the complexity of structural configurations, different materials, interface conditions, joints, etc., damping is usually determined by experiments".

When computational capability was limited, closed form solutions were developed. The usual approach is to start from Partial Differential Equations (PDEs) of motion. The first extensive discussion of damped sandwich beams was given by Ross, Ungar and Kerwin (1959) [74], based on a fourth-order partial differential equation. Their solution gave loss factors for infinite-length beams or finite beams with simply supported boundary conditions. DiTaranto (1965) [26] derived a sixth-order partial differential equation to describe the motion of the sandwich beam, enabling the analysis of finite-length beams with boundary

conditions other than just simply-supported. Mead and Markus (1969) [56] refined the theory of DiTaranto by re-deriving the partial differential equation and then extended their theory to fixed-fixed beams.

With the appearance of computers, finite element methods started to show more flexibility in modeling complex structures and boundary conditions as a result of enhanced computational capability. Carne (1975) [19] developed a two-dimensional damped beam model using MSC/NASTRAN. The base beam and the constraining layer were modeled by offset beam elements. The middle-damping layer was modeled by rectangular shear panels. The material properties of the damping layer were represented by a complex shear modulus. Though the shear storage modulus and loss factor of viscoelastic materials are frequency-dependent, they were treated as constants in modeling. Carne concluded that:

1) The necessity of a total of six boundary conditions implies that a sixth-order partial differential equation is the lowest order that could accurately describe the motion of a sandwich beam, consistent with what Mead (1973) [55] remarked.
2) The representation of complex shear modulus leads to a complex eigenvalue analysis giving complex eigenvectors thus indicated that the normal modes no longer exist as Mead and Markus (1969) concluded.

Johnson, Kienholz and Rogers (1981) [39] developed a three-dimensional plate model using the MSC/NASTRAN program. The base plate and the constraining layer were modeled by two-dimensional offset plate elements (QUAD/TRIA elements in MSC/NASTRAN). The middle-damping layer was modeled by three-dimensional solid elements (HEX/PENT elements in MSC/NASTRAN). The material properties of the middle-damping layer were all treated as real and constant so that a standard normal-modes analysis (MSC/NASTRAN solution 103) suffices. A Modal Strain Energy (MSE) method was also presented to calculate

modal loss factors from the normal-modes analysis, which is briefly described as follows. The loss factor is defined as:

$$\eta^{(r)} = \sum_{i=1}^{N} \eta_i \frac{E_{Si}^{(r)}}{E_S^{(r)}} \tag{1.11}$$

where $\eta^{(r)}$ is the system's modal loss factor at the *r*th mode, η_i is the material loss factor for material *i*, $E_{Si}^{(r)}$ is the average strain energy in material *i* when the structure deforms in natural vibration mode *r*, and $E_S^{(r)}$ is the system's overall strain energy in natural vibration mode *r*. Then to take into account the frequency-dependent material properties, a simple empirical correction has been given as:

$$\eta^{(r)'} = \eta^{(r)} \sqrt{\frac{G_2(f_r)}{G_{2,REF}}} \tag{1.12}$$

where $\eta^{(r)'}$ is the adjusted modal loss factor for the *r*th mode, $\eta^{(r)}$ is the system's modal loss factor at the *r*th mode, $G_{2,REF}$ is the core shear modulus used in normal modes calculation, and $G_2(f_r)$ is the core shear modulus at $f = f_r$ where f_r is the *r*th mode frequency calculated with core shear modulus as $G_{2,REF}$.

Carfagni and Pierini (1999) [16] did the first numerical investigation on the power input method to evaluate the effect that assumptions have on results. First, a system with eight lumped masses was analyzed. It was found that the error, which was introduced by replacing the potential energy with twice the kinetic energy at non-resonance frequencies, decreased as the natural frequencies became closer, in other words, as modal coupling became stronger. [Note: this feature enables the power input method to do well where the free-decay method can not.] Further numerical investigations included modeling a flat plate for modal analysis for the first 10 modes using ANSYS to determine experimental discretization plan. [Note: so

far this is the only analytical work using the power input method concept on plate-type structures.] It was concluded that "with the number of portions being equal, the error increased as the frequency increased". This is because as the frequency increases, the deflection shape of the plate becomes more complex, which makes the nodes less representative of the vibratory features.

Bloss and Rao (2002) [9] did a parametric study by modeling spring/mass/damper systems. It was observed that both the decay method and the power input method yielded accurate results. But for highly damped structures, the decay method gave significantly lower loss factors than the power input method.

To model the frequency-dependency of viscoelastic material properties, several other finite element methods appeared, namely the Golla-Hughes-McTavish (GHM) [54] method, the Augmented Thermodynamic Fields (ATF) [42] method and Anelastic Displacement Field (ADF) [47] method. These methods augment the usual finite element model by introducing internal dissipation coordinates. For example, in the GHM method, the material property data of viscoelastic material are curve-fitted to a polynomial first, with coefficients reflecting the material properties of the viscoelastic damping layer. The Laplace Transform is then used so this polynomial can be incorporated into the Laplacian domain governing equations of the structure. This way, the frequency-dependent material properties are taken into account with the price of increased computational cost. The results of these augmented finite element methods are concluded to be more accurate than the commonly-used modal strain energy method proposed by Johnson, Kienholz and Rodgers (1981). However, the additional dissipation coordinates prevent these finite element methods from using commercially available software.

Based on the above literature survey, it is identified that the current gaps in analytical methods are:

1) Modeling of the frequency-dependency of viscoelastic material properties in constrained layer damping treatment: the commonly-used modal strain energy method uses only constant material properties, followed by an approximate correction.
2) Using commercially available finite element software (MSC/NASTRAN) to ease and standardize the process, overcoming the limitation of augmented finite element model methods caused by introducing internal dissipation coordinates.
3) Exploring new analytical procedures to estimate damping in engineering structures.

Besides the above gaps, there is also a need to compare experimental and analytical estimation of damping over an extended frequency range.

1.4.2. Analytical Methods for Particle Damping

Due to the complex interaction involved in particle damping, a comprehensive analytical method is not yet available [31]. Current methods can be generally categorized into three groups:

1) Equivalent model. Papalou and Masri (1996) [63] proposed an approximate single-particle damper model, aimed to predict the root mean square response. Nayfeh, Verdirame and Varanasi (2002) [62] developed 3-D shell equations to model powders as a compressible fluid with complex speed of sound for qualitative explanation.
2) Semi-empirical methods. Friend and Kinra (2000) [33] developed an analytical method, assuming that all particles move as a lumped mass. An “effective coefficient

of restitution" is adopted to minimize analytical and experimental discrepancies. Xu (2004) [90] presented an empirical method where the damping capacity is determined by curve-fitting based on extensive experiments.

3) Explicit Discrete Element Method (DEM). This method tracks the individual motion of each particle [25][76]. As a result, it reveals more accurately the impact and friction in between particles, given that the impact and friction mechanism is accurately modeled. But, it also requires high computational cost. So, it is practical only for a small number of particles enclosed in a few cavities.

In this research, glass microbubbles are used as the damper, considering their low density compared to metal particles. But current methods do not offer quick quantitative damping estimation that fits for the design of particle damping using glass microbubbles.

2. Structures with Viscoelastic Damping

Studies on structures with viscoelastic damping include experimental work and analytical work. Results are presented and summarized in this chapter. The results described in this section are published in Reference [49].

2.1. Experimental Study

Experimental setup used in this research is described first and then responses obtained through experiments and finite element computations are compared.

2.1.1. Experimental Setup

All three commonly-used methods mentioned in Section 1.3 are applied in this research. For the modal curve-fitting method and the power input method, a shaker is used as the mechanical excitation, as shown in Figure 2.1(a). For the free decay method, a speaker is used as the noise excitation, because it eliminates the shaker armature interference.

For both shaker and speaker excitation, a pseudo-random excitation signal is usually used to generate broadband responses. Test articles are suspended by a light and soft spring to simulate free boundary conditions. The other end of the spring is attached to a massive and stiff frame, so vibrational energy is reflected back to the test article with minimum energy loss at the boundary. Wolf Jr. (1984) [88] provided a rule-of-thumb for designing suspension systems: to simulate free boundary conditions, the first rigid body mode under the constraint of the suspension should be no more than 1/10 of the first elastic mode. For example, the most dominant rigid body mode (the vertical translational mode) of a damped aluminum plate

is measured to be at 1.4 Hz, which is much less than 1/10 of the plate's first bending mode 91Hz/10=9.1 Hz.

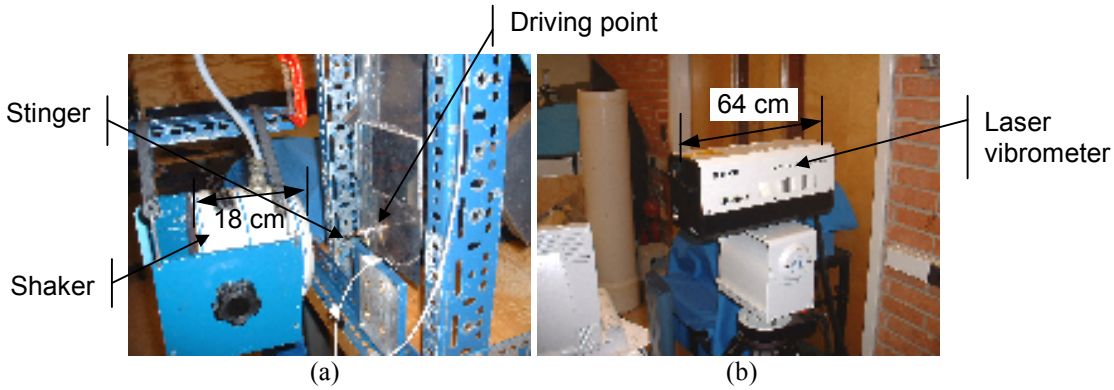

Figure 2.1 Experimental instruments. (a) A shaker attached to the test article through a force transducer and an aluminum connector; (b) Polytec OFV 056 laser scanning head.

The response of the test article is measured using a Polytec OFV 056 scanning laser vibrometer, a non-contact measuring instrument, with built-in excitation signal generator, as shown in Figure 2.1(b). STAR software is used for modal curve-fitting analysis. A typical experimental setup is illustrated in Figure 2.2. Tests are done at room temperature, approximately 20 °C.

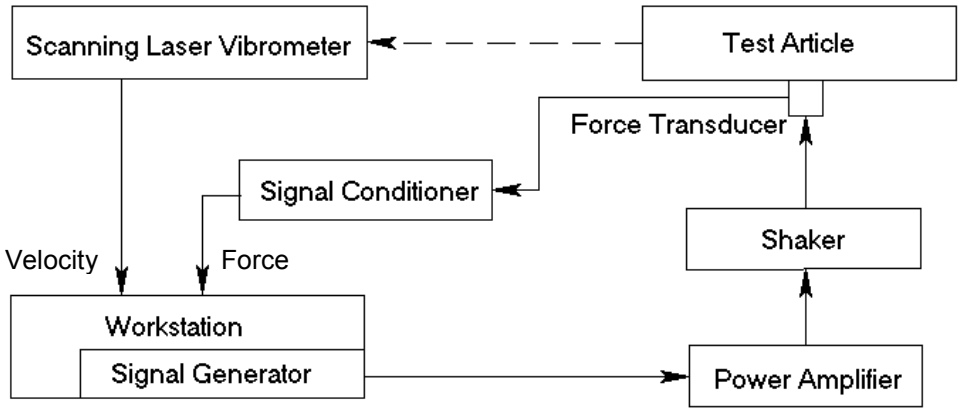

Figure 2.2 A typical experimental setup in this research.

Aluminum alloy plates are chosen as test articles to simulate aerospace structures, especially structural skin panels. Uniformly damped and non-uniformly (partially covered)

damped plates are manufactured. Sandwich honeycomb composite beams and plates are also used. The damping material used here is viscoelastic-damping polymer, 3M F9469PC. To make sure of the good bonding between the viscoelastic material and the structure, surfaces are cleaned before attachment and vacuum is drawn after attachment to apply a pressure to about 1×10^5 Pascal.

2.1.2. Comparison of Experimental Responses with Analytical Responses

In this section, the comparison is between the measured and predicted mobility responses of an aluminum plate with full coverage constrained layer damping. The purpose is to compare the analytical methods validated in Section 2.2.4 with the experimental methods.

Table 2.1 Description of the plate with full coverage constrained layer damping

	Material	Dimensions (m)	Mass (g)
Base layer	CLAD 2024-T3	0.349×0.2029×0.0016002	311
Damping layer	3M F9469PC at 20°C	0.349×0.2029×0.000127	3
Constraining sheet	CLAD 2024-T3	0.349×0.2029×0.000508	30

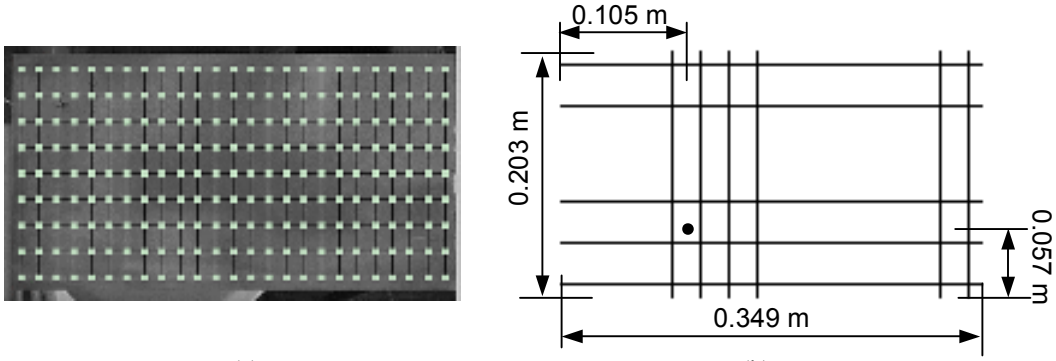

(a) (b)

Figure 2.3 Aluminum plate with full coverage constrained layer damping. (a) The plate as a test article with scanning points defined; (b) the plate as a finite element model with the driving point illustrated.

The sandwich aluminum plate is designed and manufactured with a configuration as shown in Table 2.1. An analytical finite element model is built to obtain analytical responses. The base layer and the constraining layer are modeled as QUAD4 elements and the damping

layer is modeled as HEX8 elements. The total degrees of freedom are 5890. Please see Appendix A for detail definitions of materials mentioned in Table 2.1.

Both measured and predicted mobility responses, at two representative frequencies, are shown in Figure 2.4. From the comparison, agreement can be seen between measured and predicted mobility responses. Another purpose of this comparison is to illustrate the different response characteristics of a plate in low and high frequency ranges, which is consistent with the explanation in Reference [24] Chapter 4 that "for low-frequency measurements on a sample of small dimensions, one may consider the test sample as a spring. At intermediate and high frequencies, the sample then acts more like a wave-carrying distributed system. At very high frequencies, one generally determines material data by considering the test samples to be semi-infinite continua".

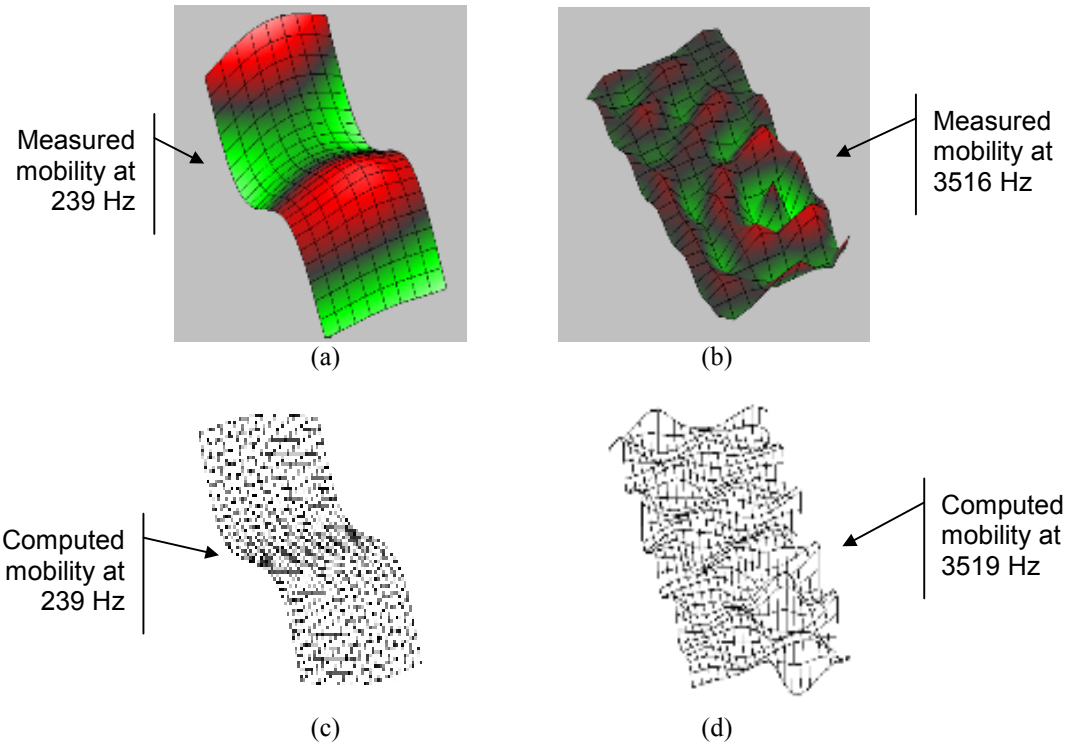

Figure 2.4 Comparison of the measured and predicted responses of a damped aluminum plate. (a) Measured mobility at 239 Hz; (b) measured mobility at 3516 Hz; (c) computed mobility at 239 Hz; (d) computed mobility at 3519 Hz.

2.2. Analytical Study

2.2.1. Viscoelasticity

Strictly speaking, there is no pure elastic material because in reality all materials deviate from Hooke's law in some way. Viscoelastic materials have elements of both of elastic and viscous properties. Whereas elasticity is usually the result of bond-stretching along crystallographic planes in an ordered solid, viscoelasticity is the result of the diffusion of atoms or molecules inside of an amorphous material, e.g., glasses, rubbers and high polymers. Much of the viscoelastic behavior can be described in terms of a simple combination of elastic and viscous phenomena:

1) The elastic components can be modeled as springs of elastic constant E, given the formula $\sigma = E\varepsilon$, where σ is the stress; E is the elastic modulus and ε is the strain that occurs under the given stress.
2) The viscous components can be modeled as dashpots such that the stress-strain rate relationship can be given as $\sigma = v\, d\varepsilon/dt$ where v is the viscosity coefficient, and $d\varepsilon/dt$ is the time derivative of strain.

Some common phenomena in viscoelastic materials are [45]:

1) If the stress is held constant, the strain increases with time (creep).
2) If the strain is held constant, the stress decreases with time (relaxation).
3) The effective stiffness depends on the rate of application of the load.
4) If cyclic loading is applied, hysteresis (a phase lag) occurs, along with a dissipation of mechanical energy.
5) Acoustic waves experience attenuation.
6) Rebound of an object following an impact is less than 100%.

Among the common viscoelastic phenomena, two types of behavior are of major engineering interest: transient properties (creep and relaxation) and dynamic response to alternating load.

For transient properties, there are three commonly-used 1-DOF models (as shown in Figure 2.5), namely, the Maxwell model, the Kelvin-Voigt model and the standard linear solid model (a.k.a., three element model).

The Maxwell model represents viscoelastic materials by an elastic spring and a viscous damper connected in series:

$$\frac{d\varepsilon_{Total}}{dt} = \frac{d\varepsilon_{Damper}}{dt} + \frac{d\varepsilon_{Spring}}{dt} = \frac{\sigma}{\nu} + \frac{1}{E}\frac{d\sigma}{dt}. \tag{2.1}$$

Letting

$$\sigma = \sigma_0 \exp(i\omega t) = (E' + iE'')\varepsilon, \tag{2.2}$$

Equation (2.1) yields:

$$E'' + iE'' = E\frac{i\omega\lambda}{1 + i\omega\lambda}, \tag{2.3}$$

which leads to:

$$E' = \frac{\omega^2\nu^2 E}{E^2 + \omega^2\nu^2} \text{ and } E'' = \frac{\omega\nu E^2}{E^2 + \omega^2\nu^2}. \tag{2.4}$$

The Kelvin-Voigt model represents viscoelastic materials by an elastic spring and viscous damper connected in parallel:

$$\sigma = E\varepsilon + \nu\frac{d\varepsilon}{dt}. \tag{2.5}$$

The standard linear solid model represents viscoelastic materials by an elastic spring (elastic 1 with modulus E_1) and a viscous damper connected in series, then together connected to another elastic spring (elastic 2 with modulus E_2) in parallel:

$$\frac{d\varepsilon_{Tot}}{dt} = \frac{\frac{E_2}{\nu}\left(\frac{\nu}{E_2}\frac{d\sigma}{dt} + \sigma - E_1\varepsilon\right)}{E_1 + E_2}. \tag{2.6}$$

Following the same treatment presented earlier for the Maxwell model, the Kelvin-Voigt model and the standard linear solid model yield their own expressions for moduli E' and E'', which is comparable to Equation (2.4).

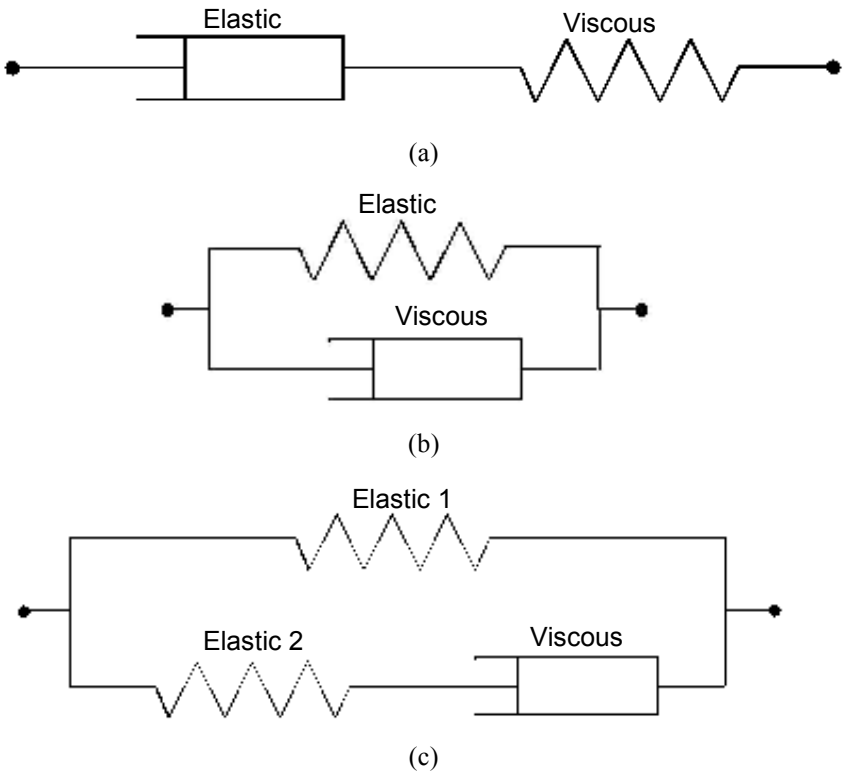

Figure 2.5 Models of viscoelastic materials. (a) Maxwell model; (b) Kelvin-Voigt model; (c) standard linear solid model.

The Maxwell model says that stress decays exponentially with time, which is accurate for most polymers, but it is unable to predict creep. Kelvin-Voigt model is good at modeling creep, but does not function well as to relaxation. The standard linear solid model is more accurate than the Maxwell and Kelvin-Voigt models in modeling viscoelastic responses.

Generalized models of viscoelastic materials can be built to simulate more complex behaviors, as shown in Figure 2.6.

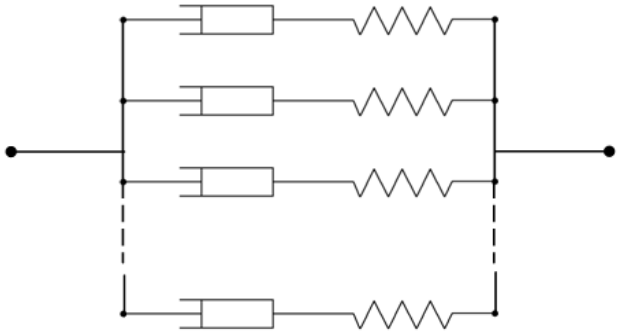

(a)

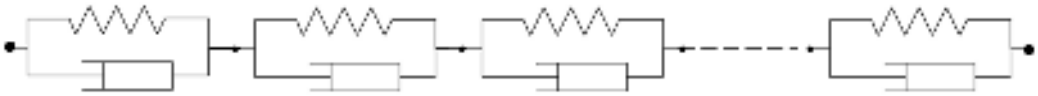

(b)

Figure 2.6 Generalized models of viscoelastic materials. (a) Generalized Kelvin model; (b) Generalized Maxwell model.

The differential equation of any generalized model of the Kelvin or Maxwell type has the form [31]

$$\sigma + p_1\dot{\sigma} + p_2\ddot{\sigma} + \ldots = q_0\varepsilon + q_1\dot{\varepsilon} + q_2\ddot{\varepsilon} + \ldots \tag{2.7}$$

or

$$\sum_{k=0}^{m} p_k \frac{d^k\sigma}{dt^k} = \sum_{k=0}^{n} q_k \frac{d^k\varepsilon}{dt^k} \tag{2.8}$$

The above equation can also be written as

$$\mathrm{P}\sigma = \mathrm{Q}\varepsilon \tag{2.9}$$

where P and Q are differential operators:

$$\mathrm{P} = \sum_{k=0}^{m} p_k \frac{d^k}{dt^k},\ \mathrm{Q} = \sum_{k=0}^{n} q_k \frac{d^k}{dt^k} \tag{2.10}$$

Equations (2.7), (2.8) and (2.9) are the constitutive equation which describes the mechanical behavior of a viscoelastic material. When the constitutive equation is subjected to

the Laplace transformation, there results the following algebraic relation between the Laplace transforms $\bar{\sigma}(s)$ and $\bar{\varepsilon}(s)$ of stress and strain

$$\sum_{k=0}^{m} p_k s^k \bar{\sigma} = \sum_{k=0}^{n} q_k s^k \bar{\varepsilon} \tag{2.11}$$

It maybe written in the forms

$$\mathsf{P}(s) \cdot \bar{\sigma} = \mathsf{Q}(s) \cdot \bar{\varepsilon} \tag{2.12}$$

in which $\mathsf{P}(s)$ and $\mathsf{Q}(s)$ are polynomials in s,

$$\mathsf{P}(s) = \sum_{0}^{m} p_k s^k \,,\ \mathsf{Q}(s) = \sum_{0}^{n} q_k s^k \tag{2.13}$$

which have the same coefficients as the differential operators P and Q.

For steady-state dynamic response to alternating load, the stress can be written as

$$\varepsilon = \varepsilon_0 e^{i\omega t} = \varepsilon_0 (\cos \omega t + i \sin \omega t) \tag{2.14}$$

When we introduce the above ε into Equation (2.8), we see that the stress must have a factor $e^{i\omega t}$, that is

$$\sigma = \sigma_0 e^{i\omega t} \tag{2.15}$$

Equation (2.8) then reads

$$\sum_{k=0}^{m} p_k \sigma_0 (i\omega)^k e^{i\omega t} = \sum_{k=0}^{n} q_k \varepsilon_0 (i\omega)^k e^{i\omega t} \tag{2.16}$$

After cancellation of $e^{i\omega t}$, this may be solved for the stress amplitude

$$\sigma_0 = \varepsilon_0 \frac{\sum q_k i^k \omega^k}{\sum p_k i^k \omega^k} = \varepsilon_0 \frac{\mathsf{Q}(i\omega)}{\mathsf{P}(i\omega)} \tag{2.17}$$

where P and Q are the polynomials introduced before. Evidently σ_0 is a complex quantity and may be written as

$$\sigma_0 = \sigma' + i\sigma'' \tag{2.18}$$

whence

$$\sigma = \sigma_0 e^{i\omega t} = (\sigma' + i\sigma'')(\cos\omega t + i\sin\omega t) \tag{2.19}$$

After separation of real and imaginary parts

$$\sigma = (\sigma'\cos\omega t - \sigma''\sin\omega t) + i(\sigma''\cos\omega t + \sigma''\sin\omega t) \tag{2.20}$$

Thus, for steady-state dynamic response to alternating load, there is a phase lag between stress and strain (Section 1.6 in reference [22] and Section 5.1 in reference [31]). For stresses and strains that are not too large, the linear viscoelastic properties under dynamic loading can be described by a frequency dependent complex modulus $E^*(i\omega)$. The linear relation is:

$$\sigma(\omega,t) = E^*(i\omega)\varepsilon(\omega,t) \tag{2.21}$$

Under periodic loading, both the stress and the strain are harmonic and $E^*(i\omega)$ is given by real and imaginary parts as

$$E^*(i\omega) = E'(\omega) + iE''(\omega) \tag{2.22}$$

$E'(\omega)$ and $E''(\omega)$ are usually called the storage modulus and loss modulus, respectively. In this research, the viscoelastic materials dissipate energy mostly through shear deformation. So, the shear modulus G^* replaces the Young's modulus E^*, which yields:

$$\tau(\omega,t) = G^*(i\omega)\gamma(\omega,t) \tag{2.23}$$

and

$$G^*(i\omega) = G'(\omega) + iG''(\omega) \tag{2.24}$$

G' and G'' are usually called shear storage modulus and shear loss modulus. The shear moduli are directly provided by the manufacturer in a nomograph [1] and then incorporated into the finite element models.

Following the above definition, the shear loss factor is:

$$\eta = \frac{G''}{G'} \tag{2.25}$$

which leads to the expression of viscoelastic shear modulus $G^* = G'(1+i\eta)$.

2.2.2. Finite Element Modeling of Viscoelastic Materials for Steady-State Analysis

One necessary condition for analytical studies of viscoelastically-damped structures is to model the viscoelastic damping material accurately. The finite element method is used to model the structure. In the MSC.Patran/Nastran 2005 r2 finite element package, viscoelastic materials are modeled using the following method.

$$[M]\{\ddot{x}(t)\} + [B]\{\dot{x}(t)\} + [K]\{x(t)\} = \{P(\omega)\}e^{i\omega t} \tag{2.26}$$

In the frequency domain,

$$[-\omega^2 M + i\omega B + K]\{u(\omega)\} = \{P(\omega)\} \tag{2.27}$$

$$[B] = [B^1] + [B^2] \tag{2.28}$$

where $[B^1]$ is the damping matrix generated through "CVISC" and "CDAMPi" Bulk Data cards (damping elements); $[B^2]$ holds the damping terms generated through direct matrix input, e.g., on the "DMIG" (Direct Matrix Input at Grid points) Bulk Data card. These would be needed to model discrete dampers, which does not apply to this research.

In frequency response analysis, the parameters “G” and “GE” on the MATi entry do not form a damping matrix. Instead, they form the following complex stiffness matrix:

$$[K] = (1+ig)[K^1] + [K^2] + i[K^4] \tag{2.29}$$

where g is the overall structural damping coefficient specified through the “PARAM” Bulk Data card. $[K^1]$ is the stiffness matrix for structural elements. This would be appropriate if all elements had the same damping properties, which is not the case here. $[K^2]$ is the stiffness

terms generated through direct matrix input, e.g., "DMIG" Bulk Data card, which is not done here. [K^4] is the element damping matrix generated by the multiplication of individual element stiffness matrices by an element damping, g_e, entered on the MATi Bulk Data card; g_e is the element structural damping coefficient ("GE" on the appropriate MATi entry).

Applying Equation (2.29) on viscoelastic elements, the stiffness matrix may be written in the form [60]:

$$[K]_V = \{[1 + g_{REF} TR(f)] + i[g + g_{REF} TI(f)]\}[K^4] \tag{2.30}$$

where the two tables $TR(f)$ and $TI(f)$ are used to represent the real and imaginary components of the shear modulus. Briefly the equations are [60]:

$$TR(f) = \frac{1}{g_{REF}}\left(\frac{G'(f)}{G_{REF}} - 1\right) \tag{2.31}$$

$$TI(f) = \frac{1}{g_{REF}}\left(\frac{G''(f)}{G_{REF}} - g\right) \tag{2.32}$$

where G_{REF} is the reference shear modulus (G on MAT1 card); g_{REF} is the reference element damping (GE on MAT1 card); g is the overall structural damping (defined by PARAM Bulk Data card). It is specified in the application manual that this formulation may be used for direct frequency response analysis (MSC/NASTRAN 2005 r2 solution 108). This method has been proved effective in the present research.

Literature on modeling the viscoelastic material properties in constrained layer damping using commercially available finite element software are rarely seen. Belknap (1991) [6] pointed out that the complex frequency-dependent shear modulus could be modeled using MSC/NASTRAN 2005 r2 by inputting two tabular functions. However, no analytical results were presented. Chang (1992) [20] used the same method to model a single degree-of-

freedom system to find the resonant frequency. They both referred to the MSC/NASTRAN 2005 r2 application manual [60].

The viscoelastic material used in this research (3M™ F9469PC) has different material properties from commonly-used elastic materials, as shown in Table 2.2. Its properties are complex, and are both frequency- and temperature-dependent. The mechanical properties are given by the manufacturer in a nomograph, as shown in Appendix A. Extracted material properties of F9469PC are plotted in Figure 2.7 and listed in Appendix A.

Table 2.2 Characteristics of viscoelastic material properties

	Temperature-dependent	Frequency-dependent	Complex
Shear modulus	X	X	X
Poisson's ratio	-	X	-
Loss factor	X	X	-

Besides the shear modulus and loss factor information, there is another important parameter: Poisson's ratio. However, in the data sheet provided by the manufacturer 3M [1], the Poisson's ratio is briefly mentioned as "approximately 0.49". Austin and Inman (2000) [4] commented that "two independent material properties are needed for an isotropic material, but historically only the shear modulus of viscoelastic materials are measured" and "authors who need a second material property (besides the shear modulus) generally guess Poisson's ratio to be between 0.3 and 0.5". Bianchini and Lesieutre (1994) [7] mentioned that "the low frequency Poisson's ratio of F9469PC is 0.49 showing behavior similar to that of an incompressible solid. At high frequency, the Poisson's ratio of F9469PC is comparable to that of stiff polymers, here 0.3" (but they used a constant, 0.49 for 10-2000 Hz anyways). So based on the above survey, the frequency-dependency of the Poisson's ratio is interpolated as shown in Figure 2.7.

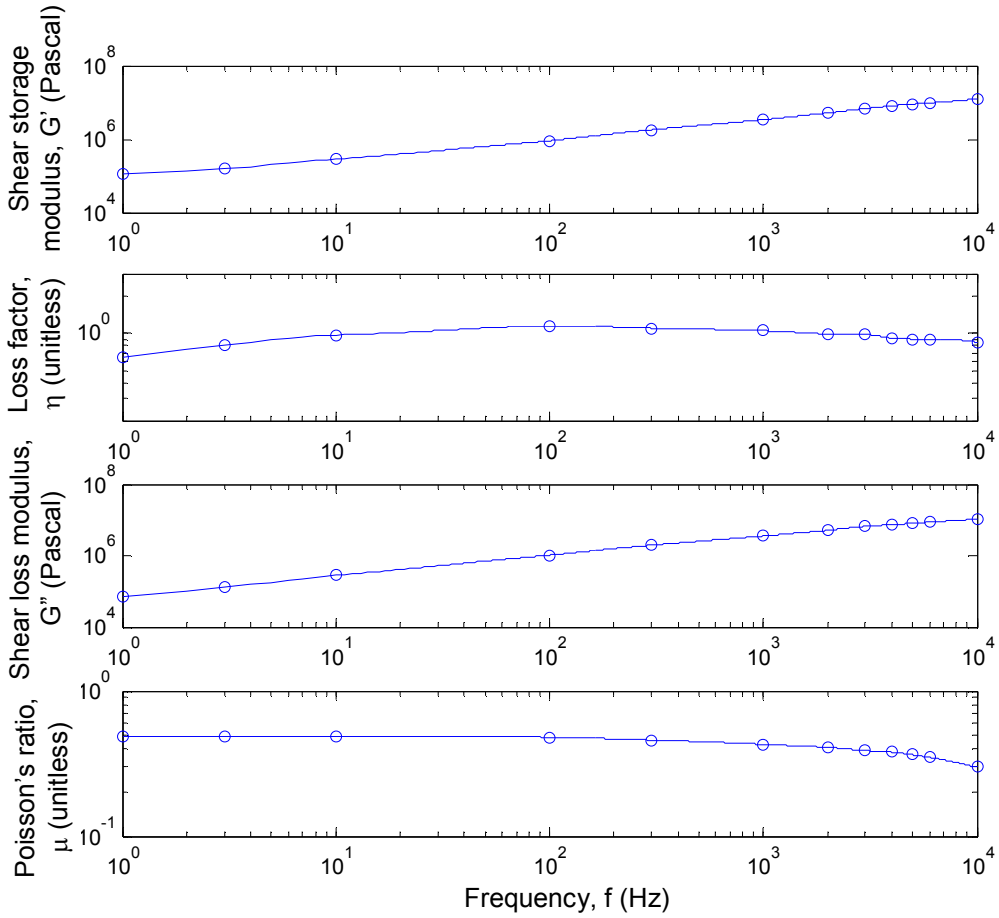

Figure 2.7 Material properties of 3M F9469PC at 20 °C used in this research extracted from manufacturer's nomograph.

2.2.3. Finite Element Modeling of Sandwich Structures with Viscoelastic Core

Composite plate models (for instance, using the "PCOMP" card in MSC/NASTRAN) cannot be used because they fail to represent the strong variations of in-plane strains through the thickness [64] [65]. Due to the fact that "the energy in the viscoelastic material is almost exclusively linked to shear deformation" [65], modeling sandwich structures with viscoelastic core requires that the shear deformation be accurately represented.

There are three commonly-used finite element models for sandwich structures with viscoelastic core, as shown in Figure 2.8. Briefly, the features of the above three models can be summarized as

1) Model (a) is relatively simple and thus is commonly-used.
2) Model (b) is the most complex one and can be used to model curved sandwich plates, because the offset plate elements in model (a) do not correctly represent the curved inside and outside layers [58].
3) Model (c) exhibits a better convergence rate than model (a), but due to the extra nodes, the computational cost increases.

Considering computational accuracy, model (c) is used in this research.

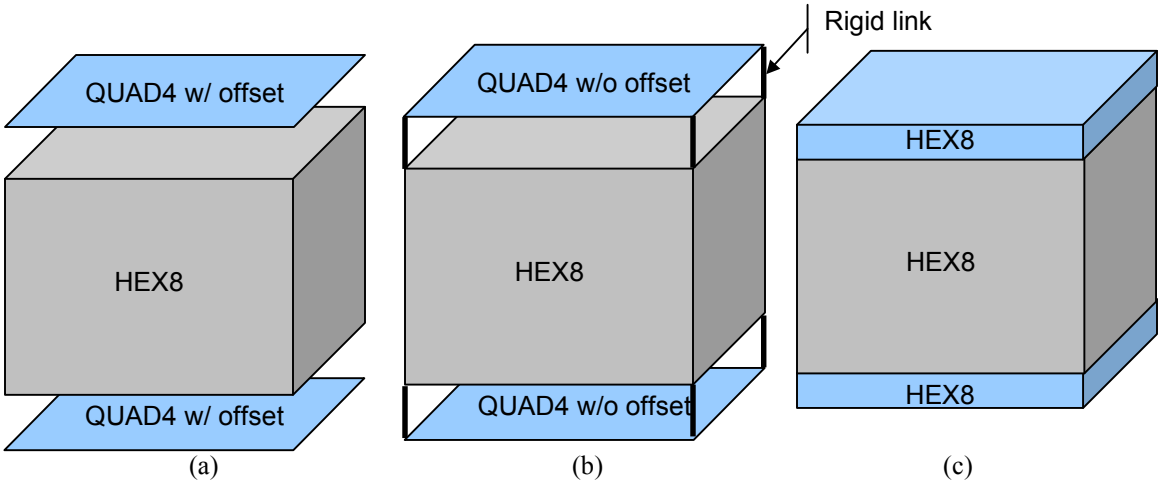

Figure 2.8 Finite element models of a sandwich structure with viscoelastic core (facesheets are in blue and viscoelastic core is in grey). (a) Plate elements with offsets of half of the plate thickness, attached to solid elements; (b) plate elements with translational degrees-of-freedom connected to solid elements by rigid links; (c) solid elements for all three layers.

One thing that needs to be avoided in finite element modeling is shear locking. Shear locking is caused by an inaccurate displacement field of linear quadrilateral or hexahedral elements. Illustrated on the left of Figure 2.9 is the real deflection shape of a bending element and on the right its linear representation. It can be seen that though the extension on the top

and the compression at the bottom are modeled, an unreal shear stress is introduced by the linear model. This excessive shear absorbs strain energy, thus the element reaches equilibrium with smaller nodal displacements because of shear locking. This representation under-predicts the bending displacements and over-predicts the stiffness. To avoid shear locking, the thickness/length ratio of solid elements should be kept above 1/5000 [42]. This requirement is satisfied in this research, with worst case as 1/100.

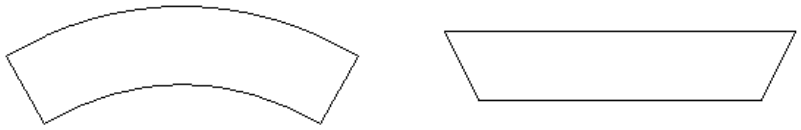

(a) (b)

Figure 2.9 Real and approximate linear representations of bending deflections. (a) Real representation; (b) linear representation.

2.2.4. Validation of Finite Element Modeling

2.2.4.1. Convergence Study

To achieve balance between accuracy and computing costs, a convergence study is performed to determine a reasonable modeling configuration. Five models of different discretization are built and compared against each other. Frequency and modal strain energy ratio results of the fiftieth natural mode is presented because it is a representative plate-bending mode and it is within the interested frequency range.

Calculations show convergence to three significant figures for both resonance frequencies and strain energy ratios as the degrees of freedom reach 38940, as shown in Figure 2.10 and Table 2.3. So, configuration 3 is chosen as the baseline model of current research.

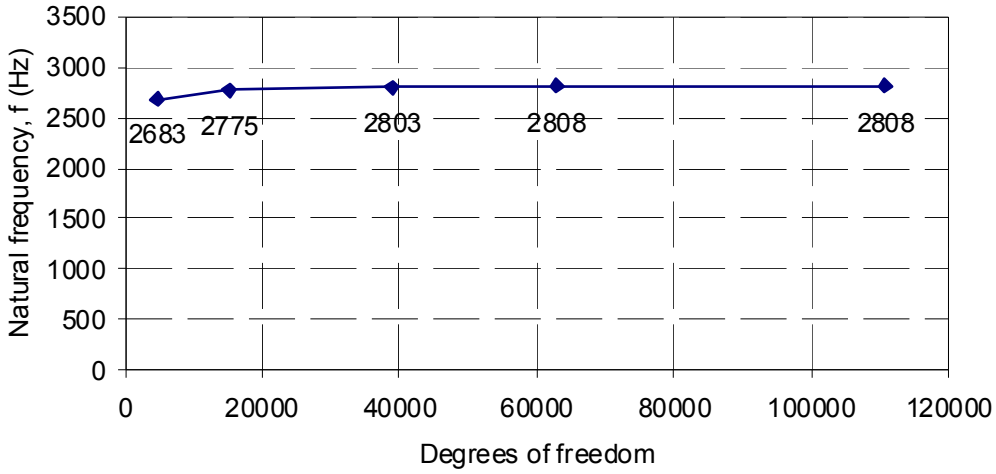

(a)

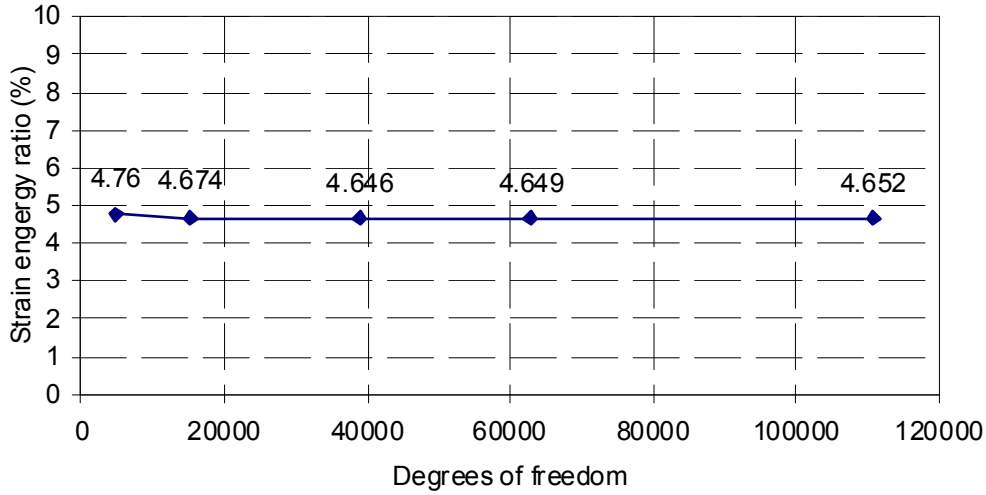

(b)

Figure 2.10 Convergence study of a partially-covered sandwich plate. (a) Natural frequencies; (b) strain energy ratios.

Table 2.3 Convergence study of in-plane discretization

Configuration	DOF	Frequency (Hz)	Strain energy ratio (%)
1	4788	2683	4.760
2	15252	2775	4.674
3	38940	2803	4.646
4	62865	2808	4.649
5	110715	2808	4.652

2.2.4.2. Through-thickness Discretization

Current references use one solid element in the thickness direction to model the layers of sandwich plates [39] [43]. But no study has been presented to prove its validity. So, three models are built and compared. Model 1, 2 and 3 respectively have one, two and four solid elements in the thickness direction for each layer.

Loss factors by the modal strain energy results are shown in Figure 2.11. It can be seen that discretization in the through-thickness direction does not appreciably affect the strain energy ratios in the viscoelastic core layer. The three discretization configurations yield almost identical results over a broad frequency range from 0 to 3000 Hz, with loss factor markers in Figure 2.11 overlapping each other at all modes. Also, the displacement, amplified about 30,000 times, is plotted in Figure 2.12. It can be seen that the displacement is almost linear through the thickness of the viscoelastic layer. Thus, the common practice of using one layer of solid elements for each sandwich component is justified.

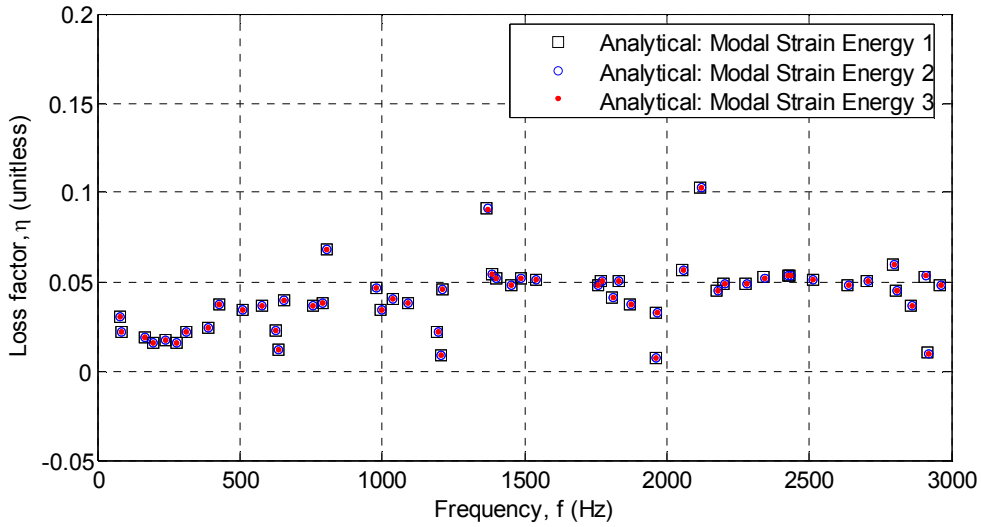

Figure 2.11 Through-thickness discretization study using the modal strain energy method (model 1: one solid element for each layer; model 2: two solid elements for each layer; model 3: four solid elements for each layer).

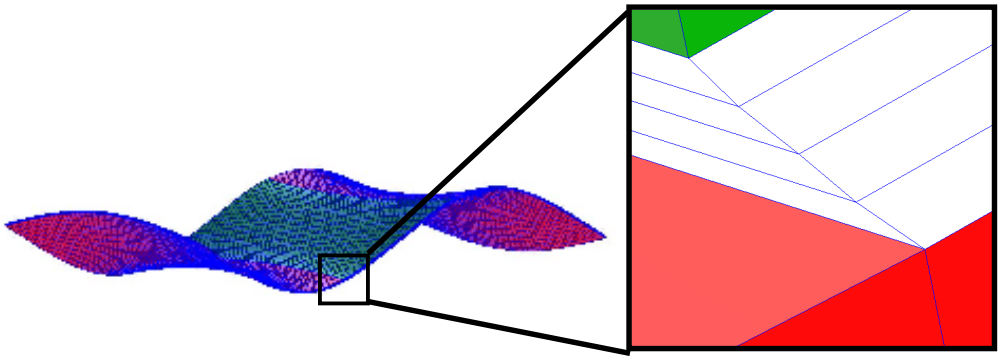

Figure 2.12 Displacement of the viscoelastic layer in relation to the displacement of the base layer and the constraining layer.

2.2.5. Comparison of Analytical Responses with Published Responses

In this section, the comparison is between our analytical results with other published results: Lu and Everstine (1980) [52]. The purpose is to verify the finite element modeling procedure in this research.

A 24.1875"×1" sandwich steel beam with viscoelastic core and free boundary conditions at two ends with is modeled. The two steel layers are modeled as QUAD4 elements and the viscoelastic layer is modeled as HEX8 elements. 4850 total degrees of freedom are used. Please see Table 2.4 for configuration details and Figure 2.13 for calculated mechanical impedance results. All mechanical properties of the materials mentioned in Table 2.4 are listed in Appendix A.

Table 2.4 Configuration of Lu and Everstine's (1980) [52]beam

	Thickness (in)	Material
Constraining layer	0.25	"Steel" modeled as low alloy steel AISI 4130
Damping layer	0.004	"Acrylic base VEM" modeled as 3M F9469PC
Base layer	0.25	"Steel" modeled as low alloy steel AISI 4130

It can be seen in Figure 2.13 that though the material properties of the steel layer and the viscoelastic layer are assumed (because they are not specified in [52]), the finite element

model predicts the impedance responses with consistency with regard to natural frequencies and magnitude of response. The discrepancy is believed to be due to modeling differences (e.g., material properties, etc.).

Thus, the modeling procedure is shown to produce minor discrepancies with regard to mobility predictions.

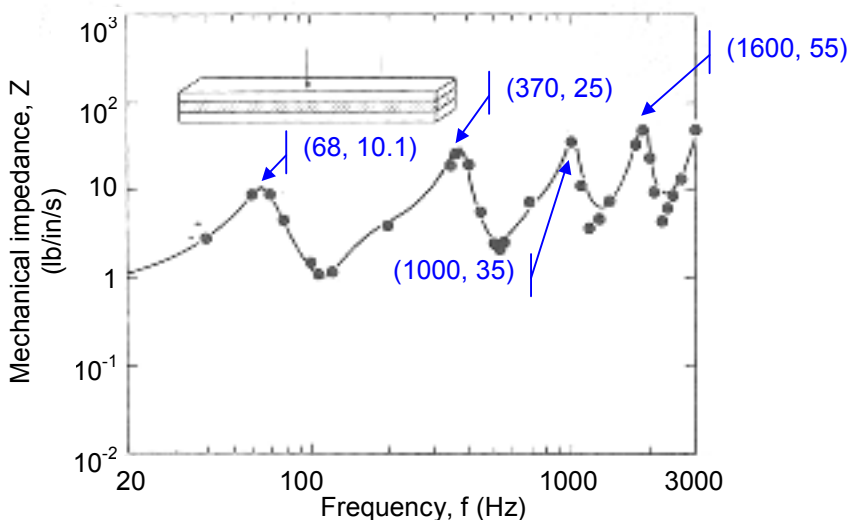

(a)

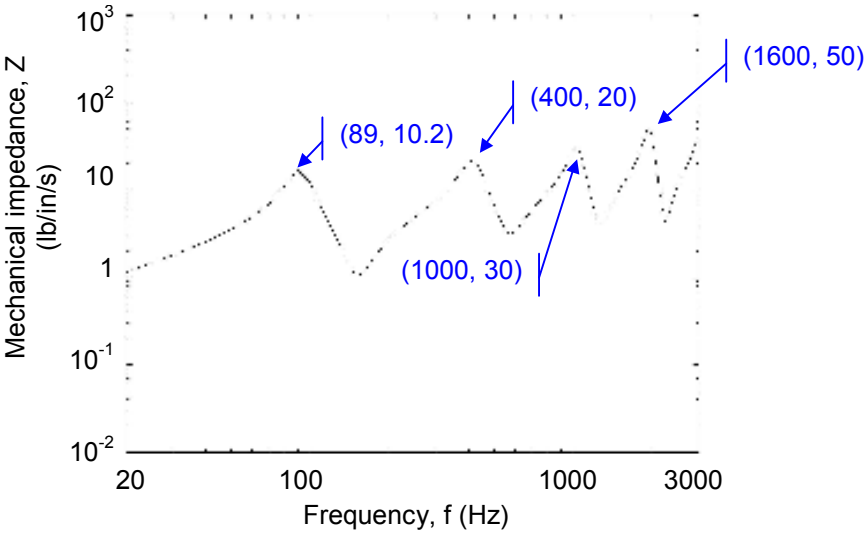

(b)

Figure 2.13 Comparison of mechanical impedance results of Lu and Everstine's (1980) [52] beam. (a) Lu and Everstine's result (Solid line: experimental results; Dots: Nastran results); (b) Present result of this research.

2.2.6. Mathematical Model of Sandwich Plates with Viscoelastic Core: Theoretical Approach Compared with Finite Element Method

In this section, the basic mathematical equations for sandwich plates with viscoelastic core are solved to obtain theoretical solutions for simply-supported boundary conditions. Mobility functions of a damped plate from theoretical solutions are compared with finite element method results.

The basic mathematical equations of vibratory bending of unsymmetrical sandwich plates are developed by means of variational methods [22]. The transverse displacement is *w*, and the in-plane displacement components are u_i, v_i, i=1, 2 and 3. The quantities μ_1 and μ_3 are the Poisson's ratios, and E_1 and E_3 are the elastic moduli of the face layers 1 and 3. *G** is the shear modulus of the core material. The symbol (′) denotes differentiation with respect to x, star (*) with respect to y and the dot (˙) with respect to time t. The density of the composite plate is $\rho=\rho_1 h_1+\rho_2 h_2+\rho_3 h_3$ and the effective thickness is $d=h_2+(h_1+h_3)/2$. The thickness of each layer is represented by h_1, h_2 and h_3 respectively.

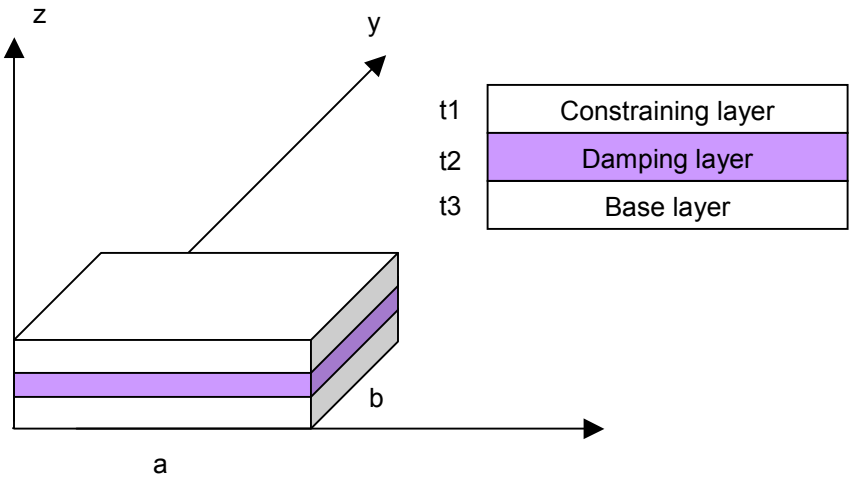

(a) (b)

Figure 2.14 Geometry of the sandwich plate with viscoelastic core. (a) Sign convention; (b) thicknesses of the 3 layers.

The maximum strain energy of the sandwich plate, *SE*, is

$$SE = \iint \Bigg[\frac{E_1 t_1}{2(1-\mu_1^2)} \Big\{ u_1'^2 + \mu_1 u_1' v_1^* + v_1^{*2} + \mu_1 v_1^* u_1' + \frac{(1-\mu_1)}{2} \Big(u_1^{*2} + v_1'^2 + 2u_1^* v_1' \Big) \Big\}$$

$$+ \frac{E_3 t_3}{2(1-\mu_3^2)} \Big\{ u_3'^2 + \mu_1 u_3' v_3^* + v_3^{*2} + \mu_3 v_3^* u_3' + \frac{(1-\mu_3)}{2} \Big(u_3^{*2} + v_3'^2 + 2u_3^* v_3' \Big) \Big\}$$

$$+ \frac{E_1 t_1^{\,3}}{24(1-\mu_1^2)} \Big\{ w''^2 + 2\mu_1 w'' w^{**} + w^{**2} + 2(1-\mu_1) w'^{*2} \Big\} \tag{2.33}$$

$$+ \frac{E_3 t_3^{\,3}}{24(1-\mu_3^2)} \Big\{ w''^2 + 2\mu_3 w'' w^{**} + w^{**2} + 2(1-\mu_3) w'^{*2} \Big\}$$

$$+ \frac{G^* t_2}{2} \left\{ \begin{array}{l} \left(\frac{u_1 - u_3}{t_2} \right)^2 + \left(\frac{v_1 - v_3}{t_2} \right)^2 + (w'^2 + w^{*2}) \left(\frac{d}{t_2} \right)^2 \\ -\frac{2d}{t_2} \left(w' \frac{u_1 - u_3}{t_2} + w^* \frac{v_1 - v_3}{t_2} \right) \end{array} \right\} \Bigg] dxdy$$

Assuming the plate is subjected to a normal load of intensity q, the potential energy, *PE*, is given by

$$PE = -\iint qw dxdy \tag{2.34}$$

The maximum kinetic energy, *KE*, of the plate is

$$KE = \tfrac{1}{2} \iint \dot{w}^2 dxdy$$

$$+ \tfrac{1}{2} \iint \Bigg[\rho_1 t_1 \dot{u}_1^{\,2} + \rho_3 t_3 \dot{u}_3^{\,2} + \dot{w}'^2 \frac{\rho_1 t_1^3 + \rho_3 t_3^3}{12} + \rho_1 t_1 \dot{v}_1^2 + \rho_3 t_3 \dot{v}_3^2 + \dot{w}^{*2} \frac{\rho_1 t_1^3 + \rho_3 t_3^3}{12}$$

$$+ \rho_1 t_2 \left\{ \left(\frac{\dot{u}_1 + \dot{u}_3}{2} + \dot{w}' \varepsilon_1 \right)^2 + \left(\frac{\dot{v}_1 + \dot{v}_3}{2} + \dot{w}^* \varepsilon_1 \right)^2 \right\} \tag{2.35}$$

$$+ \frac{p_2 t_2}{2} \Big\{ \big(\dot{u}_1 - u_3 - \dot{w}' \varepsilon_2 \big)^2 + \big(\dot{v}_1 - \dot{v}_3 - \dot{w}^* \varepsilon_2 \big)^2 \Big\} \Bigg] dxdy$$

According to Hamilton's principle, the stationary value of $\bar{\Phi}$ =*KE-SE-PE* is equivalent to the equilibrium state, where

$$\delta\bar{\Phi} = \int_{t_1}^{t_2} \left(\delta KE - \delta SE - \delta PE\right) dt \tag{2.36}$$

Performing the variation term by term, the following equation of motion are obtained for arbitrary virtual displacements

$$\gamma_1\left\{u'' + (1/2)(1+\mu_1)v_1'^{*} + (1/2)(1-\mu_1)u_1^{**}\right\} + \gamma_2\left\{\left(c/t_2^2\right)w' - \left(u_1 - u_3\right)/t_2^2\right\}$$

$$-\rho_1 t_1 \ddot{u}_1 - \rho_2 t_2\left(\ddot{u}_1/3 + \ddot{u}_3/6 + \ddot{w}'\varepsilon_3\right) = 0$$

$$\gamma_1\left\{v_1^{**} + (1/2)(1+\mu_1)u_1'^{*} + (1/2)(1-\mu_1)v_1''\right\} + \gamma_2\left\{\left(c/t_2^2\right)w^{*} - \left(v_1 - v_3\right)/t_2^2\right\}$$

$$-\rho_1 t_1 \ddot{v}_1 - \rho_2 t_2\left(\ddot{v}_1/3 + \ddot{v}_3/6 + \ddot{w}^{*}\varepsilon_3\right) = 0$$

$$\gamma_3\left\{u_3'' + (1/2)(1+\mu_3)v_3'^{*} + (1/2)(1-\mu_3)u_3^{**}\right\} - \gamma_2\left\{\left(c/t_2^2\right)w' - \left(u_1 - u_3\right)/t_2^2\right\}$$

$$-\rho_3 t_3 \ddot{u}_3 - \rho_2 t_2\left(\ddot{u}_1/6 + \ddot{u}_3/3 + \ddot{w}'\varepsilon_4\right) = 0$$

$$\gamma_3\left\{v_3^{**} + (1/2)(1+\mu_3)u_3'^{*} + (1/2)(1-\mu_3)v_3''\right\} - \gamma_2\left\{\left(c/t_2^2\right)w^{*} - \left(v_1 - v_3\right)/t_2^2\right\}$$

$$-\rho_3 t_3 \ddot{v}_3 - \rho_2 t_2\left(\ddot{v}_1/6 + \ddot{v}_3/3 + \ddot{w}^{*}\varepsilon_4\right) = 0$$

$$\left(D_1 + D_3\right)\nabla^4 w - \gamma_2\left(c/t_2^2\right)\left\{c\left(w'' + w^{**}\right) - u_1'' + u_3'' - v_1^{*} + v_3^{*}\right\}$$

$$-(1/12)\left(\rho_1 t_1^3 + \rho_3 t_3^3\right)\left(\ddot{w}'' + \ddot{w}^{**}\right)$$

$$-\rho_2 t_2\left\{\varepsilon_3\left(\ddot{u}_1' + \ddot{v}_1^{*}\right) + \varepsilon_4\left(\ddot{u}_3' + \ddot{v}_3^{*}\right) + \left(\varepsilon_1^2 + \varepsilon_2^2/12\right)\left(\ddot{w}'' + \ddot{w}^{**}\right)\right\}$$

$$+\rho\ddot{w} + Q(x,y)\,g(t) = 0$$

$$\nabla^4 w = \frac{\partial^4 w}{\partial x^4} + 2\frac{\partial^4 w}{\partial x^2 \partial y^2} + \frac{\partial^4 w}{\partial y^4} \tag{2.37}$$

$$\varepsilon_3 = (1/12)(t_3 - 2t_1)$$

$$c = (1/2)(2t_2 + t_1 + t_3),\ \gamma = E_i t_i / (1 - \mu_i^2),\ i = 1, 3,\ \gamma_2 = G_2 t_2$$

$$\varepsilon_4 = (1/12)(2t_3 - t_1),\ \varepsilon_1 = (t_3 - t_1)/4,\ \varepsilon_2 = (t_1 + t_3)/2$$

$$D_i = \frac{E_i t_i^3}{12(1-\mu_i^2)},\ \mathrm{i} = 1,3,\ \rho = \rho_1 t_1 + \rho_2 t_2 + \rho_3 t_3 \tag{2.38}$$

In deriving the equations of motion, the following assumptions are made:

1) A plane transverse to the middle plane before bending remains plane and perpendicular to the middle plane after bending
2) Transverse displacement at a section does not vary along thickness.
3) All displacements are small.
4) There is perfect continuity at the interfaces and no slip occurs.
5) The extension effect in the core is ignored and stresses in the core are considered negligible.

For the viscoelastic core, the complex moduli are

$$G_2^* = G_2(1 + i\eta_2),\ E_2^* = E_2(1 + i\eta_2) \tag{2.39}$$

For simply supported boundary conditions, it is assumed that

$$u_1 = \sum_{m=1}^{\infty}\sum_{n=1}^{\infty} U_{1mn} \cos\frac{m\pi x}{a} \sin\frac{n\pi y}{b} \sin\omega t$$

$$u_3 = \sum_{m=1}^{\infty}\sum_{n=1}^{\infty} U_{3mn} \cos\frac{m\pi x}{a} \sin\frac{n\pi y}{b} \sin\omega t$$

$$v_1 = \sum_{m=1}^{\infty}\sum_{n=1}^{\infty} V_{1mn} \sin\frac{m\pi x}{a} \cos\frac{n\pi y}{b} \sin\omega t \tag{2.40}$$

$$v_3 = \sum_{m=1}^{\infty}\sum_{n=1}^{\infty} V_{3mn} \sin\frac{m\pi x}{a} \cos\frac{n\pi y}{b} \sin\omega t$$

$$w = \sum_{m=1}^{\infty}\sum_{n=1}^{\infty} W_{mn} \sin\frac{m\pi x}{a}\sin\frac{n\pi y}{b}\sin\omega t$$

The loading function is assumed to be

$$Q(x,y)g(t) = \sum_{m=1}^{\infty}\sum_{n=1}^{\infty} Q_{mn} \sin\frac{m\pi x}{a}\sin\frac{n\pi y}{b}\sin\omega t \tag{2.41}$$

For a concentrated load $Q(x,y)$ at the point of application x_0, y_0 $(x_0 = a/2, y_0 = b/2)$,

$$Q(x,y) = \sum_{m=1}^{\infty}\sum_{n=1}^{\infty} \frac{4F_0}{ab} \sin\frac{m\pi}{a}\sin\frac{n\pi}{2}\sin\frac{n\pi y}{b} \tag{2.42}$$

where F_0 is the amplitude. Following the normal procedure, the Fourier components of the transverse displacement W_{mn} can be obtained as follows:

$$\begin{bmatrix} d_2^R + id_2^I & d_4 & -d_3^R - id_3^I & 0 & -d_1^R - id_1^I \\ d_4 & e_2^R + ie_2^I & 0 & -d_3^R - id_3^I & -e_1^R - ie_1^I \\ -d_3^R - id_3^I & 0 & f_2^R + if_2^I & f_3^R & -f_1^R - if_1^I \\ 0 & -d_3^R - id_3^I & f_3^R & g_2^R + ig_2^I & -g_1^R - ig_1^I \\ -h_2^R & -h_2^R - ih_c^I & -h_3^R - ih_3^I & -h_5^R - ih_5^I & h_1^R + ih_1^I \end{bmatrix} \begin{bmatrix} U_{1mn} \\ V_{1mn} \\ U_{3mn} \\ V_{3mn} \\ W_{mn} \end{bmatrix} = \begin{bmatrix} 0 \\ 0 \\ 0 \\ 0 \\ Q_{mn} \end{bmatrix} \tag{2.43}$$

where

$$Q_{mn} = \frac{4F_0}{ab}\sin\frac{m\pi}{2}\sin\frac{n\pi}{2}\Big/\left(E_3\frac{m\pi}{a}\right)$$

$$d_1^I = \frac{1}{2t_2}(2t_2 + t_1 + t_3)\frac{G_2}{E_3}\eta_2 = \delta_{23}\left(1 + \frac{1+\theta_{13}}{2\theta_{23}}\right)\eta_2$$

$$d_1^R = \frac{1}{2t_2}(2t_2 + t_1 + t_1)\frac{G_2}{E_3} + \rho_2 t_2\omega^2\frac{1}{E_3}\frac{t_3 - 2t_1}{12} = \delta_{23}\left(1 + \frac{1+\theta_{13}}{2\theta_{23}}\right) + \frac{\lambda\gamma_{23}}{12}\frac{\theta_{23}}{\gamma_{13}}(1 - 2\theta_{13})$$

$$d_4 = \frac{E_1 t1}{E_3(1-\nu_1)}\frac{1}{2}\left(\frac{n\pi}{b}\right) = \frac{a_{13}\theta_{13}\beta n\gamma}{2(1-\psi_{13}\nu_3)}$$

$$d_2^I = \frac{G_2 a}{E_3 t_2 m\pi}\eta_2 = \frac{\delta_{23}}{\theta_{23}\beta m}\eta_2$$

$$d_2^R = \frac{E_1 t_1}{E_3\left(1-\mu_1^2\right)}\frac{m\pi}{a} + \frac{E_1 t_1}{E_3\left(1+\mu_1\right)}\frac{1}{2}\frac{\left(n^2\pi^2/b^2\right)}{\left(m\pi/a\right)} - \frac{\rho_1 t_1 \omega^2}{E_3\left(m\pi/a\right)} - \frac{\rho_2 t_2 \omega^2/3}{E_3\left(m\pi/a\right)}$$

$$+\frac{G_2}{E_3 t_2\left(m\pi/a\right)} = \frac{a_{13}\theta_{13}}{1-\nu_1^2}\left\{m\beta + \frac{1-\nu_1}{2}\gamma^2\beta^2\frac{n^2}{\beta m}\right\} + \frac{\delta_{23}}{\theta_{23}\beta m} - \frac{\lambda}{\beta m}\theta_{13} - \frac{\lambda}{\beta m}\frac{\gamma_{23}}{\gamma_{13}}\frac{1}{3}\theta_{23}$$

$$d_3^I = \frac{G_2}{E_3}\frac{1}{t_2}\frac{a}{m\pi}\eta_2 = d_2^I,$$

$$d_3^R = \frac{G_2}{E_3}\frac{1}{t_2}\frac{a}{m\pi} + \frac{\rho_2 t_2 \omega^2 a}{6E_3\left(m\pi\right)} = \frac{1}{\beta m}\left(\frac{\delta_{23}}{\theta_{23}} + \lambda\frac{\gamma_{23}}{\gamma_{13}}\frac{\theta_{23}}{6}\right),$$

$$e_1^I = \frac{G_2}{E_3}\frac{c}{t_2}\frac{n\pi/b}{m\pi/a}\eta_2 = \frac{n}{m}\gamma d_1^I$$

$$e_1^R = \frac{G_2}{E_3}\frac{c}{t_2}\frac{n\pi/b}{m\pi/a} + \frac{\rho_2 t_2 \omega^2}{E_3\left(m\pi/a\right)}\frac{n\pi/b}{12}\frac{t_3-2t_1}{12} = \frac{n}{m}\gamma d_1^R$$

$$e_2^I = \frac{G_2\eta_2}{E_3 t_2\left(m\pi/a\right)} = d_2^I$$

$$e_2^R = \frac{\alpha_{13}\theta_{13}}{1-\psi_{13}^2\nu_3^2}\left\{\frac{n^2}{m}\gamma^2\beta + \frac{1}{2}\left(1-\psi_{13}\nu_3\right)\beta m\right\} + \frac{\delta_{23}}{\theta_{23}\beta m} - \frac{\lambda}{\beta m}\left(\theta_{13} + \frac{\gamma_{23}}{\gamma_{13}}\frac{\theta_{23}}{3}\right)$$

$$f_1^I = -\frac{G_2}{E_3 t_2}\frac{1}{2}\left(2t_2 + t_1 + t_3\right)\eta_2 = -d_1^I$$

$$f_1^R = -\frac{G_2}{E_3 t_2}\frac{1}{2}\left(2t_2 + t_1 + t_3\right) + \frac{\rho_2 t_2 \omega^2}{E_3}\frac{1}{12}\left(2t_3 - t_1\right) = \frac{\lambda\gamma_{23}}{\gamma_{13}}\frac{\theta_{23}}{12}\left(2-\theta_{13}\right) - \delta_{23}\left(1 + \frac{1+\theta_{13}}{2\theta_{23}}\right)$$

$$f_2^I = \frac{G_2\eta_2}{E_3 t_2\, m\pi/a} = d_3^I = d_2^I$$

$$f_2^R = \frac{t_3}{1-\nu_3^2}\left(\frac{m\pi}{a}\right) + \frac{t_3}{1-\nu_3^2}\frac{1-\nu_3}{2}\frac{n^2\pi^2}{b^2}\Bigg/\left(\frac{m\pi}{a}\right) + \frac{G_2}{E_3 t_2\left(m\pi/a\right)}$$

$$-\frac{\rho_3 t_3 \omega^2}{E_3\left(m\pi/a\right)} - \frac{1}{3}\frac{\rho_2 t_2 \omega^2}{E_3\left(m\pi/a\right)} = \frac{1}{1-\mu_3^2}\left(m\beta + \frac{1-\mu_3}{2}\gamma\beta\frac{n^2}{m}\right) + \frac{\delta_{23}}{\theta_{23}\beta m} - \frac{\lambda}{\beta m}\left(\frac{1}{\gamma_{13}} + \frac{\gamma_{23}}{\gamma_{12}}\frac{\theta_{23}}{3}\right)$$

$$g_1^I = -\frac{G_2}{E_3 t_2}\left(\frac{n\pi}{b}\right)\Big/\left(\frac{m\pi}{a}\right)\frac{1}{2}\left(2t_2 + t_1 + t_3\right)\eta_2 = \frac{n}{m}\gamma f_1^I = -\frac{n}{m}\gamma d_1^I$$

$$g_1^R = -\frac{G_2}{E_3 t_2}\left(\frac{n\pi}{b}\right)\Big/\left(\frac{m\pi}{a}\right)\frac{1}{2}\left(2t_2 + t_1 + t_3\right) + \frac{\rho_2 t_2 \omega^2}{E_3\, m\pi/a}\frac{n\pi}{b}\frac{2t_3 - 1}{12} = \frac{n}{m}\gamma f_1^R$$

$$g_2^I = d_2^I$$

$$g_2^R = \frac{1}{1-\mu_3^2}\left(\frac{n^2}{m}\beta\gamma^2 + \frac{1-\mu_3}{2}m\beta\right) + \frac{\delta_{23}}{\theta_{23}\beta m} - \frac{\lambda}{\gamma_{13}\beta m} - \frac{\lambda}{3}\frac{\gamma_{23}}{\gamma_{13}}\frac{\theta_{23}}{\beta m}$$

$$h_2^I = \frac{G_2}{E_3 t_2}\frac{1}{2}\left(2t_2 + t_1 + t_3\right)\eta_2 = d_1^I$$

$$h_2^R = \frac{G_2}{E_3 t_2}\frac{1}{2}\left(2t_2 + t_1 + t_3\right) + \frac{\rho_2 t_2 \omega^2}{E_3}\frac{1}{12}\left(t_3 - 2t_1\right) = d_1^R$$

$$h_4^R = \frac{G_2}{E_3 t_2}\frac{1}{2}\left(2t_2 + t_1 + t_3\right)\left(\frac{n\pi}{b}\Big/\frac{m\pi}{a}\right) + \frac{\rho_2 t_2 \omega^2}{E_3\, m\pi/a}\frac{n\pi}{b}\frac{t_3 - 2t_1}{12} = e_1^R$$

$$h_4^I = \frac{G_2}{E_3 t_2}\frac{1}{2}\left(2t_2 + t_1 + t_3\right)\left(\frac{n\pi}{b}\Big/\frac{m\pi}{a}\right)\eta_2 = e_1^I$$

$$h_3^I = -\frac{G_2}{E_3 t_2}c\eta_2 = f_1^I = -d_1^I$$

$$h_3^R = -\frac{G_2}{E_3 t_2}c + \frac{\rho_2 t_2}{E_3}\omega^2\frac{2t_3 - t_1}{12} = f_1^R,$$

$$h_5^I = -\frac{G_2}{E_3 t_2}c\eta_2\left(\frac{n\pi}{b}\Big/\frac{m\pi}{a}\right) = g_1^I$$

$$h_5^R = -\frac{G_2}{E_3 t_2}c\left(\frac{n\pi}{b}\Big/\frac{m\pi}{a}\right) + \frac{\rho_2 t_2 \omega^2}{E_3 m\pi / a}\left(\frac{n\pi}{b}\right)\frac{2t_3 - t_1}{12} = g_1^R$$

$$h_5^I = m\beta\left(1 + \frac{n^2}{m^2}\gamma^2\right)\left\{1 + \frac{1+\theta_{13}}{2\theta_{23}}\right\}^2 \delta_{23}\eta_2\theta_{23}$$

$$h_1^R = m^3\beta^3\left[\left\{\frac{\alpha_{13}\theta_{13}^3}{12\left(1-\psi_{13}\mu_3^2\right)}\right\}\left\{1+2\gamma^2\frac{n^2}{m^2}+\frac{n^4}{m^4}\gamma^4\right\}+\frac{\theta_{23}}{\beta^2 m^2}\left(1+\gamma^2\frac{n^2}{m^2}\right)\left(1+\frac{1+\theta_{13}}{2\theta_{23}}\right)^2\delta_{23}\right.$$

$$\left.-\lambda\left[\frac{m\beta}{12}\left(1+\frac{n^2\gamma^2}{m^2}\right)\left\{\theta_{13}^2+\frac{1}{\gamma_{13}}+\frac{\gamma_{23}}{\gamma_{13}}\theta_{23}\left(1+\theta_{13}^2-\theta_{13}\right)\right\}+\frac{1}{\beta m}\left(\theta_{13}+\frac{\gamma_{23}}{\gamma_{13}}\theta_{23}+\frac{1}{\gamma_{13}}\right)\right.\right. \quad (2.44)$$

Also

$$\lambda = \rho_1\omega^2 t_3^2/E_3$$

$$\psi_{13} = \mu_1/\mu_3$$

$$\theta_{13} = t_1/t_3$$

$$\theta_{23} = t_2/t_3$$

$$\gamma_{13} = \rho_1/\rho_3$$

$$\alpha_{13} = E_1/E_3$$

$$\beta = \pi t_3/a$$

$$\gamma = a/b$$

$$\delta_{23} = G_2/E_3 \quad (2.45)$$

A damped sandwich steel plate is used as an example, as shown in Figure 2.15. Theoretical solutions as driving point mobilities are obtained from the procedure described above. Twenty five expansion terms are used to calculate the displacements. A finite element model is built and MSC/Nastran 2005 r2 direct frequency response solution 108 is used to compute mobilities at the driving point. The dimensions of the simply-supported sandwich plate are 14 in×14 in. HEX8 elements are used for all three layers. Materials and thicknesses are listed in Table 2.5. Please see Appendix A for detailed mechanical properties defined in the finite element model.

Table 2.5 Description of the steel sandwich plate with viscoelastic core for theoretical and finite element method comparison

	Material	Thickness (in)
Base layer	Steel AISI 4130	0.125
Damping layer	3M F9469PC at 20°C	0.006
Constraining layer	Steel AISI 4130	0.125

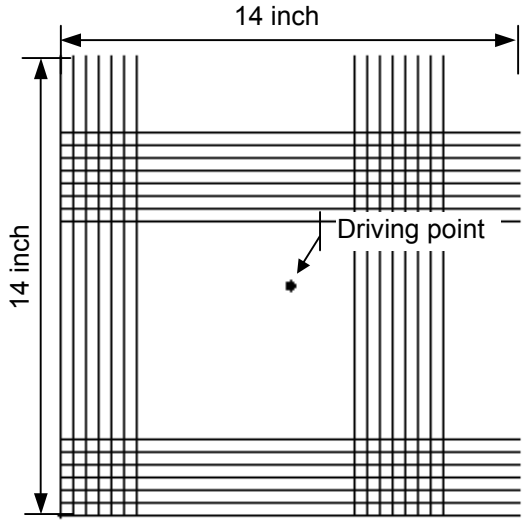

Figure 2.15 Finite element model of the steel sandwich plate with viscoelastic core.

Mobility functions at the driving point are chosen to be compared because they help represent the input power in the analytical power input method, which a new analytical damping estimation procedure introduced in a later section (Section 2.2.7) uses. Mobility functions obtained from both the theoretical equations and finite element model are compared in Figure 2.16. General agreement is noted on modal frequencies and mobility magnitudes, with discrepancy diminishing with frequency. As discussed later, damping estimation at low frequency is systemically problematic. Differences of the two results are believed to be that in the finite element model only one layer of nodes can be defined as simply-supported. But there are four layers of nodes for this sandwiched plate modeled with three layers of HEX8 solid elements. Choosing only one layer of the nodes in the finite element model does not strictly agree with the simply-supported boundary condition as defined in the theoretical equations. [However, free boundary conditions are used for all later examples in this

research, which avoids the above-mentioned boundary conditions discrepancy.] Of course, this boundary condition discrepancy is more of a factor for the fundamental mode which has only one half sine wave in the mode shape.

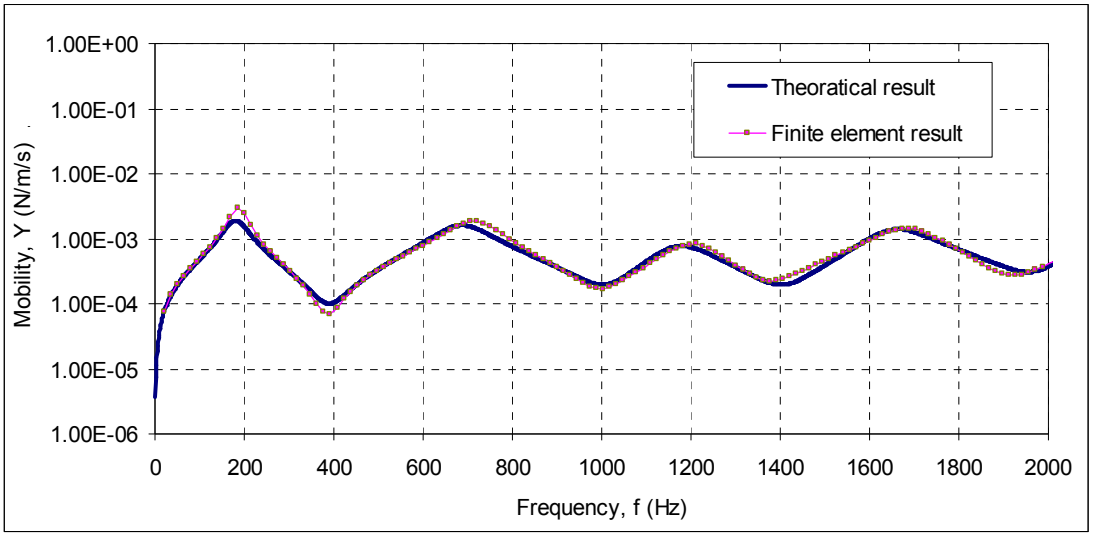

Figure 2.16 Comparison of theoratical results and finite element results of the steel sandwich plate with viscoelastic core.

2.2.7. Analytical Power Input Method

The analytical estimation of loss factors is different from the experimental estimation in that the finite element method can directly calculate the total energy E_{Tot}. Instead of replacing it with twice the average kinetic energy, E_K, the total energy E_{Tot} is calculated directly in a direct frequency response solution (MSC/NASTRAN solution 108) as a summation of the average kinetic energy, E_K and the average strain energy, E_S. Then if the dissipated power P_D can be determined, it makes up a new procedure to estimate damping.

The input power takes an alternative form as [11] [27]

$$P_D = P_I = \overline{F_f(t) \cdot V_f(t)} = \overline{F_f{}^2(t)}\,\mathrm{Re}\left[Y_{ff}(\omega)\right] = \frac{1}{2}\left|F_f(\omega)\right|^2 \mathrm{Re}\left[Y_{ff}(\omega)\right] \qquad (2.46)$$

where $F_f(\omega)$ is the Fourier transform of $F_f(t)$. In addition, the driving point mobility $Y_{ff}(\omega)$ can be calculated in the finite element method too. Thus, the loss factor can be written as

$$\eta = \frac{\frac{1}{2}\left|F_f(\omega)\right|^2 \mathrm{Re}\left[Y_{ff}(\omega)\right]}{\omega\left(E_S + E_K\right)} \tag{2.47}$$

So from the above equation, a new procedure of estimating loss factors is proposed [49]. Moreover, the frequency-dependency of the viscoelastic material is taken into account by the method described in Section 2.2.1. Examples of loss factor estimation of different damping configurations are included in later sections.

2.2.8. Validation of Analytical Power Input Method

To check the validity of the new analytical procedure, a test finite element model is built and the loss factor is computed. A rectangular plate under a point excitation at the center is given dimensions, material properties and boundary conditions consistent with structural panels found in passenger enclosures, with a constant loss factor as 0.1. The plate is modeled as a 0.36×0.24 m, aluminum alloy 2024-T3 plate (See Appendix A for detailed definition of material properties in the finite element model.) with free boundary conditions. QUAD4 elements are used with total degrees of freedom as 12505. Then MSC/NASTRAN 2005 r2 direct frequency response solution 108 is computed to obtain the mobility function at the driving point, the average strain energy, and the average kinetic energy of the system at each excitation frequency. Then Equation (2.47) is applied to estimate loss factors. The results are shown in Figure 2.17.

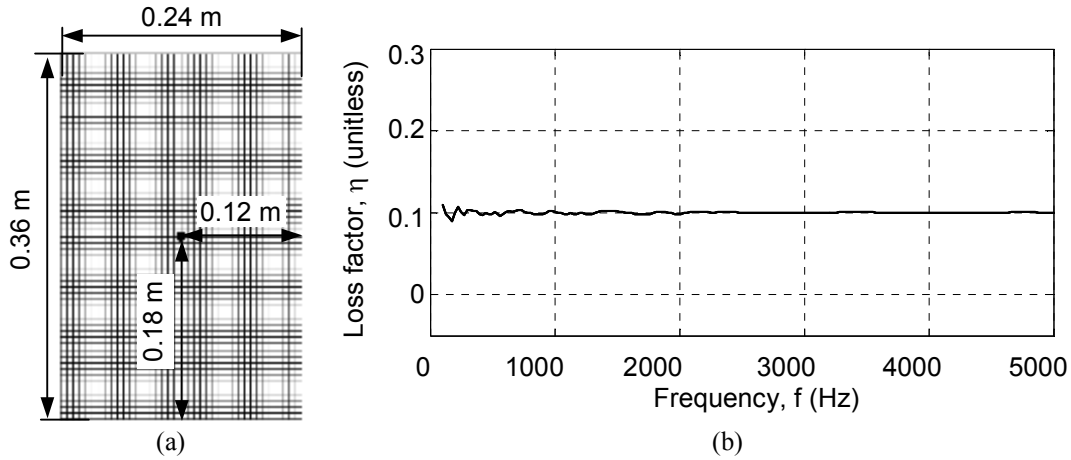

Figure 2.17 Validation of the analytical power input method. (a) The finite element model of the plate with the driving point defined; (b) The calculated loss factor of the plate.

It can be seen from the result that the new analytical procedure estimates the loss factor of this plate as 0.1 with only small discrepancies in the low modal density frequency range. So this new procedure faithfully evaluates the damping characteristics of the plate. Starting from this point, the new method is applied for further loss factor estimation of more complex structures.

2.3. Results and Discussion

In this section, results of two aluminum plates with constrained layer damping (partial coverage and full coverage) and two composite honeycomb sandwich beams with stand-off constrained layer damping (aluminum stand-off and Plexiglas stand-off) are presented and discussed. All material properties used in the finite element models are listed in Appendix A.

2.3.1. Aluminum Plate with Partial Coverage Constrained Layer Damping

The aluminum plate with a partial constrained layer damping treatment is as shown in Table 2.6. The partial damping treatment is placed in the central portion of the plate, as

shown in Figure 2.18. The driving point is placed at the center of undamped region. The plate has free boundary conditions on all edges since it is suspended by a light elastic spring.

The finite element model of the plate has 12,980 nodes. All three layers are modeled as HEX8 solid elements. There are 38,940 total degrees of freedom. All material properties defined in the finite element model can be found in Appendix A. The finite element model has free boundary conditions on all edges.

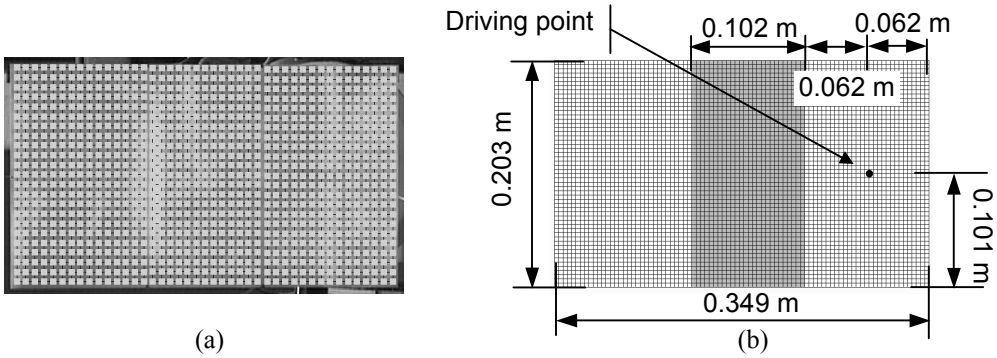

Figure 2.18 Plate with partial coverage constrained layer damping. (a) The plate as a test article with scanning points defined; (b) the plate as a finite element model with the excitation point illustrated.

Table 2.6 Description of the plate with partial coverage constrained layer damping

	Material	Dimensions (m)	Mass (g)
Base layer	CLAD 2024-T3	0.349×0.2029×0.0016002	313.7
Damping layer	3M F9469PC at 20°C	0.2029×0.10186×0.000127	2.6
Constraining sheet	CLAD 2024-T3	0.2029×0.10186×0.000508	29.1

2.4.1.1. Comparison of Experimental Methods

Results from the experimental power input method are compared with commonly-used experimental methods, namely, the free decay method and the modal curve-fitting method. In the power input method, the plate is divided into 989 portions to minimize the discretization error (the description of the convergence study is skipped for the purpose of brevity). Since this plate has a non-uniform damping treatment, the mass m_i is not constant over the plate. In

the free decay method, a speaker is used as the excitation. In the modal curve-fitting method, STAR modal analysis software is used.

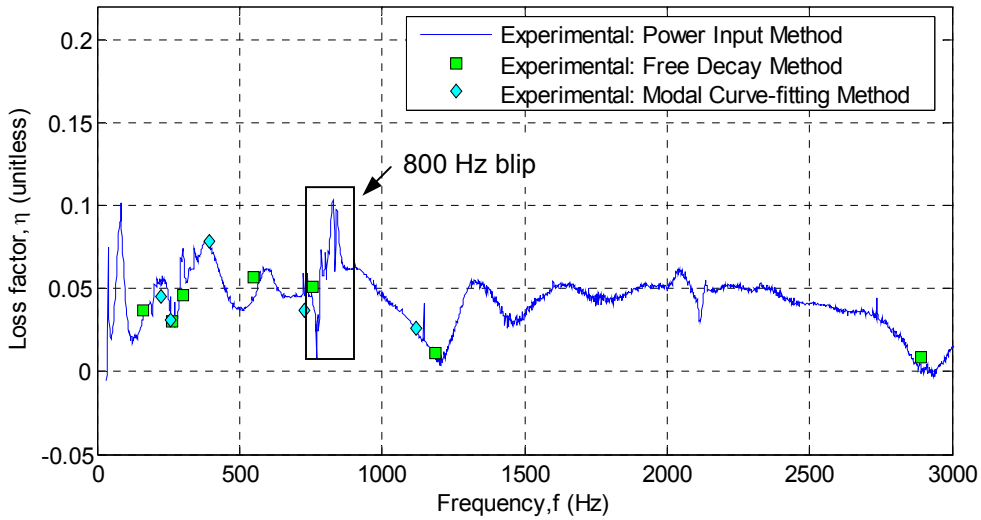

Figure 2.19 Loss factors of the aluminum plate with partial coverage constrained layer damping by experimental power input method, free decay method and modal curve-fitting method.

It can be seen from the comparison in Figure 2.19 that all three experimental methods yield essentially consistent results. Note that the power input method gives damping estimation over a broad frequency range, rather than just at several discrete estimations in the low frequency range. There are several things to note:

1) The two lowest frequency spikes at 39 Hz and 85 Hz are found to be the first two resonances of the test article/shaker system.

2) The blip around 800 Hz is found to be a test artifact related to the stinger length. The stinger length effect is noted in Figure 2.20, where loss factor estimation discrepancies in the 2400-2600 Hz range are seen to be a function of the stinger length. From experience, it is generally recommended to use a stinger with medium length (3-5 cm) for the test articles used, which range from 1 to 3 lbs.

3) At around 2900 Hz, negative loss factors with very small magnitudes are observed (worst case: -0.003). This is found to be a test artifact due to the measurement error of the driving point mobility. As can be seen in Equation (1.10) $\eta(\omega) = \mathrm{Re}\left[Y_{ff}(\omega)\right] \Big/ \sum_{i=1}^{N} m_i \omega \left|Y_{if}(\omega)\right|^2$, the sign of loss factor is totally determined by the real part of the driving point mobility. In a real test, the laser vibrometer can only measure the front side of the plate instead of the back side where the driving point really is. Thus, if the phase lag between the two sides is greater than 90°, a negative real part of the driving point mobility is measured (worst case: -28.4×10^{-6} m/sec/N), which leads to a slightly negative loss factor.

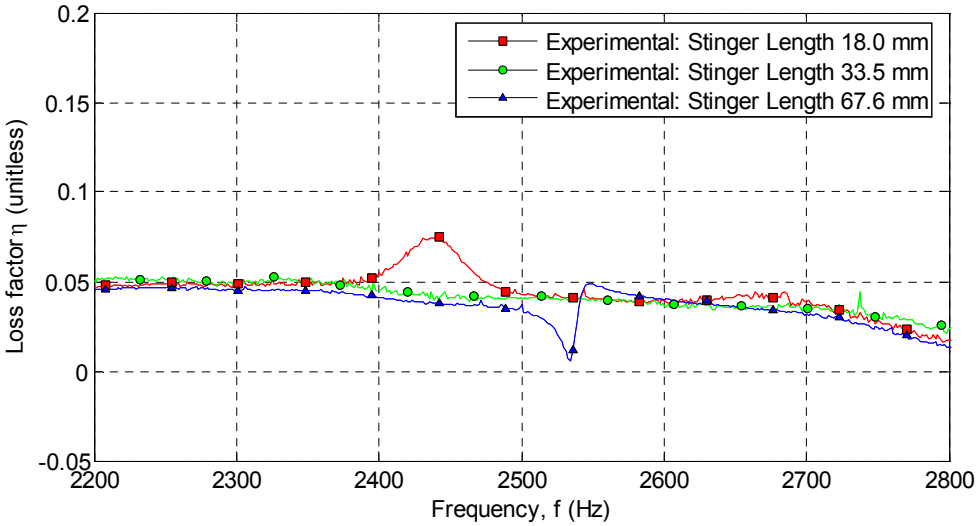

Figure 2.20 Loss factor results of the aluminum plate with partial coverage constrained layer damping in 2400-2600 Hz obtained using different stinger lengths.

2.4.1.2. Comparison of Analytical Methods

In this section, the analytical power input method is compared with the most commonly-used analytical method, namely, the modal strain energy method. Analytical results are based on the finite element method using MSC/NASTRAN 2005 r2.

The analytical power input method is used to estimate loss factors from the direct frequency response solution (MSC/NASTRAN solution 108). Frequency Response Functions (FRFs) of the driving point and the strain energy of the whole structure at each frequency are extracted. Since this is a non-uniformly damped structure, the *i*th portion's mass m_i is not constant over the plate.

For the purpose of comparison, the modal strain energy method is used to estimate loss factors using the normal mode solution (MSC/NASTRAN solution 103). Strain energy ratios are extracted. It is noted that the modal strain energy method tends to overestimate loss factors [83] [84]. The error increases with the loss factor of the viscoelastic material η_{VEM} and goes to zero as $G_2/G_1 \to 0$ [84]:

$$\frac{\Delta\eta}{\eta} = \frac{\eta^{(r)} - \eta}{\eta} = \left\{ {\eta_{VEM}}^2 \left[\frac{G_2}{G_1} + \frac{G_3}{G_2}\left(\frac{G_2}{G_1}\right)^2 \right] \right\} \Bigg/ \left\{ 1 + \frac{G_2}{G_1} + \frac{G_3}{G_2}\left(\frac{G_2}{G_1}\right)^2 \right\} \tag{2.48}$$

In this research, this error is estimated by the material properties of the viscoelastic material at 5000 Hz: $\eta_{VEM} = 0.9$, $G_2 = 9\times10^6$ Pa and the material properties of the aluminum: $G_1 = G_3 = 7.45\times10^{10}$ Pa. The error (2.36×10^{-8}) turns out to be harmless to the loss factor results in this research.

Loss factor results are shown in Figure 2.21. The two analytical methods yield results which show modestly good agreement once one considers several reasons to discount some features of the two results. First, at certain frequencies (e.g., 2118 Hz and 2913 Hz), the modal strain energy method yields "abnormally" high or low loss factors estimations. A closer look into the corresponding mode shapes reveals the reason. As shown in Figure 2.22(a), at 2118 Hz, the mode shape involves large displacement in the central damped region. So as a result, the ratio of strain energy stored in the viscoelastic material to the strain

energy of the whole plate is high, leading to high loss factor estimation in the modal strain energy method. However, since the excitation is placed at the node line of this mode, the power input method, which is based on the frequency response solution, "skips" this high loss factor. The same case is true for 805 Hz and 1369 Hz. At 1961 Hz, the driving point is at a node line, but the damped region does not have much deformation, hence low loss factor. It is the opposite at 2913 Hz: since the excitation is placed at the anti-node line of this mode, the power input method "catches" the low loss factor. The effect is the same at 1207 Hz.

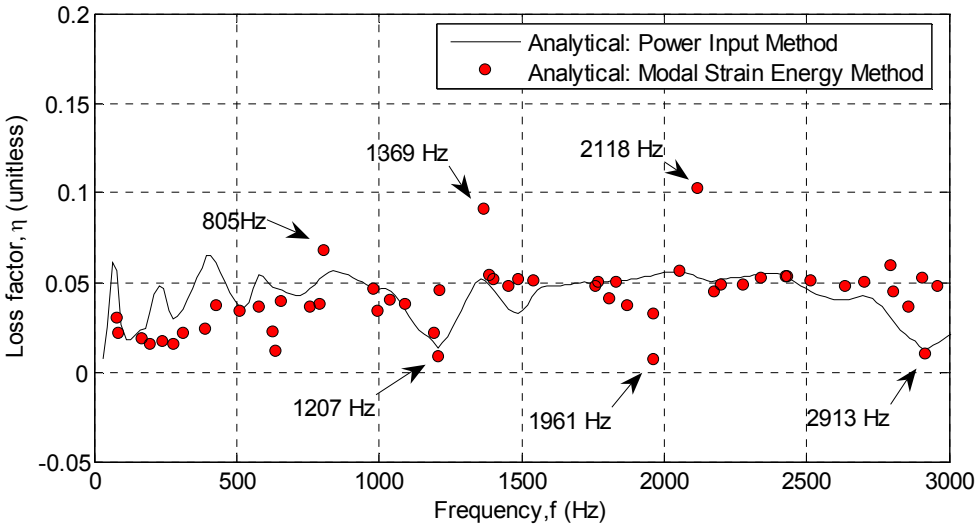

Figure 2.21 Loss factors of the aluminum plate with partial coverage constrained layer damping by analytical power input method and modal strain energy method.

To summarize, in the frequency range from 800 to 3000 Hz, the analytical power input method "skips" a mode if the driving point is at a node line and "catches" a mode is the driving point is near an anti-node line. The high loss factors belong to modes that have high deformation in the damped region and the low loss factors belong to modes that have little deformation in the damped region due to the low strain energy density in the viscoelastic materials.

There are other discrepancies that remain, in particular the regions of loss factor overpredictions in the low modal density frequency range (below 700 Hz), which will be discussed in Section 2.3.2.3. In general, based on the excitation location, the analytical power input method loss factor result can be different from what the modal strain energy method predicts. It also demonstrates that a partially covered plate can have very low loss factors in modes where the strain energy density in the damped region is low.

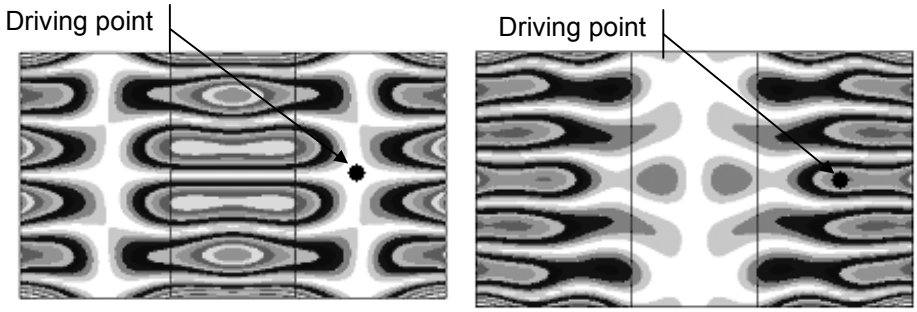

Figure 2.22 Selected mode shapes of the plate with partial coverage constrained layer damping. (a) Mode shape at 2118 Hz; (b) mode shape at 2913 Hz.

2.4.1.3. Comparison of Experimental and Analytical Methods

Two comparisons are made in this section:

1) The first compares the analytical power input method and the modal strain energy method with commonly-used experimental methods, namely, the free decay method and the modal curve-fitting method.
2) The second compares the analytical power input method with the experimental power input method.

The first comparison is shown in Figure 2.23, which uses Figure 2.21 as a basis. It can be seen that analytical power input method shows better consistency with the two commonly-used experimental methods (the free decay method and the modal curve-fitting method).

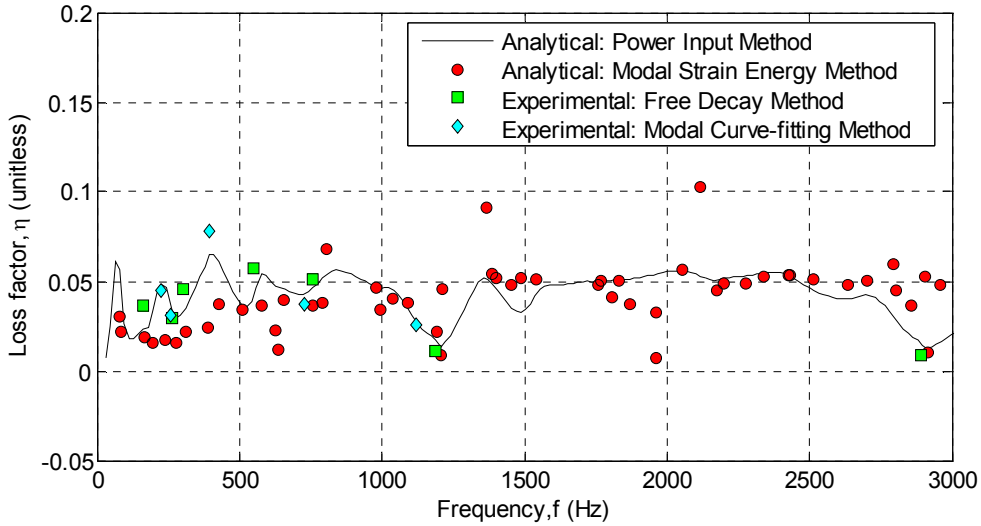

Figure 2.23 Comparison of loss factors of the plate with partial coverage constrained layer damping by the analytical power input method and the modal strain energy method with the experimental free decay method and the modal curve-fitting method.

The second comparison is shown in Figure 2.24. It can be seen that the experimental power input method and analytical power input method yield generally consistent loss factor estimations, although there is appreciable disparity in the low modal density frequency range.

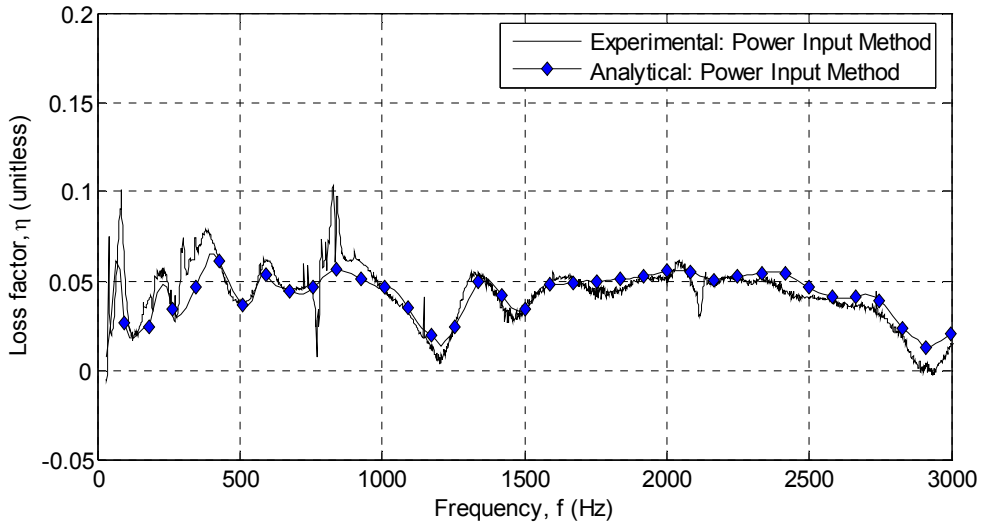

Figure 2.24 Loss factors of the plate with partial coverage constrained layer damping by the experimental power input method and analytical power input method.

From the comparison of experimental and analytical results discussed above, it can be concluded that:

1) Constrained layer damping can significantly increase the dissipation loss factor for plate structures. The mean value of experimental loss factors is 0.043, comparing to a loss factor about 0.003 for aluminum alloy alone.
2) Generally good agreement between the analytical and experimental power input method is observed, especially at high modal densities (1000-2500 Hz)
3) Both the analytical power input method and the modal strain energy method give consistent estimation with the experimental power input method, for moderately damped structures (e.g., $\eta \approx 0.05$). But overall, the analytical power input method gives results which are more in agreement with experimental results than the modal strain energy method does, as shown in Figure 2.23.

2.3.2. Aluminum Plate with Full Coverage Constrained Layer Damping

The aluminum plate with uniform constrained layer damping is as described in Table 2.7. The driving point is at the center of the damped plate, as shown in Figure 2.25(b). The plate has free boundary conditions on all edges since it is suspended by a light elastic spring. The plate is divided into 989 portions to minimize discretization errors, as shown in Figure 2.25(a). The same data reduction procedure is used as explained in Section 2.3.1.

All three layers are modeled as HEX8 solid elements. The finite element model of the plate has 24,644 nodes. There are 73932 total degrees of freedom. All material properties defined in the finite element model can be found in Appendix A. The finite element model has free boundary conditions on all edges.

Table 2.7 Description of the plate with full coverage constrained layer damping treatment

	Material	Dimensions (m)	Mass (g)
Base layer	5052-H34	0.347×0.201×0.003055	572.1
Damping layer	3M F9469PC at 20°C	0.347×0.201×0.000127	8.9
Constraining sheet	CLAD 2024-T3	0.347×0.201×0.000508	98.1

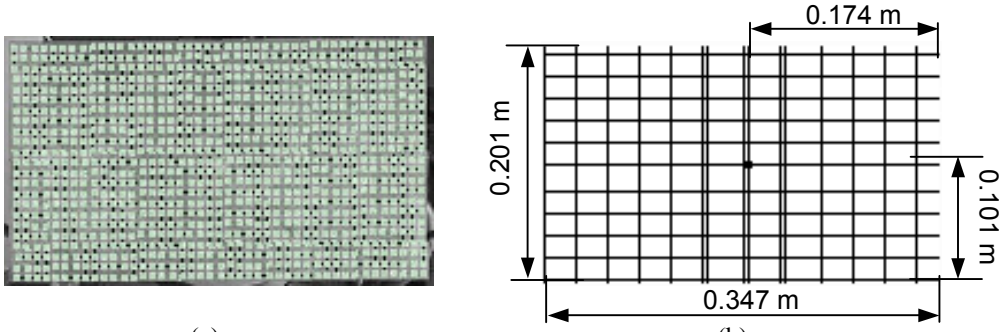

(a) (b)

Figure 2.25 Plate with full coverage constrained layer damping. (a) The plate as a test article with scanning points defined; (b) the plate as a finite element model with the excitation point illustrated.

2.3.2.1. Comparison of Experimental Results

The experimental power input method and the free decay method are used to characterize damping. The modal curve-fitting method does not fit here because it is hard to identify any clear modes for this highly damped plate.

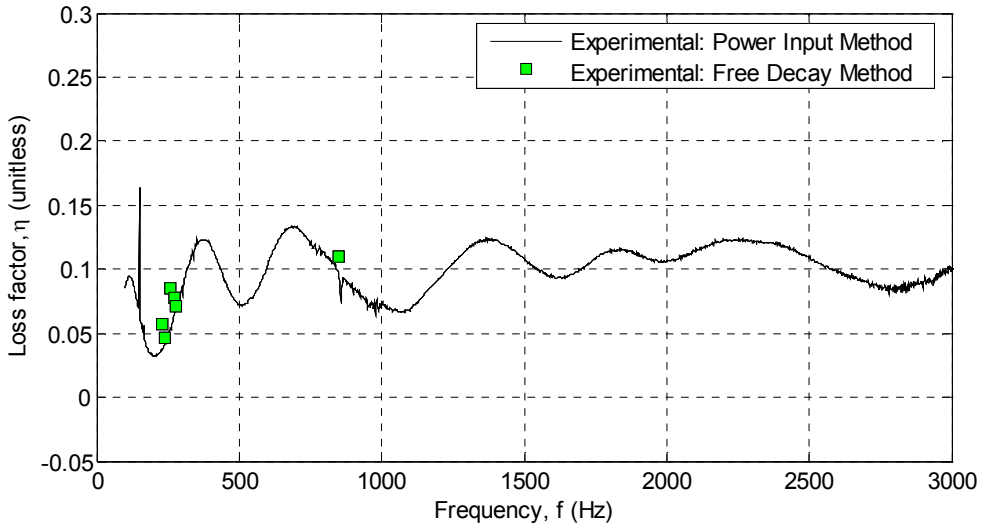

Figure 2.26 Loss factors of the plate with full coverage constrained layer damping by the experimental power input method and free decay method.

As shown in Figure 2.26, a loss factor as high as 0.13 is observed. Overall, this fully-covered plate exhibits a much higher damping than the partially-covered plate. It can be seen that the two experimental methods yield consistent loss factors, but the free decay method fails to give damping estimation above 1000 Hz where free decay time histories are hard to obtain for this highly-damped plate.

2.3.2.2. Comparison of Analytical Results

Results by the analytical power input method and the modal strain energy method are plotted together with results by the experimental free decay method for the purpose of comparison, as shown in Figure 2.27. The two analytical methods agree with each other very well above 1500 Hz. Below 1500 Hz the analytical power input method conforms to the experimental free decay method much better than the modal strain energy method does, for this heavily damped structure.

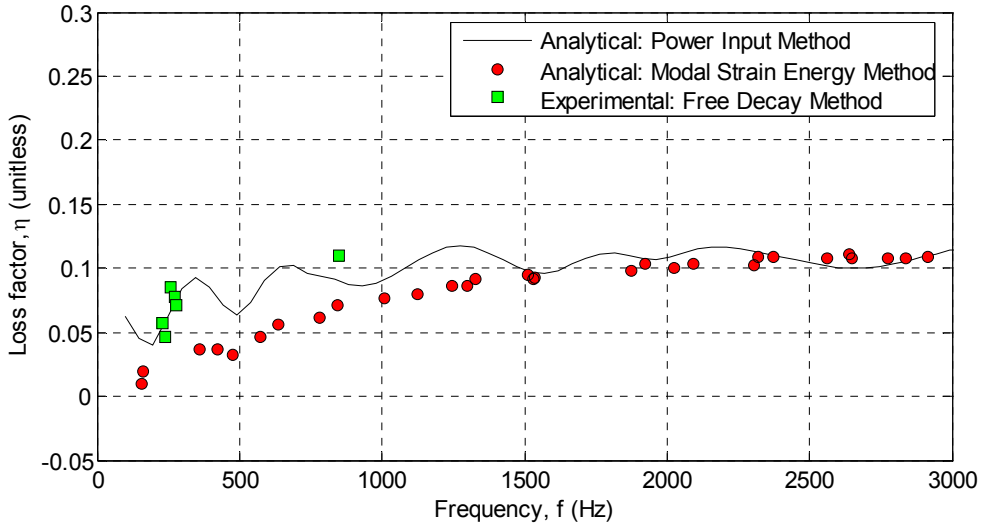

Figure 2.27 Loss factors of the plate with full coverage constrained layer damping by the analytical power input method, modal strain energy method and free decay method.

2.3.2.3. Comparison of Experimental Power Input Method and Analytical Power Input Method Results

An apparent correlation between the analytical power input method and the experimental power input method results is observed in the frequency range 1500-2500 Hz, which corresponds to a region of relatively high modal density, as shown in Figure 2.28.

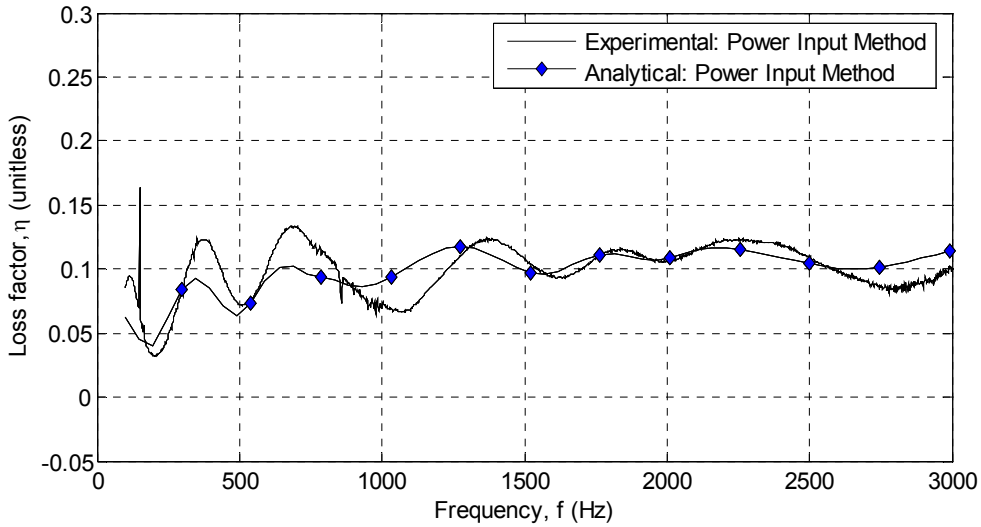

Figure 2.28 Loss factors of the plate with full coverage constrained layer damping by the experimental power input method and analytical power input method.

The experimental power input method yields higher loss factor estimations than the analytical power input method in the low modal density range, which in this case is below 1000 Hz. A possible reason is that in an actual test, losses occur, e.g., due to radiation damping, interactions with test specimen supports, lateral vibration of the stinger, etc. These factors, which are not taken into account in the analytical model, will result in more energy being dissipated in the actual test than the analytical model predicts—which results in a larger value of the experimentally-estimated loss factor. Perhaps the reason these additional loss factors (which add to the numerator of Equation (1.1)) make so much of a difference in loss

factor estimation, is that the total system energy (in the denominator of Equation (1.1)) is rather small when the plate is being excited at an anti-resonance.

The reason for the oscillatory estimations at low frequencies is believed to be due to the existence of frequency bands wherein the plate becomes more or less responsive in bending [30]. Figure 2.29 is the loss factor predictions from Figure 2.28 in the 100-2000 Hz frequency range.

The local minimum in the range of 150-250 Hz and 450-600 Hz, as shown in Figure 2.29, is first inspected. The "valleys" of relatively low loss factors seem to correspond to the deflected mode shapes which closely match a primarily bending mode. For instance, Figure 2.30 (a) and Figure 2.31 (a) show, respectively, the fundamental bending mode shapes for the "long" and "short" lateral dimensions of the damped plate. These mode shapes are very easily excited at "nearby" frequencies by application of the mechanical excitation at the center of the plate, as shown in Figure 2.30 (b) and Figure 2.31 (b). All other deflection shapes in the vicinity of 157 Hz and 475 Hz are very similar to the two mode shapes at 157 Hz and 475 Hz. As such, a plausible explanation is that the fundamental bending modes dominate the response in the frequency range wherein the response closely resembles the easily excited mode shapes.

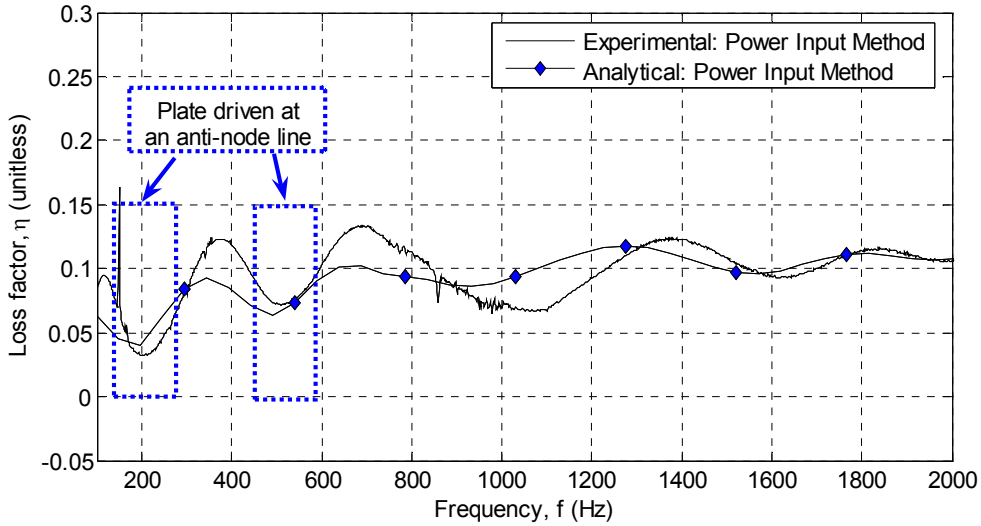

Figure 2.29 Low Loss factors of the plate with full coverage constrained layer damping driven at an anti-node line by the experimental power input method and analytical power input method.

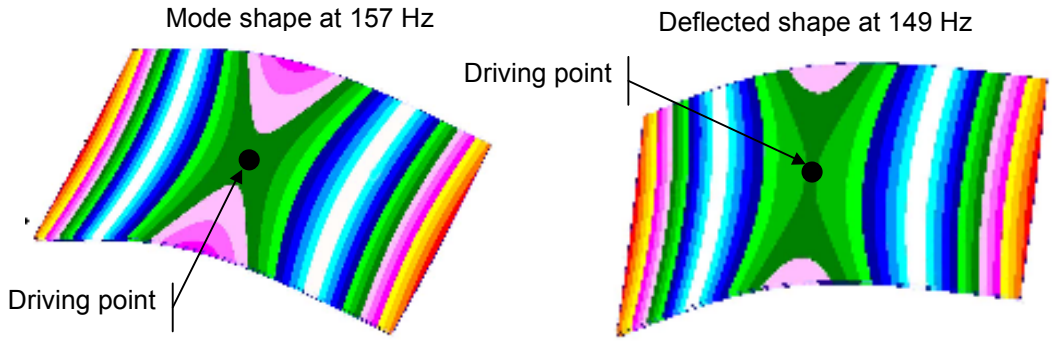

(a) (b)

Figure 2.30 The mode shape of the plate with full coverage constrained layer damping at 157 Hz and the deflection shape in the vicinity of this mode. (a) The mode shape at 157 Hz; (b) deflection shape at 149 Hz.

Mode shape at 475 Hz

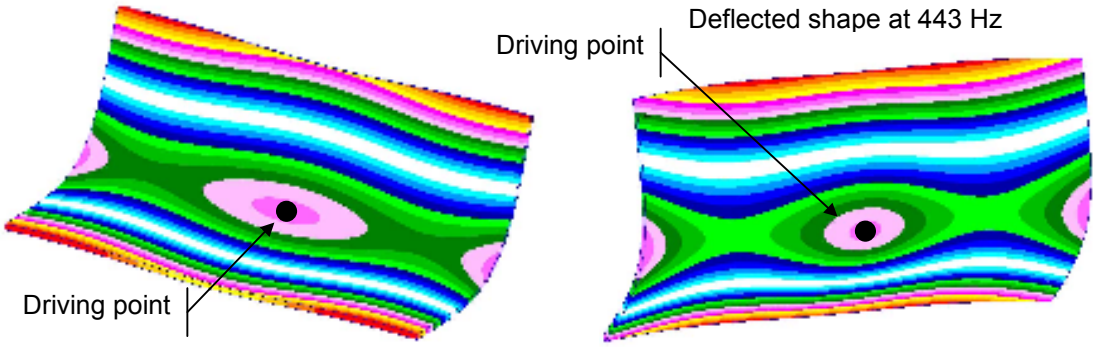

Figure 2.31 The mode shape of the plate with full coverage constrained layer damping at 475 Hz and the deflection shape in the vicinity of this mode. (a) The mode shape at 475 Hz; (b) deflection shape at 443 Hz.

By comparison, the local maximum in the range of 300-450 Hz and 600-750 Hz, as shown in Figure 2.32, is inspected. The explanation for the frequency ranges with relatively high loss factors may involve the fact that in these ranges, the excitation point is on a node line of the mode shape at 360 Hz and 635 Hz, as shown in Figure 2.33 (a) and Figure 2.34 (a). Clearly, the center of the plate is a suboptimal force application point for these modes (due to the presence of a node line). In fact, none of the deflected shapes resemble these mode shapes, as shown in Figure 2.33 (b) and Figure 2.34 (b). For excitation at a node line, a substantial amount of energy is expended translating the center of mass of the plate. In such cases, the energy input at the drive point is high relative to total strain energy of the response, therefore higher predicted loss factors result. In other frequency ranges (near primarily bending frequencies), the fraction of energy required to excite the primarily bending modes is relatively low, therefore lower loss factors result.

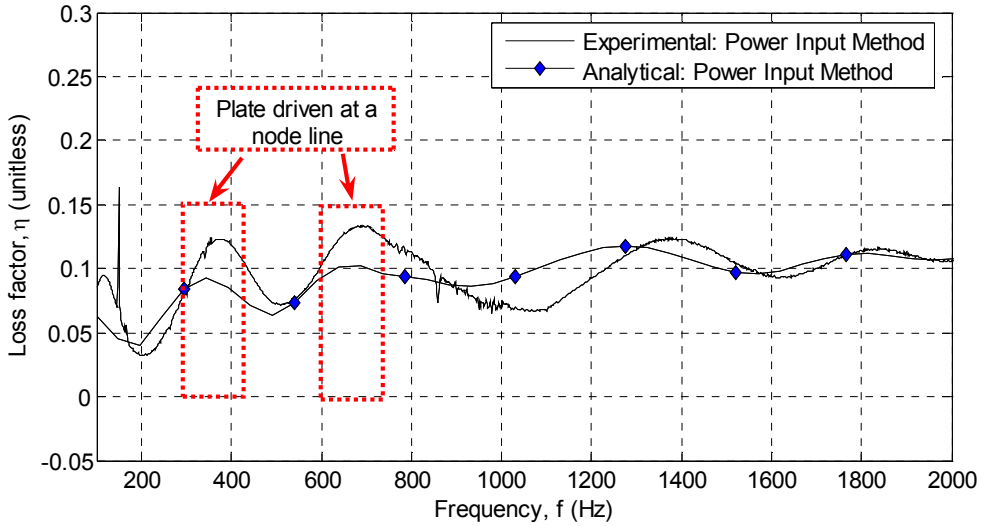

Figure 2.32 High loss factors of the plate with full coverage constrained layer damping driven at a node line by the experimental power input method and analytical power input method.

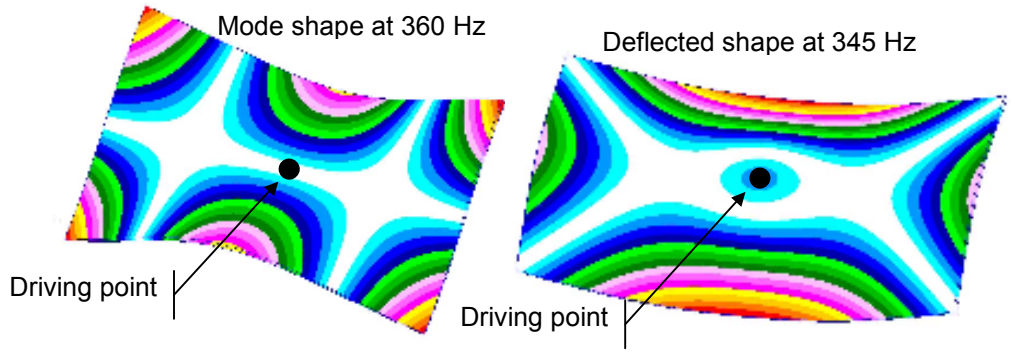

Figure 2.33 The mode shape of the plate with full coverage constrained layer damping at 475 Hz and the deflection shape in the vicinity of this mode. (a) The mode shape at 475 Hz; (b) deflection shape at 443 Hz.

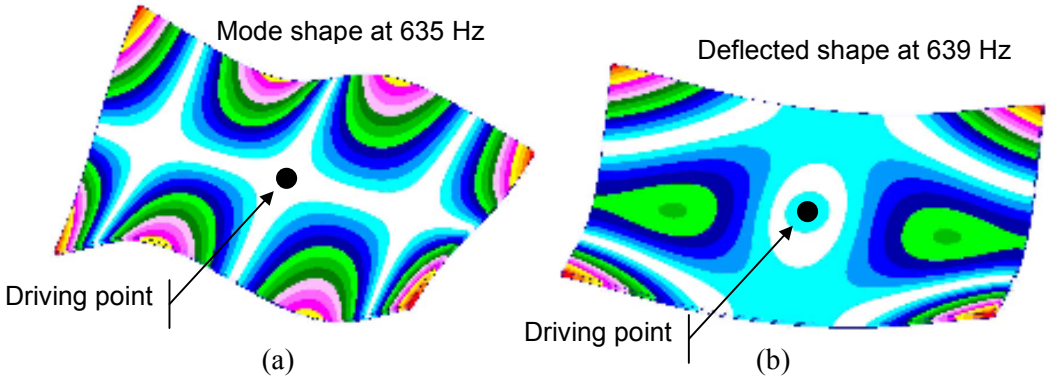

Figure 2.34 The mode shape of the plate with full coverage constrained layer damping at 475 Hz and the deflection shape in the vicinity of this mode. (a) The mode shape at 635 Hz; (b) deflection shape at 639 Hz.

2.3.3. Composite Honeycomb Sandwich Beam with Aluminum Stand-Off Constrained Layer Damping

Carbon-fiber reinforced plastic composite structures usually possess high specific stiffness. The bending stiffness will be further increased by adding a honeycomb layer in between carbon facesheets, which is common for aircraft fuselage and bulkhead structures. In contrary to riveted metal structures, composite honeycomb sandwich structures have low intrinsic damping, due to lack of friction between structural components. So added damping becomes necessary for noise reduction.

In this research, aluminum alloy 2024-T3 is first chosen as the stand-off material, considering stiffness, material availability, etc. The manufactured stand-offs are in 1 cm×1 cm squares, 1 mm apart. The 1 mm groves are cut to reduce the bending stiffness of the aluminum stand-offs. The stand-offs are bonded to carbon facesheets by epoxy under vacuum pressure, then a damping layer and a constraining layer are added, as shown in Figure 2.35 and Table 2.8. The beam has free boundary conditions on all edges as it is suspended by two light elastic springs.

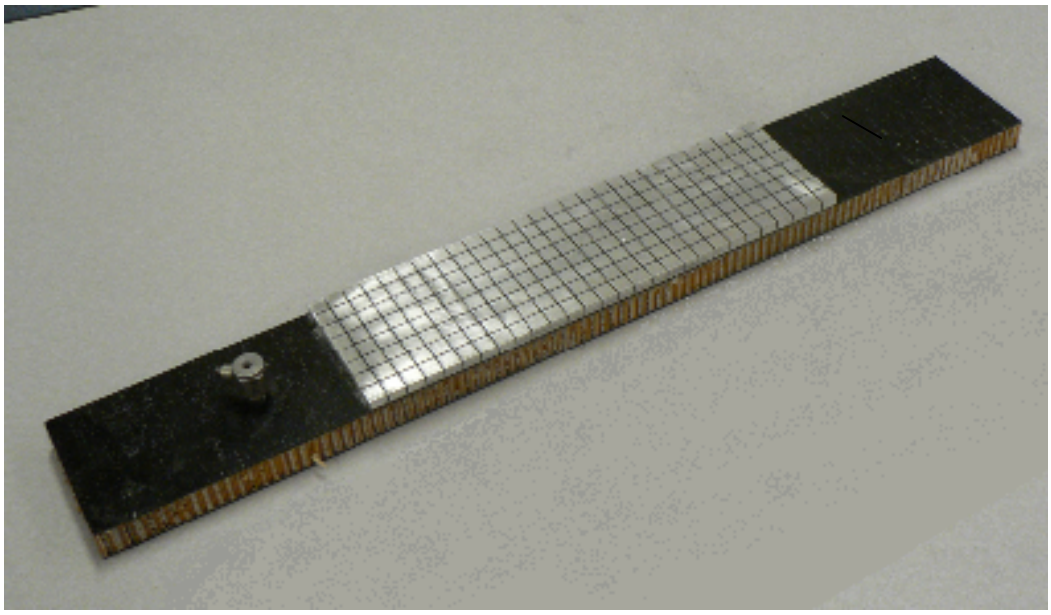

(a)

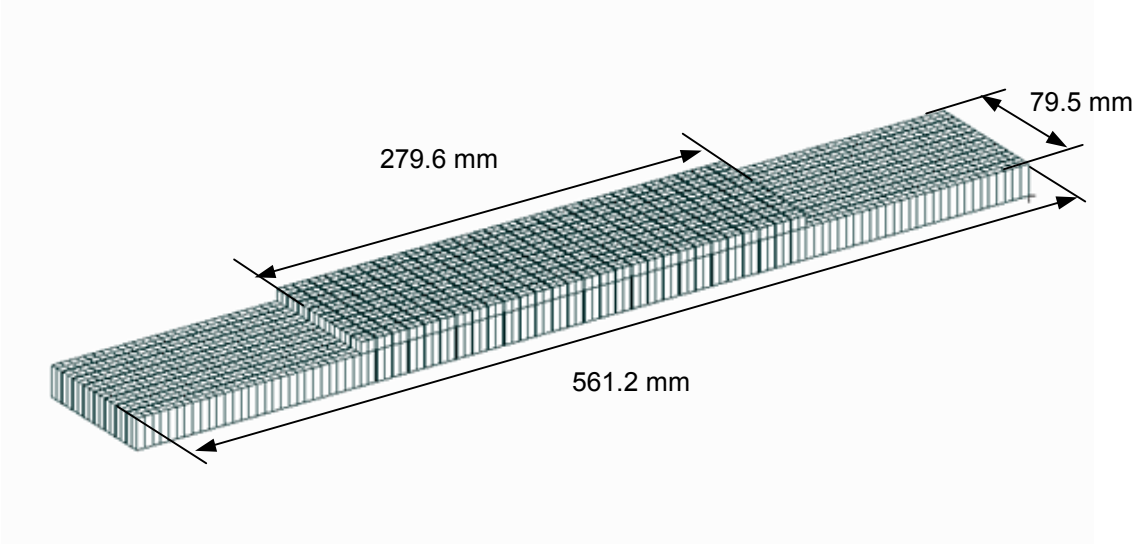

(b)

Figure 2.35 Composite honeycomb sandwich beam with aluminum stand-off constrained layer damping treatment. (a) The beam as a test article; (b) the beam as a finite element model.

Table 2.8 Description of the plate with aluminum stand-off constrained layer damping

Component	Material	Thickness (in)	Length and width (mm)
Carbon/Epoxy face sheet	IM7/3501-6	0.037 [0/90/90/0]	561.2×79.46
Honeycomb core	Nomex 1/8-3.0	0.66	561.2×79.46
Carbon/Epoxy face sheet	IM7/3501-6	0.037 [0/90/90/0]	561.2×79.46
Stand-off	2024-T3	0.25	279.6×79.46
Damping layer	3M F9469PC at 20°C	0.005	279.6×79.46
Constraining layer	Clad 2024-T3	0.02	279.6×79.46

The finite element model of the plate has 17236 nodes. The total degrees of freedom are 79298. The two composite facesheets and the constraining layer are modeled as QUAD4 elements. The honeycomb, stand-offs and the viscoelastic layer are modeled as HEX8 solid elements. All material properties defined in the finite element model can be found in Appendix A. The finite element model has free boundary conditions on all edges.

Experimental and analytical power input method results are shown in Figure 2.36. Conclusions include:

1) Stand-off constrained layer damping yields a significantly higher damping level than generic constrained layer damping, with less damping material (222 cm^2 for SOCLD beam vs. 697 cm^2 for fully covered monolithic CLD plate vs. 207 cm^2 for partially covered monolithic CLD plate).
2) The same correlation as shown in Section 2.3.2.3 is observed in between the two results. The modeling issues related to the frequency mismatch between the local loss factor maxima and minima seem to be the same.
3) The discrepancy between experimental and analytical results may be due to lack of accurate material property information on carbon fiber composites and honeycomb core. Also the aluminum stand-off on the test article is more massive than in the model because a thin layer of aluminum is left to act as linkage between neighboring stand-off units. This will make the actual stand-off more stiff, which is consistent with the results in Figure 2.36.

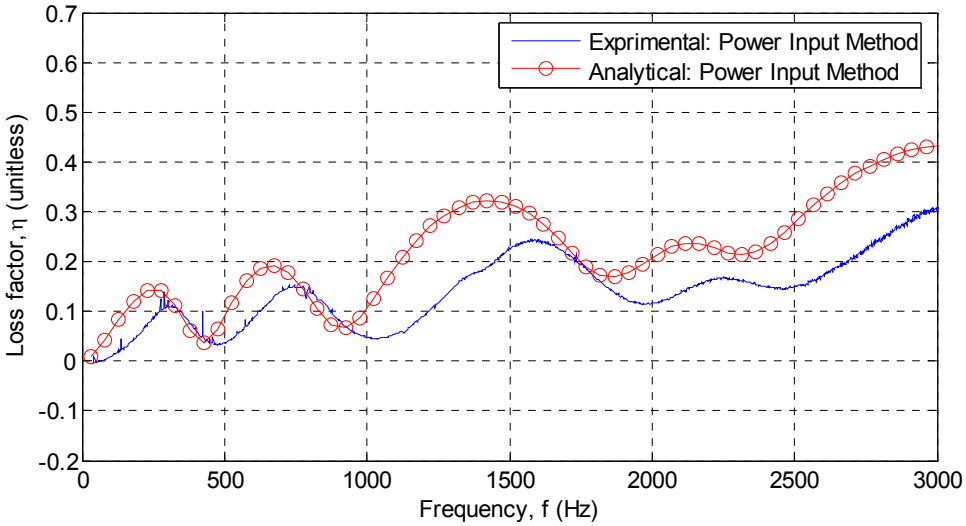

Figure 2.36 Loss factors of the composite honeycomb sandwich beam with aluminum stand-off constrained layer damping treatment by the experimental power input method and analytical power input method.

2.3.4. Composite Honeycomb Sandwich Beam with Plexiglas Stand-Off Constrained Layer Damping

Cutting thin groves in an aluminum alloy plate is not an easy task, so Plexiglas is explored as an alternative. The beam is shown in Figure 2.37 and Table 2.9. The beam has free boundary conditions on all edges since it is suspended by two light elastic springs.

The two composite facesheets and the constraining layer are modeled as QUAD4 elements. The finite element model of the plate has 17,236 nodes. There are 79,298 total degrees of freedom. The honeycomb, stand-offs and the viscoelastic layer are modeled as HEX8 solid elements. All material properties defined in the finite element model can be found in Appendix A. The finite element model has free boundary conditions on all edges.

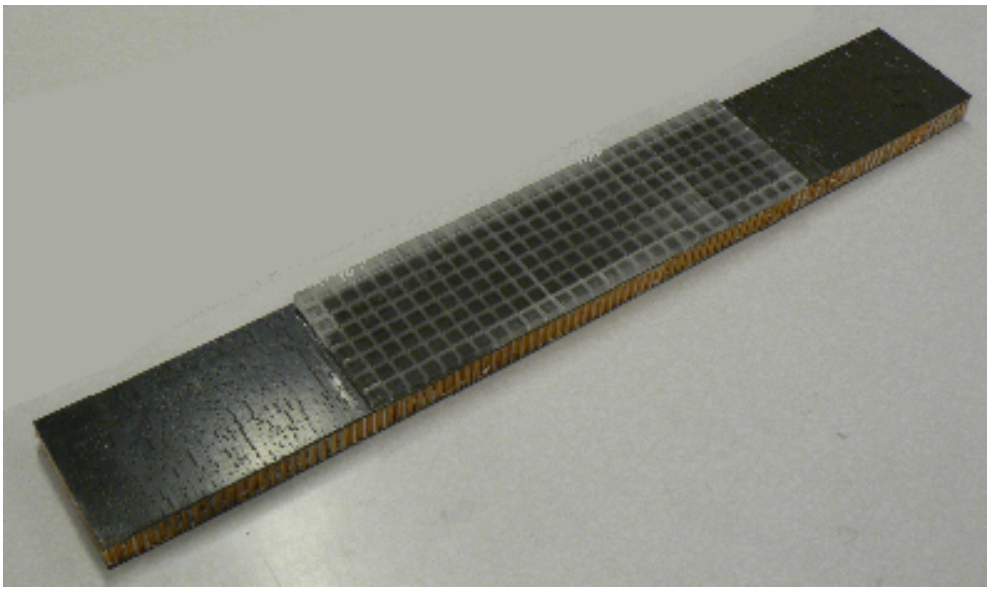

(a)

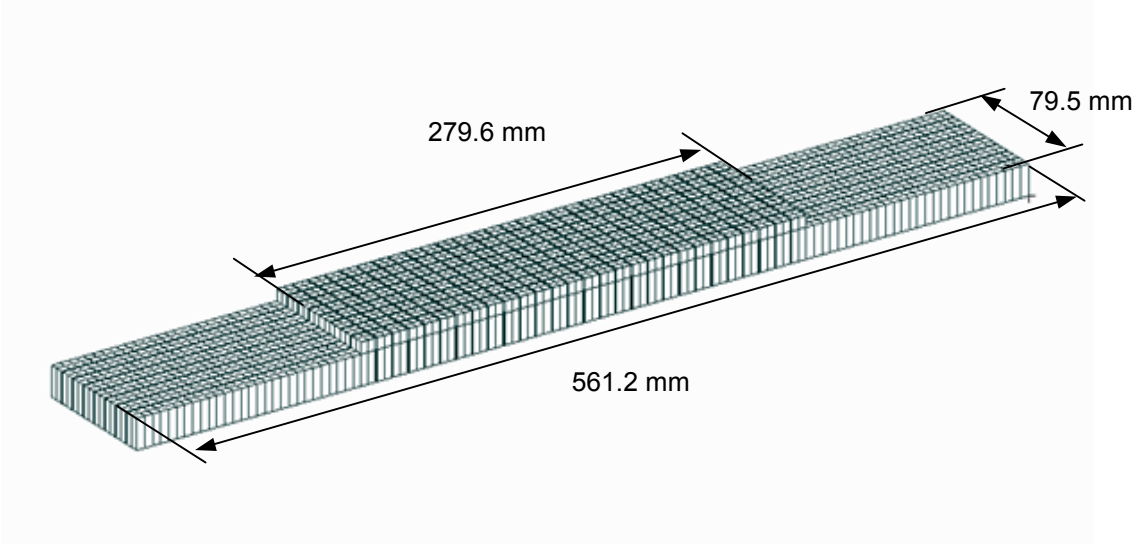

(b)

Figure 2.37 Composite honeycomb sandwich beam with Plexiglas stand-off constrained layer damping treatment. (a) The beam as a test article; (b) the beam as a finite element model.

Table 2.9 Description of the beam with Plexiglas stand-off constrained layer damping

Component	Material	Thickness (in)	Length and width (mm)
Carbon/Epoxy face sheet	IM7/3501-6	0.037 [0/90/90/0]	561.2×79.46
Honeycomb core	Nomex 1/8-3.0	0.66	561.2×79.46
Carbon/Epoxy face sheet	IM7/3501-6	0.037 [0/90/90/0]	561.2×79.46
Stand-off	Plexiglas (Cast acrylic)	0.25	279.6×79.46
Damping layer	3M F9469PC at 20°C	0.005	279.6×79.46
Constraining layer	Clad 2024-T3	0.02	279.6×79.46

Experimental and analytical power input method results are shown in Figure 2.38. Conclusions include:

1) Stand-offs made of Plexiglas yield a lower damping level than stand-offs made of aluminum, which is due to the stiffness difference. The overall damping level of Plexiglas stand-offs is still significantly higher than that of generic constrained layer damping.
2) Issues of correlation between the experimental power input method and the analytical power input method noted in Section 2.3.3 are observed, but to a slightly lower degree.
3) Discrepancy between experimental and analytical results may be due to lack of accurate material property information on carbon fiber composites and honeycomb core.

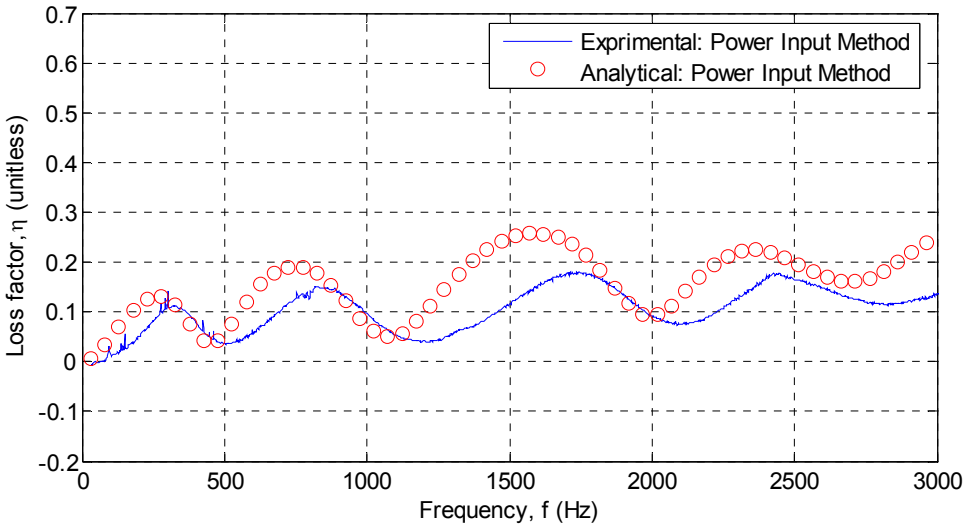

Figure 2.38 Loss factors of the composite honeycomb sandwich beam with Plexiglas stand-off constrained layer damping by the experimental power input method and the analytical power input method.

A summary of viscoelastic damping examples is listed in Figure 2.39 and Table 2.10. From the summary, it can be seen that:

1) Partial coverage constrained layer damping offers the most weight-efficient damping solution for flexible structures (e.g., metallic plates).
2) In cases where additional weight is not a concern, full coverage constrained layer damping offers higher damping.
3) Partial coverage Plexiglas stand-off constrained layer damping is a more weight-efficient damping solution for structures with high specific stiffness (e.g., composite honeycomb sandwich beams) than aluminum stand-off constrained layer damping.
4) Aluminum stand-off constrained layer damping, being the heaviest, yields the highest damping level.

Table 2.10 Summary of viscoelastic damping examples

	Partial coverage CLD	Full coverage CLD	Partial coverage Plexiglas SOCLD	Partial coverage aluminum SOCLD
Mean loss factor from 0 to 3000 Hz	0.0434	0.0997	0.1037	0.1357
Coverage area (cm^2)	207	697	222	222
Mass of VEM (g)	2.63	8.85	2.82	2.82
Mass of overall treatment (g)	31.73	106.9	171.8	352.3
Mean loss factor/VEM mass (1/g)	0.0165	0.0113	0.037	0.048
Mean loss factor/overall treatment mass (1/g)	0.0014	0.00093	0.0006	0.00038

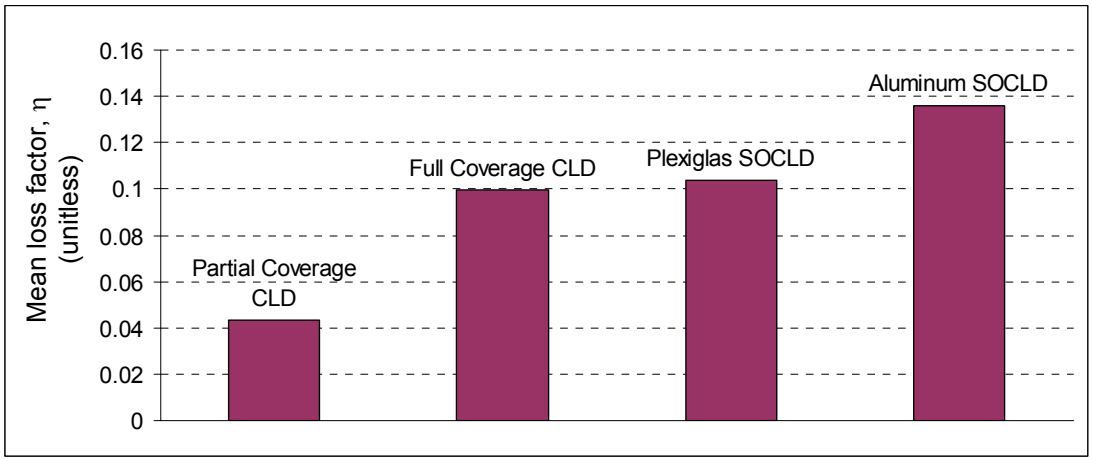

(a)

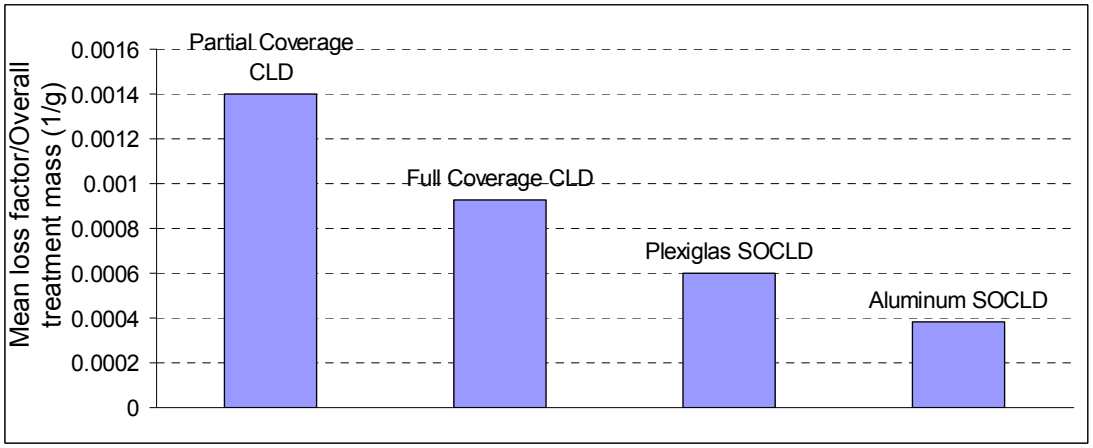

(b)

Figure 2.39 Summary of viscoelastic damping examples. (a) Mean loss factor from 0 to 3000 Hz; (b) ratio of mean loss factor to overall treatment mass.

3. Structures with Particle Damping

Experimental and analytical studies have been completed on plates with particle damping treatments. Loss factor results are presented, compared and analyzed. The results described in this section are published in Reference [51]. It is observed that fluid resonances become more apparent as the fill ratio increases [50]. So the particle damping examples shown here all have 100% fill ratio. The experimental setup is the same with that described in Chapter 2.

3.1. Fluid Analogy

The analytical model is a simple fluid resonance analogy. Under external excitations, the particles behave largely as fluid. If we treat the particles as a compressible fluid, the resonance frequencies of compressible fluid in a cavity with two ends closed are:

$$f_n = \frac{nc}{2d}, \; n=1, 2, 3 \ldots \tag{3.1}$$

where d is depth of the particle layer (here is the honeycomb thickness) and c is the longitudinal wave speed. The resonance frequencies of compressible fluid in a cavity with two ends open are the same, as shown in Figure 3.1.

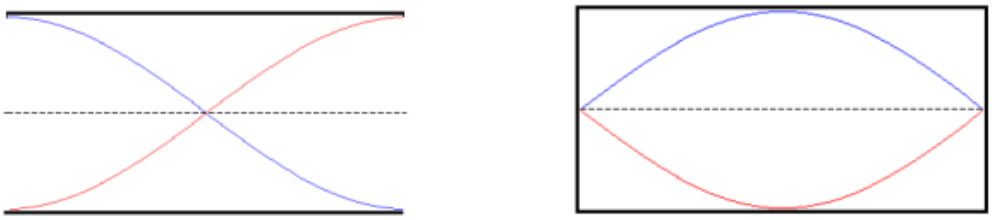

(a) (b)

Figure 3.1 Particle displacement mode shape by a fluid resonance analogy in a cavity. (a) Two ends open; (b) two ends closed.

3.1.1. Measurement of Particle Longitudinal Wave Speeds

The performance of particle dampers is closely influenced by particle resonances in the cavity. Particle resonances are determined by the intrinsic particle property: the longitudinal wave speed. Therefore, this property is measured to facilitate further inspections of particle damping.

However, the longitudinal wave speed, c ,in glass microbubbles can only be quantified with difficulty. For K1 particles, wave speeds ranging from 58 m/s [85] and 69 m/s [62] to 100 m/s [87] are found in the literature. No literature has been found on the wave speed of K20 and K37 particles. The measuring method in Reference [62] is adopted to evaluate the longitudinal wave speed in this research.

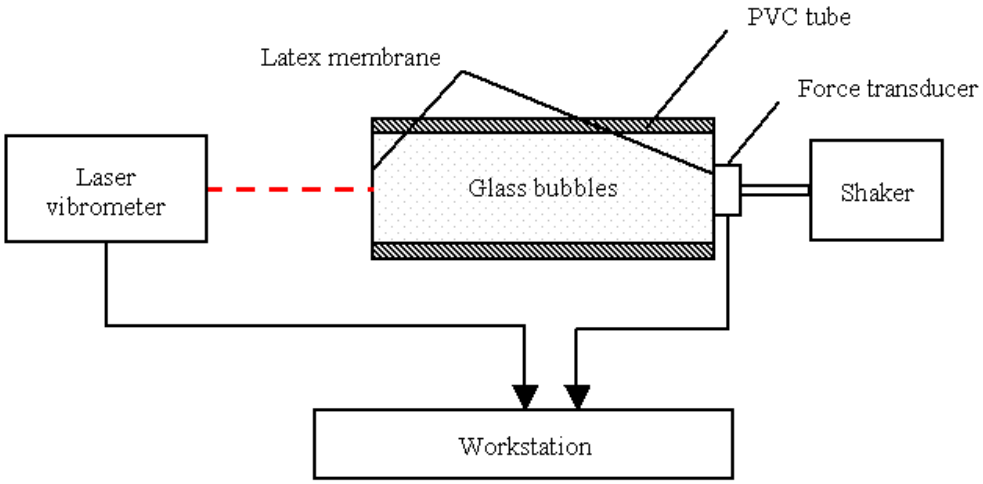

Figure 3.2 Experimental setup for longitudinal wave speed measurements of particles.

The two ends of the particle-filled PVC tubes (8.43 cm) are closed by latex membranes to simulate open ends. The tube diameter is selected so gravity will not cause excessive particle settling in the cross section, as illustrated in Figure 3.3, where the root mean square mobilities for the large tube (which has more gravity-caused setting) clearly show a non-uniform distribution. Thus, bottom particles are not as involved in resonances as the top particles are,

which leads to difficulty measuring particle resonances. A tube with smaller diameter shows more uniform resonance.

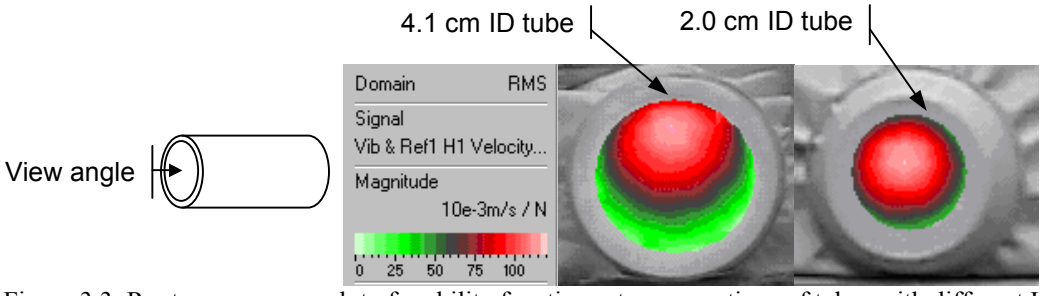

Figure 3.3 Root mean square plot of mobility functions at cross sections of tubes with different Inner Diameters (ID).

For a tube with two open ends, the resonance frequencies are the same with two ends closed: $f_n = nc/(2d)$, $n=1, 2, 3\ldots$ The first resonance in the cavity is measured and presented in Figure 3.4. Both magnitude and phase information are plotted. For K1 particles, the first resonance frequency of the particles is found to be at 398.4 Hz. Therefore, c for K1 is determined as 67.1 m/s. For K20 particles, the first resonance frequency of the particles is found to be at 316.4 Hz. Therefore, c for K20 is determined as 53.4 m/s. For K37 particles, the first resonance frequency of the particles is found to be at 232.8 Hz. Therefore, c for K37 is determined as 39.3 m/s.

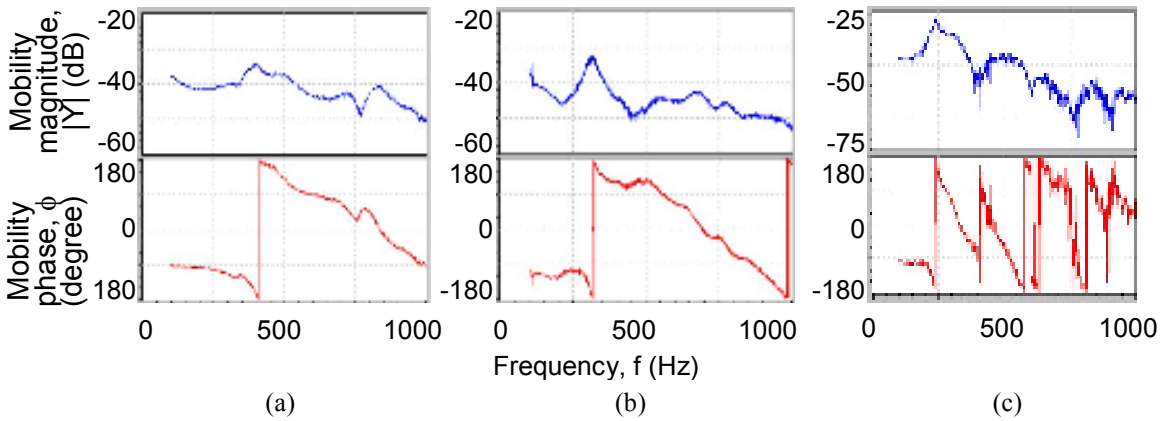

(a) (b) (c)

Figure 3.4 Measured mobility resonances of the glass microbubbles in the 2 cm inner diameter tube. (a) K1 microbubbles; (b) K30 microbubbles; (c) K37 microbubbles.

3.1.2. Measurement of Particle Internal Friction

Consider the fact that the two major energy loss modes of particle dampers are:

1) Inelastic collisions.

2) Friction among particles and between particles and the walls of the enclosure.

The first mode is unlikely to be the major energy loss mode because the glass microbubbles are expected to be elastic in this low excitation application. Thus, the second mode dominates the energy loss. As a result, inter-particle friction is a key property in evaluating particle damping treatments. However, the internal friction information of the glass bubbles is not provided by the manufacturer. Therefore, tests of internal friction are done on the particles.

The internal friction is evaluated in two ways: the angle of repose test and the flowability test, which is shown in Figure 3.5 and Figure 3.6, respectively.

The measured angle of repose for K1 is apparently smaller than K20 and K37, indicating a lower internal friction in K1 particles than in K20 and K37 particles (Please note that according to the angle of repose classification in Reference [28], K1, K20 and K37 particles are all classified as very fine free-flowing materials).

The flowability test instrument is designed referring to Reference [29]: 130 ml of glass microbubbles is allowed to freely flow out of a funnel starting from rest. An average of three measurements is taken for both of the angle of repose test and the flowability test.

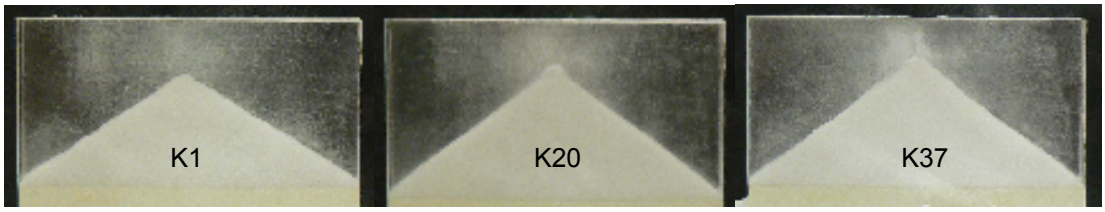

(a) (b) (c)

Figure 3.5 Angle of repose test of different glass microbubbles. (a) K1; (b) K20; (c) K37.

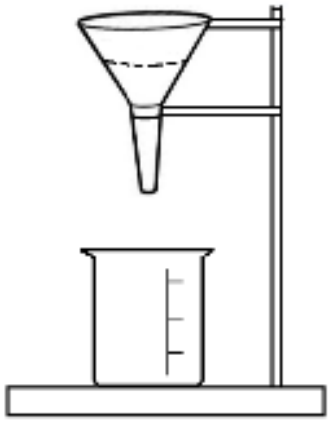

Figure 3.6 Schematic of flowability test instrument.

As shown in Table 3.1, the flow time results are consistent with the angle of repose test results, indicating a higher internal friction in K20 and K37 particles than K1 particles.

Table 3.1 Internal friction tests of K1, K20 and K37 glass microbubbles

Particle Type	Angle of repose (°)	Average flow time (second)
K1	32.5	3.57
K20	35.0	4.09
K37	37.2	4.11

3.2. Metallic Honeycomb Sandwich Plates with Different Particle Damping Treatments

Sandwich honeycomb composite plates are manufactured as the base structure. The configuration of the sandwich honeycomb plate as a baseline structure is shown in Table 3.2. Three damping configurations, as shown in Table 3.3, are tested. 3M™ Glass Bubbles (tiny hollow glass microspheres) are filled into the cells of honeycomb core to a 100% packing ratio and then enclosed by face sheets, as shown in Figure 3.7. 3M™ K1, K20 and K37 particles are used. The driving point position is placed at the center of the plate, as shown in Figure 3.7(a). The rest of the experimental setup is the same as that described in Section 2.1.

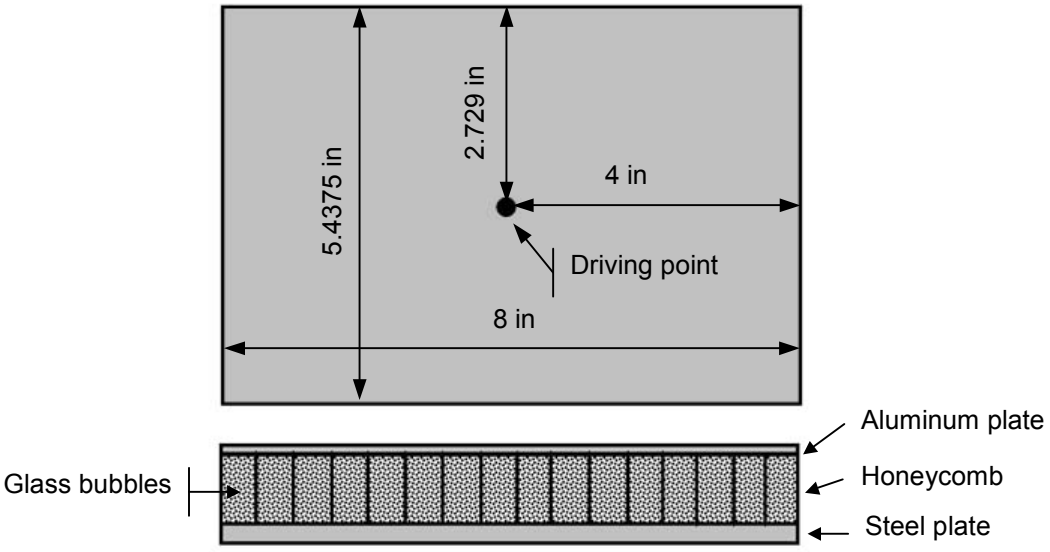

(a)

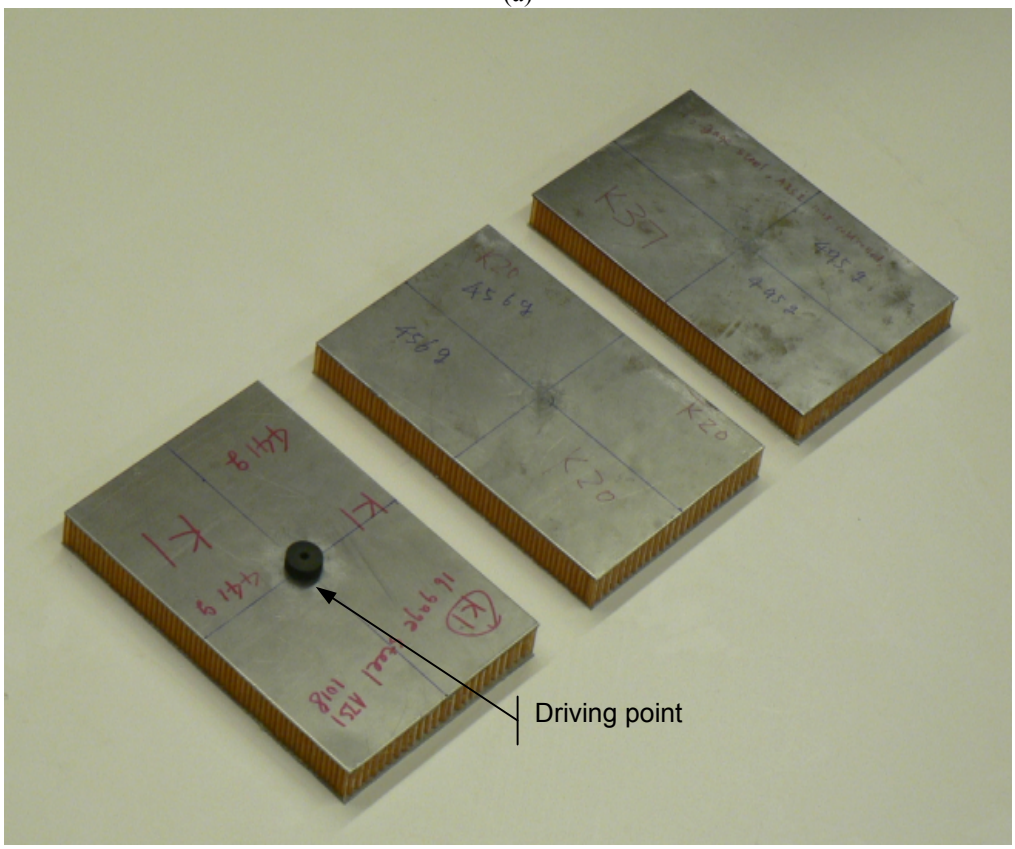

(b)

Figure 3.7 Sandwich honeycomb plates with particle damping. (a): Schematic of damped plates; (b): the three specimens filled with different particles.

Table 3.2 Description of metallic sandwich honeycomb plates

Component	Material	Thickness (in)	Length and width (in)
Aluminum face sheet	Clad 2024-T3	0.032	$5\,7/16 \times 8$
Honeycomb core	Nomex 1/8-3.0	0.66	
Steel base sheet	AISI 1018	0.0625	

Table 3.3 Description of K1, K20 and K37 glass microbubbles

Particle Type	Particle density [1] (g/cm^3)	Average particle diameter [1] (μm)	Total mass of the damped plate (g)
K1	0.125	65	441
K20	0.20	60	456
K37	0.37	45	495

With the properties measured in Section 3.1 in hand, it is convenient to inspect the damping measurement, as shown in Figure 3.8. It can be observed from the comparison in Figure 3.8 that:

1) The experimental power input method and modal curve-fitting method give consistent results, but the power input method offers more damping information other than just at a small number of frequencies. In particular, the experimental power input method allows one to identify the distinct frequency bands within which the damping is substantially higher.
2) Glass microbubbles, when filled into honeycomb cells, can significantly increase damping for sandwich honeycomb plates in distinct frequency bands. Moreover, the frequencies at which damping peak values occur follow the same trend as the friction indices measured in Section 3.1.
    a) The K1 specimen loss factor result shows a “hump” with the maximum value of 0.095 near 2000 Hz. By the fluid resonance model described in Section 3.1, since K1 particles have a measured longitudinal wave speed of 67.1 m/s, the first

particle resonance is found to be at 2001 Hz, which explains the peak damping in the vicinity of this frequency.

b) The K20 specimen has a more distinct peak value of 0.16 around 1439 Hz. The fluid resonance model predicts the first particle resonance to be at 1591 Hz, which is again consistent with the experimental measurement.

c) The K37 has an even more distinct peak value of 0.22 around 1077 Hz, compared to the predicted resonance frequency at 1171 Hz.

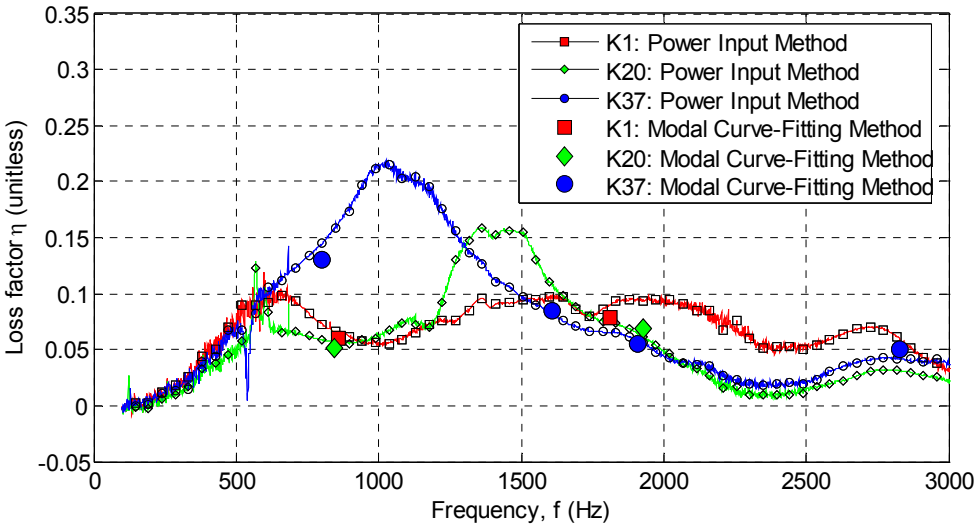

Figure 3.8 Comparison of loss factors of metallic sandwich honeycomb plates with K1, K20 and K37 particles by the experimental power input method and the modal curve-fitting method.

A summary of particle damping examples is listed in Table 3.4 and plotted in Figure 3.9. It can be seen from the summary that:

1) K37 particles offer the highest damping level but add the most weight to the base structure due K37 particles' high density compared to K1 and K20.

2) K20 particles also offer an impressive damping capability which is a more weight-efficient damping solution than K37 particles.

3) K1 particles offer somewhat lower damping through a somewhat broad frequency range, but provide the best damping to weight ratio.

4) In general, particle is more efficient if the frequency at which the damping is needed can be made to coincide with the frequency at which the loss factor peaks.

Table 3.4 Summary of particle damping examples

	K1	K20	K37
Max loss factor from 0 to 3000 Hz	0.095	0.16	0.22
Mean loss factor from 0 to 3000 Hz	0.068	0.056	0.078
Mass of particles (g)	26.9	43.0	79.6
Max loss factor/mass of particles (1/g)	0.0035	0.0037	0.0028
Mean loss factor/mass of particles (1/g)	0.0025	0.0013	0.0010

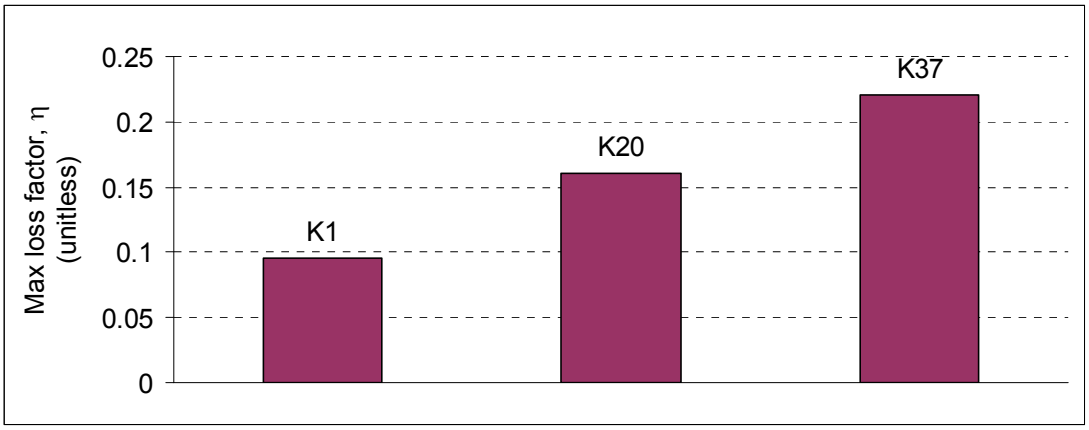

(a)

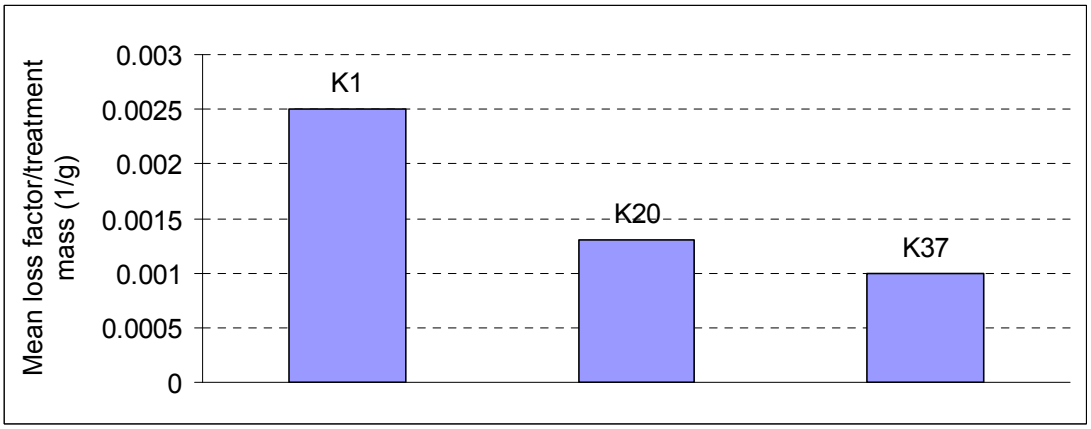

(b)

Figure 3.9 Summary of particle damping examples. (a) Max loss factor; (b) ratio of mean loss factor to treatment mass.

4. Closure

4.1. Summary

Both experimental and analytical methods of loss factor estimation have been investigated on two of the most commonly-used passive damping treatments: constrained layer damping and particle damping.

In summary, the major work in this research includes:

1) Design and manufacture of constrained layer damping, stand-off constrained layer damping and particle damping treatments for both monolithic and sandwich-construction beams and plates.
2) Measurement of loss factors for structural panels representative of passenger enclosures in vehicles using the standard modal curve-fitting method, the free-decay method and the power input method.
3) Estimation of loss factors for beams and plates with conventional constrained-layer-damping treatments and stand-off constrained-layer-damping treatments using the analytical modal strain energy method and the new analytical power input method.
4) Resolution of experimental and analytical methods of damping loss factor estimation for structural panels with conventional and stand-off constrained layer damping.
5) Measurement of wave speeds in glass microbubbles used as particle dampers.
6) Resolution of frequency bands of high measured damping loss factor for particle damping in structural panels with the wave speed of particles.

4.2. Original Contributions to the Field of Structural Acoustics

1) A new analytical power input method is proposed, validated and applied to monolithic and sandwich-construction panels with both conventional and stand-off constrained layer damping configurations. The frequency-dependency of the viscoelastic materials is directly taken into account in the finite element model used. This method, then, provides a viable analysis tool for panel constrained layer damping design.
2) Reasons for the frequency-dependent fluctuation of loss factor estimations characteristic of the power input methods are explained for the first time in the literature.
3) Experiments to measure the wave speeds of glass microbubbles in cylindrical enclosures were conducted.
4) Predicted cavity resonance frequencies, calculated from microbubble wave speeds, were successfully correlated to frequencies of peak damping loss factor in sandwich panels with microbubbles particle damping installed in the honeycomb core.
5) Experiments to measure the internal friction of various types of microbubbles were conducted and correlated in a relative sense with wave speeds and therefore with frequency of peak damping loss factor.

4.3. Conclusions

1) In frequency ranges where other commonly-used experimental methods apply, the experimental power input method yields results consistent with the two most commonly used experimental methods, the free decay method and the modal curve-fitting method

2) In the frequency range associated with high modal density, the analytical power input method yields results consistent with the (analytical) modal strain energy method and the experimental power input method.
3) In the low frequency range associated with low modal density, the experimental and analytical power input methods—with a single point of force/power input—both predict damping loss factors which oscillate between substantial over-prediction and near-agreement with the (analytical) modal strain energy method.
    a. This effect is a direct result of the point at which the excitation occurs
        i. If the excitation point is at a node line for the mode shapes and deflection response shapes in a broad frequency range, these methods will overpredict the damping loss factor.
        ii. If the excitation point is at an anti-node for the mode shapes and deflection response shapes in a broad frequency range, these methods will more accurately predict the damping loss factor.
    b. The analytical power input method predicts a slightly higher loss factor than the modal strain energy method at the frequencies at which the analytical power input method results are at a local minimum. It is expected that if a different excitation point is used, the analytical power input method would have different local minimums. This suggests one can estimate the damping loss factor in the low modal density range by "constructing" a curve through the local minimums of the loss factor curve determined by testing.
4) In the low modal density frequency ranges where both the experimental and analytical power input methods over-predict loss factor:

a. For monolithic plates with conventional constrained layer damping,
    i. The experimental power input method predicts even higher loss factors than the analytical power input method.
    ii. The frequencies at which the overpredictions occur tend to agree between the experimental and analytical methods.
b. For sandwich plates
    i. The analytical power input method predicts even higher loss factors than the experimental method.
    ii. The frequencies at which the overpredictions occur are always lower for the analytical model, suggesting the modeling process for sandwich plates and/or stand-off damping treatments underpredicts the structural stiffness of the panel and indicates needed improvement.

5) The fluid resonance model can predict at which frequency the peak damping performance will be for particle dampers made of glass microbubbles. This can be used to tune particle dampers to function at a specific frequency, which leads to the possibility of suppressing noise/vibration in a specified narrow frequency range (e.g., take-off fan blade passage frequency).
6) Results show that the internal friction indices can predict the relative relationship between peak damping values. It can be used as a particle selection index.

4.4. Notes on Applying the Analytical Power Input Method

1) Discretization in the finite element model should be fine enough to capture the feature size of the frequency response deflection so that there are at least 6-8 elements for a half sine wave.
2) Results show that the displacement in the viscoelastic layer of constraint layer damping is not strictly linear. So, more than one solid element should be used for the viscoelastic layer if the computational resource allows.

4.5. Notes on Applying the Experimental Power Input Method

3) The test article should have the velocity measured at points with a spacing that is capable of capturing the smallest vibration "feature" desired. This can be achieved by using an analytical model to determine the wavelength of the smallest feature of the mode shapes for the highest frequency under study. Then, there should be no less than 2 measurement points over the span of the smallest feature.
4) The shaker armature and stinger should not have a mass over 1/3, but ideally more like 1/10 of the mass of the test article.
5) The shaker, armature and stinger should have a higher resonance frequency than the highest frequency of interest.
6) Very long or short stinger lengths should be avoided:
    a. Not so long that the stinger vibrates laterally.
    b. Not so short that the shaker and test article respond in "pendulum modes" (both lateral and torsional)

4.6. Recommendations for Future Work

1) For either the analytical or experimental power input method, the estimated damping loss factors are dependent on the excitation position at which a mechanical shaker is used as excitation source. Therefore, implementing multiple excitation positions are desirable. In other estimation methods, for example, the Impulse Response Decay Method (IRDM), multiple hammer excitation positions are used to obtain a more accurate damping estimation for those structures. Implementing multiple driving point positions would be very simple in the analytical power input method, and is feasible for the experimental method.
2) A method to use acoustic excitation would be a great improvement to the experimental power input method and the analytical power input method to expand their applicability, especially to structures more complex than a flat structural panel.
3) A laser vibrometer can not easily measure the driving point mobility because the shaker will tend to block the view from the laser to the point of force application. In the current work, all response velocities were measured on the other side of the panel from the shaker. As reported, at high frequency, this leads to prediction of a negative driving point mobility measurement (when the force is 90 degrees out of phase with the measured velocity). It would be a great improvement to the experimental power input method if this test difficulty can be overcome in future works.
4) For more complex and built-up structures, the analytical power input method will not raise particular difficulties. But the experimental method would require scanning surfaces individually and rotating the specimen/shaker if the laser cannot

"see" all of the structure. Therefore, methods to provide high quality velocity measurements for a "roving" laser vibrometer would be needed. Manually-positioned accelerometers may be used instead.

5) A finite element specially-developed to model a thin viscoelastic layer should be investigated. This element would need to satisfy the displacement and force compatibilities expected in a viscoelastic continuum.

Reference

[1] 3M Glass Bubbles Production Information, 3M Specialty Materials Department, St. Paul, Minnesota, 2005

[2] 3M Viscoelastic Damping Polymers Technical data, 3M Bonding System Division, St. Paul, Minnesota, USA http://multimedia.mmm.com/mws/mediawebserver?WWWWWWECOgjWpzXWizXWWW6U4GRh6wF0-

[3] Adams, Douglas Scott, Efficient finite element modeling of thin-walled structures with constrained viscoelastic layer damping, AIAA/ASME/A SCE/AHS/ASC Structures, Structural Dynamics and Materials Conference and Exhibit, 37th, Salt Lake City, UT, Apr. 15-17, 1996, Technical Papers. Part 4, pp. 2079-2085, AIAA-1996-1651

[4] Austin, E. A. and Inman, D. J., Some Pitfalls of Simplified Modeling for Viscoelastic Sandwich Beams, ASME Journal of Vibration and Acoustics, Vol. 122, No. 4, 2000, pp. 434-439

[5] Austin, Eric M. and Johnson, Conor D., Passive damping technology, International Congress on Recent Developments in Air- and Structure-Borne Sound and Vibration, 2nd, Auburn Univ., AL, Mar. 4-6, 1992, Proceedings. Vol. 1 (A93-55851 24-31), pp. 181-188

[6] Belknap, Frank M., Vibration reduction of composite structures using constrained layer damping techniques, AIAA/ASME/ASCE/AHS/ASC Structures, Structural Dynamics, and Materials Conference, 32nd, Baltimore, MD, Apr. 8-10, 1991, Technical Papers. Pt. 3 (A91-31826 12-39). Washington, DC, American Institute of Aeronautics and Astronautics, 1991, pp. 2391-2396, AIAA-1991-1128

[7] Bianchini, E. and Lesieutre, G., Viscoelastic constrained-layer damping - time domain finite element modeling and experimental results. SDM Conference, 1994, AIAA paper 94-1652-CP, pp. 2666–2676

[8] Bies, D. A. and Hamid, S., In situ determination of loss and coupling loss factors by the power injection method, Journal of Sound and Vibration, 1980, Vol. 70, pp. 187-204

[9] Bloss, B. and Rao, M.D., "Measurement of Damping In Structures by the power input method," Experimental Techniques, Vo. 26, No. 3, 2002, pp. 30-33 http://www.me.mtu.edu/~mrao/et-paper-brandon-revised.pdf

[10] Bloss Brandon C. and Rao, Mohan D. Estimation of frequency-averaged loss factors by the power injection and the impulse response decay methods, The Journal of the Acoustical Society of America, Vol. 117(5), May 2005, pp. 240-249

[11] Bolduc, Maxime, Acquiring Statistical Energy Analysis Damping Loss Factor for Complex Structures with Low to High Damping Characteristics, PhD dissertation, University of Sherbrooke, Quebec, Canada, August 2007.

[12] Brown, K. T. and Norton, M. P., Some Comments on the Experimental Determination of Modal Densities and Loss Factors for Statistical Energy Analysis Applications, Journal of Sound and Vibration, Vol. 102, no. 4, 1985, pp. 588-594

[13] Buehrle, Ralph D., Gibbs, Gary P., Klos, Jacob and Mazur, Marina, Modeling and Validation of Damped Plexiglas Windows for Noise Control, 44th AIAA/ASME/ASCE/AHS/ASC Structures, Structural Dynamics, and Materials Conference, Norfolk, Virginia, AIAA 2003-1870, April 7-10, 2003, pp. 10, AIAA, 2003

[14] Buehrle, Ralph D., Klos, J. and Gibbs, G. P., Damped Windows for Aircraft Interior Noise Control, Noise-Con 2004, Baltimore, Maryland, USA, 12-14, July 2004, pp. 899-910

[15] Carfagni, M., Lenzi, E. and Pierini, M., The Loss Factor as a Measure of Mechanical Damping, Proceedings of the 16th International Modal Analysis Conference, 1998, pp.580-584

[16] Carfagni, M. and Pierini, M., Determining the Loss Factor by the power input method (PIM), Par t 1: Numerical Investigation, Journal of Vibration and Acoustics, July 1999, Vol. 121, pp. 417-421

[17] Carfagni, M. and Pierini, M., Determining the Loss Factor by the power input method (PIM), Part 2: Experimental Investigation with Impact Hammer Excitation, Journal of Vibration and Acoustics, July 1999, Vol. 121, pp. 422-428

[18] Carfagni, M., Citti, P., Pierini, M., Determining Loss Factor Using the power input method with Shaker Excitation, Proceedings of the 16th International Modal Analysis Conference, Santa Barbara, California, 2-5 Feb. 1998, pp. 585-590

[19] Carne, T., Constrained layer damping examined by finite element analysis, Society of Engineering Science 12th annual Meeting, Austin, Texas, 20-22 October 1975, Proceedings of the University of Texas, 1975, pp. 567-576

[20] Chang, Y., Linear Viscoelastic Material Properties in MSC/NASTRAN with Power Spectral Density Input, The MSC 1992 World Users' Conference Proceedings, Vol. 2, Paper No. 48, May, 1992

[21] Chu, F. H., Wang, B. P., " Experimental Determination of Damping in Materials and Structures," Damping Application for Vibration Control, Torvik, P.J., editor, ASME Winter Annual Meeting, Chicago, 1980, pp. 113-122

[22] Christensen, R.M., Theory of viscoelasticity An introduction, Second Edition, Academic Press, 1982

[23] Cremer, L, Heckl, M., Ungar, E., Structure-Borne Sound, Berlin, Springer Verlag, 1973

[24] Cremer, L., Heckl, M., Petersson, B.A.T., Structure-Borne Sound, 3rd ed, Berlin, Springer Verlag, 2005

[25] Cundall, P.A. and Strack, O., A distinct element model for granular assemblies. Geotechnique, 29, 1979, pp. 47-65

[26] DiTaranto, R. A., Theory of Vibratory Bending for Elastic and Viscoelastic Layered Finite-Length Beams, Journal of Applied Mechanics Dec. 1965, pp. 881-886

[27] De Langhe, K., An experimental – analytical SEA identification and applied validation criteria of a box type structure, Proceedings of the International Conference on Noise and Vibration Engineering, Leuven, Belgium, Sep 1994, pp. 431-446

[28] Engineer Technical Letters, Thermal Desorption, Appendix E: Design and Performance Criteria, Publication Number: TL 1110-1-173, U.S. Army Corps of Engineers, May 31, 1996, pp. E-16. http://www.usace.army.mil/publications/eng-tech-ltrs/etl1110-1-173/a-e.pdf

[29] European Pharmacopoeia, 2.9.16. Flowability, 5th ed., January 2005. Council of Europe, Strasbourg, pp. 242-243.

[30] Ewing, M.S. and Liu, W., Predicting Damping Loss Factors for Beams and Plates with Constrained Layer Damping, 49th AIAA/ASME/ASCE/AHS/ASC Structures, Structural Dynamics, and Materials Conference, April 7-10, 2008, Schaumberg, IL, AIAA 2008-2238

[31] Flugge, Wilhelm, Viscoelasticity, Springer-Verlag, Second Edition, 1975

[32] Fowler, B.L., Flint, E.M. and Olson S.E., Effectiveness and predictability of particle damping, Proceedings of SPIE (the International Society for Optical Engineering), 2003, Smart Structures and Materials 2000: Damping and Isolation, Editor: T. Tupper Hyde, April 2000, pp. 356-367

[33] FRIEND, R.D. and KINRA, V.K., Particle impact damping, Journal of Sound and Vibration, Volume 233, Issue 1, 25 May 2000, Pages 93-118

[34] Friswell, M I; Inman, D. J., Finite element models with viscoelastic damping, International Modal Analysis Conference (IMAC), 17th, Kissimmee, FL, 8-11 Feb. 1999, pp. 181-187

[35] Gade, S., and Herlufsen, H., Digital Filter techniques vs. FFT Techniques for Damping Measurements, Bruel & Kjaer Technical Review, No. 1, 1994

[36] Graesser, E. J. and Wong, C. R., The relationship of traditional damping measures for materials with high damping capacity: a review, M3D: Mechanics and Mechanisms of Material Damping, ASTM STP 1169, Kinra and Wolfenden Eds., American Society for Testing and Materials, Philadelphia, 1992, pp. 316-343

[37] Hermans L., Wyckaert K. and De Langhe K., The process to experimentally identify the statistical energy analysis parameters of industrial structures: step by step, Proceedings of the International Conference on Noise and Vibration Engineering, Leuven, Belgium, Sep 1996, pp. 171-187

[38] Huang, P. Y. H., Reinhall, P. G., Shen, I. Y., Yellin, J. M., Thickness deformation of constrained layer damping: an experimental and theoretical evaluation, Journal of Vibration and Acoustics (Transactions of the ASME), Vol. 123, no. 2, Apr. 2001, pp. 213-221

[39] Jacobsen, Finn, Measurement of structural loss factors by the power input method. Report No. 41, The acoustics laboratory, Technical University of Denmark, 1986

[40] Jacobsen, Finn, Experimental determination of structural damping. Nordic Acoustical Meeting, Aalborg, Denmark, August, 1986

[41] Johnson, C. D., Kienholz, D. A. and Rogers, L. C., Finite element prediction of damping in beams with constrained viscoelastic layers, Shock and Vibration Bull. No. 50, 1981, Part 1, pp. 71-82

[42] Johnson C. D., Kienholz, D. A., Finite Element Prediction of Damping in Structures with Constrained Viscoelastic Layers, AIAA Journal, Vol. 20, No. 9, September, 1982, pp. 1284-1290

[43] Johnson C. D., Passive Damping Technology using Viscoelastics, The 30th IEEE Conference on Decision and Control, Brighton, United Kingdom, December, 1991, pp. 2546-2551

[44] Kosmatka, J.B. and Liguore, S.L., Review of Methods to Study Constrained Layer Damping, ASCE Journal of Aerospace Engineering, Vol. 6, 1993, pp. 268-283

[45] Lakes, Roderic S., Viscoelastic solids, Mechanical Engineering Series, CRC Press, Boca Raton, FL, 1999

[46] Lesieutre, G. A. and Mingori, D. L., Finite Element Modeling of Frequency-Dependent Material Damping Using Augmenting Thermodynamic Fields, AIAA Journal of Guidance, Control, and Dynamics, vol. 13, no. 6, 1990, pp. 1040-1050

[47] Lesieutre, G. A. and Bianchini, E., Time domain modeling of linear viscoelasticity using anelastic displacement fields, ASME Journal of Vibration and Acoustics, vol. 117, No. 4, 1995, pp. 424-430

[48] Lin, R. M. and Ling, S-F., Identification of damping characteristics of viscoelastically damped structures using vibration test results, Proceedings of The Institution of Mechanical Engineers, Part C: Journal of Mechanical Engineering Science, Vol. 210, 1996, pp. 111-121

[49] Liu, W. and Ewing, M.S., Experimental and Analytical Estimation of Loss Factors of by the Power Input Method, AIAA Journal, Vol. 45, No. 2, February 2007, pp. 477-484

[50] Liu, W. and Ewing, M.S., Particle Damping of Composite Honeycomb Beams by the Power Input Method, 48th AIAA/ASME/ASCE/AHS/ASC Structures, Structural Dynamics, and Materials Conference, April 23rd, 2007, Honolulu, Hawaii, AIAA 2007-2044.

[51] Liu, W. and Ewing, M.S., Estimating Particle Damping of Honeycomb Sandwich Plates Using a Fluid analogy, 49th AIAA/ASME/ASCE/AHS/ASC Structures, Structural Dynamics, and Materials Conference, April 9th, 2008, Schaumberg, IL, AIAA 2008-2104

[52] Lu, Y.P. and Everstine, G.C., More on finite element modeling of damped composite systems, Journal of Sound and Vibration, 1980 69 (2), pp. 199-205

[53] Lyon R. H., Statistical energy analysis of dynamical systems, MIT press 1975

[54] McTavish, D. J. and Hughes, P. C., Finite element modeling of linear viscoelastic structures: The GHM method, Proceedings of the 33rd AIAA/ASME/ASCE/AHS/ASC Structures, Structural Dynamics, and Materials Conference, 1992, pp. 1753-1763

[55] Mead, D. J., governing Equations for Vibrating Constrained-Layer Damping Sandwich Plates and Beams, Journal of Applied Mechanics, Vol. 40(2), 1973, pp. 639-640

[56] Mead, D. J. and Markus, S., The forced vibration of a three-layer damped sandwich beam with arbitrary boundary conditions, Journal of Sound and Vibration, 10(2), 1969, pp. 163–175

[57] Meirovitch, Leonard, Analytical Methods in Vibrations, The Macmillan Company, New York, NY, 1967

[58] Moreira, R. and Rodrigues, J. D., Constrained damping layer treatments: The finite element modeling. Journal of Vibration and Control, Vol. 10, 2004, pp. 575-595

[59] MSC/NASTRAN 2005 Quick Reference Guide, The MacNeal Schwendler Corporation, USA, 2001

[60] MSC/NASTRAN 2005 Application Manual, Section 2.11, The MacNeal Schwendler Corporation, USA, 1983

[61] Nashif, A. D., Jones, D. I. G., Henderson, J. P., Vibration Damping, John Wiley & Sons, New York, NY, 1985

[62] Nayfeh, S.A., Verdirame, J.M. and Varanasi, K.K., Damping of Flexural Vibration by Coupling to Low-Density Granular Materials, Proceedings of SPIE, The International Society for Optical Engineering: 9th Annual International Symposium on Smart Structures and Materials, 2002, San Diego, California, Vol. 4697, pp. 158-167

[63] Papalou, A. and Masri, S.F., Performance of Particle Dampers Under Random Excitation, Journal of Vibration and Acoustics, October 1996, Volume 118, Issue 4, pp. 614-621

[64] Plouin, A. and Balmes, E., A Test Validated Models of Plates with Constrained Viscoelastic Materials, International Modal Analysis Conference, Orlando, 1999, pp. 194-200

[65] Plouin, A. and Balmes, E., Steel/viscoelastic/steel sandwich shells. Computational methods and experimental validations, International Modal Analysis Conference 2000, pages 384–390, http://www.sdtools.com/pdf/imac00damp.pdf.

[66] Plunt, J., Power injection method for vibration damping determination of body panels with applied damping treatments and trim, SAE Transactions, Vol. 100, 1991, pp. 1563-1571

[67] Plunt, J., Predictability of mid- and high frequency dynamic properties of industrial product, Eighth International Conference on Recent Advances in Structural Dynamics, Southampton, UK, 14-16 July 2003

[68] Polytec Scanning Vibrometer Software and Hardware Manual, Polytec Gmbh, Deutschland

[69] Park, Jin-Tack and Choi, Nak-Sam, Flexural Vibration Analysis of a Sandwich Beam Specimen with a Partially Inserted Viscoelastic Layer, KSME International Journal, Vol. 18 No. 3, 2004, pp. 347-356

[70] Rao, M.D., Recent Applications of Viscoelastic Damping for Noise Control in Automobiles and Commercial Airplanes, Journal of Sound and Vibration, Vol. 262, (3), 2003, pp. 457-474

[71] Ranky, M. F., and Clarkson, B. L., Frequency average loss factors of plates and shells, Journal of Sound and Vibration, 1983, Vol. 89(3), pp. 309-323

[72] Renji, K., Narayan, S. Shankar, Loss Factors of Composite Honeycomb Sandwich Panels, Journal of Sound and Vibration, Vol. 250(4), February 28, 2002, pp. 745-761

[73] Rogers, Lynn C. and Parin, Mike, Experimental results for stand-off passive vibration damping treatment, Proc. SPIE Vol. 2445, Smart Structures and Materials 1995: Passive Damping, Conor D. Johnson; Ed., pp. 374-383

[74] Ross, D., Ungar, E. E., and Kerwin Jr., E. M., Damping of Plate Flexural Vibrations by Means of Viscoelastic Laminae, in Structural Damping, ed. by J. E. Ruzicka, ASME, NY, 1959, pp. 49-88

[75] Shin, Y. S. and Maurer, G. J., Vibration Response of Constrained Viscoelastically Damped Plates: Analysis and Experiments, Journal of Finite Elements in Analysis and Design, Vol. 7 1991, pp. 291-297

[76] Simonian, S.S., Particle beam damper, Proceedings of the SPIE Conference on Passive Damping, Vol. 2445, SPIE, Newport Beach, CA, 1995, pp. 149–160

[77] Soovere, J., Drake, M. L., Miller, V. R., A Design guide for damping of aerospace structures, AFWAL Vibration Damping 1984 Workshop, Proceedings 9 pages, N86-21883 12-39, 1984

[78] Soovere, J., and Drake, M. L., Aerospace Structures Technology Damping Design Guide, Volume I-Technology Review, Technical Report AFWAL-TR-84-3089, Wright-Patterson Air Force Base, 1985

[79] Soovere, J. and Drake M. L., Aerospace structures technology damping design guide volume II-Design Guide, Technical Report AFWAL-TR-84-3089, Wright-Patterson Air Force Base, Ohio, 1985

[80] Soovere, J. and Drake M. L., Aerospace structures technology damping design guide volume III-damping material data Final Report Submitted to Flight Dynamics Laboratory, Wright-Patterson Air Force Base, Ohio, 1985

[81] Silva, Luciano Afonso da, Internal Variable and Temperature Modeling Behavior of Viscoelastic Structures - A Control Analysis, PhD dissertation, Virginia Polytechnic Institute and State University, 2003 http://scholar.lib.vt.edu/theses/available/etd-08252003-065520/unrestricted/etdLAS.pdf

[82] STAR System™ Reference Manual, Spectrural Dynamics Inc., Version 5.24.32

[83] Torvik, P. J. and Runyon, B., "On the Application of the Method of Modal Strain Energy to the Determination of Loss Factors for Damped Sandwich Beams, Proceedings, 75th Shock and Vibration Symposium, Virginia Beach, VA October 17-21, 2004

[84] Torvik, P. J. and Runyon, B., "Observations on the Accuracy of Finite Element Predictions of Constrained Layer Damping", 10th National Turbine Engine High Cycle Fatigue Conference, New Orleans, LA, March 8-11, 2005, Dayton, OH, Universal Technology Corporation, 2005

[85] Varanasi, Kripa K. and Nayfeh, Samir A., Damping of flexural vibration by low-density foams and granular materials, 2003 ASME Design Engineering Technical Conferences, 2-6 September 2003, Chicago, Illinois

[86] Veeramani, Sudha and Wereley, Norman M., Induced Strain Actuation of Sandwich Plates with Viscoelastic Damping Layers, AIAA/ASME/ASCE/AHS/ASC Structures, Structural Dynamics, and Materials Conference and Exhibit, 38th and AIAA/ASME/AHS Adaptive Structures Forum, Kissimmee, FL, Apr. 7-10, 1997

[87] Verdirame, J.M. and Nayfeh S.A., Vibration Damping of Cylindrical Shells using Low-Density, Granular Materials, 47th AIAA/ASME/ASCE/AHS/ASC Structures, Structural Dynamics, and Materials Conference, AIAA 2006-2206, 1-4, May 2006, Newport, Rhode Island

[88] Wolf Jr., J.A., The influence of mounting stiffness on frequencies measured in a vibration test, SAE paper 840480, Society of Auto motive Engineers, 1984

[89] Wu, L., Agren, A., Sundback, U., A Study of the Initial Decay Rate of Two-Dimensional Vibrating Structures in Relation to Estimates of Loss Factor, Journal of Sound and vibration, Vol. 206(5), pp. 663-684

[90] Xu, Z.W., Chan, K.W. andn Liao, W., An empirical method for particle damping design, Shock and Vibration, Vol. 11, 2004, pp. 647-664

[91] Yellin, J.M., Shen, I.Y., Reinhall, P. G., Huang, P. Y. H., An Analytical and Experimental Analysis for a One-Dimensional Passive Stand-Off Layer Damping Treatment, Journal of Vibration and Acoustics, October 2000, Vol. 122(4), pp. 440-447

[92] Zhu, G.H., Crocker M.J., and Rao, M.D., Data Processing and Accuracy Analysis of Damping Measurement, J. of the Acoustical Society of America, Vol. 85(1), 1989, pp. 171-177

Appendices

A. Definition of Material Properties

All material properties used in this research are described in this section. Materials with frequency independent mechanical properties are described in Table A.1. Mechanical properties of viscoelastic material 3M F9469PC are described in Table A.2. A manufacturer's nomograph of 3M F9469PC is shown in Figure A.1.

Table A.1 Mechanic properties of frequency independent materials

Material	Elastic modulus, E (Pascal)	Poisson's ratio, μ (unitless)	Shear modulus, G (Pascal)	Density, ρ (Kg/m^3)	Loss factor, η (unitless)
Aluminum alloy 2024-T3	7.308443e+010	0.33	-	2768	0.003
Aluminum alloy CLAD 2024-T3	7.4463379E+010	0.33	-	2768	0.003
Aluminum alloy 5052-H34	6.998179E+010	0.33	-	2685	0.003
Low alloy steel AISI 4130	1.99948e+011	0.32	-	7833.44	0.001
Plexiglas (cast acrylic)	-	0.35	1.7E9	1200.0	0.07
Film adhesive Hysol EA 9628	-	0.35	1.7E9	1153.1	0.15
Honeycomb as 3D orthotropic material	627423 in 11 direction); 313710 in 22 direction; 1.8827E8 in 33 direction	-	21373750 in 23 direction; 39300120 in 31 direction	48.06	0.024
Carbon fiber IM7/3501-6 as 2D orthotropic material	1.3119E11 in 11 direction; 1.0342E10 in 22 direction	0.3 in 12 direction	5.5158E9 in 12 direction	1460.9	0.01

Table A.2 Mechanic properties of viscoelastic material 3M F9469PC

Frequency (Hz)	Shear storage modulus, G' (Pa)	Loss factor, η (unitless)	Poisson's ratio, μ (unitless)
1	1.115*10^5	0.635	0.49
3	1.58*10^5	0.81	0.49
10	2.9*10^5	0.97	0.49
100	9.05*10^5	1.15	0.48
300	1.8*10^6	1.1	0.46
1000	3.4*10^6	1.05	0.43

Table A.2 Mechanic properties of viscoelastic material 3M F9469PC (Continued)			
2000	5.2*10^6	0.99	0.41
3000	6.8*10^6	0.98	0.39
4000	8.1*10^6	0.92	0.38
5000	9*10^6	0.9	0.365
6000	9.7*10^6	0.9	0.35
10000	1.25*10^7	0.85	0.3

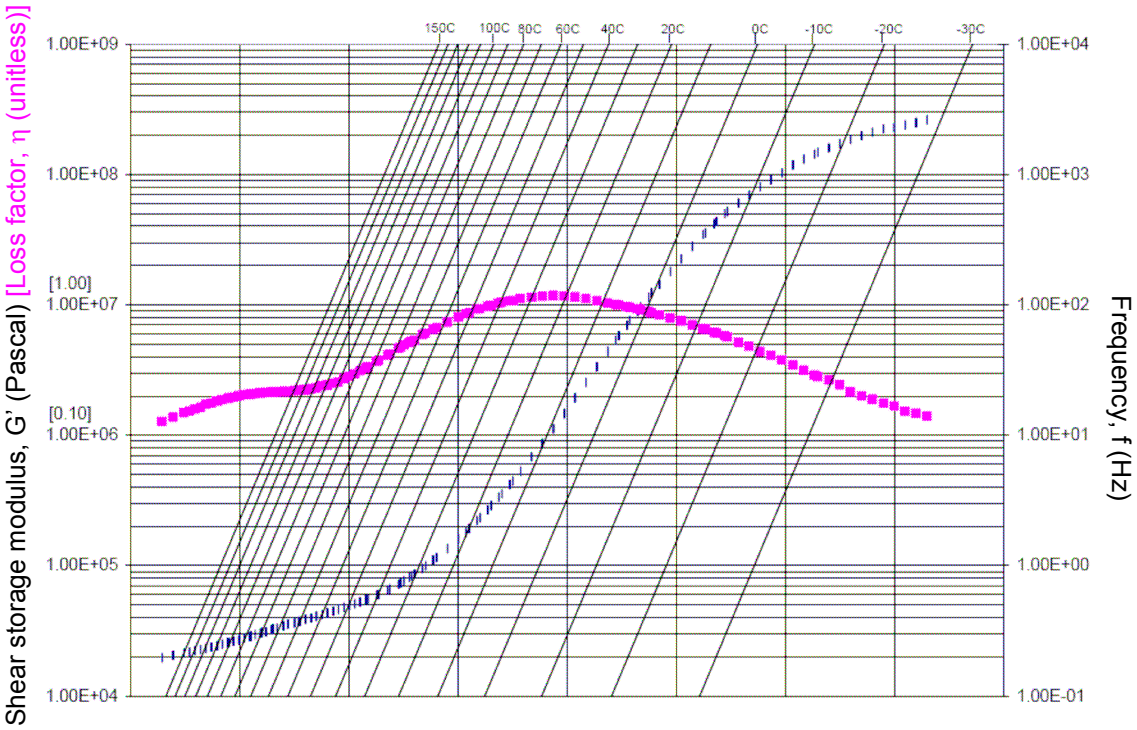

Figure A.1 Manufacturer's nomograph of 3M F9469PC.

B. Algorithm of Experimental Power Input Method in MATLAB

```
clear;
fin=fopen('K20_100_pd31.asc');      %input from asc file
N=551;  %number of total scanning points
f=276;  %reference point number
Nfft=6337;
df=1.563; %frequency resolution
f1=100;  %starting freq of the scan
f2=10000;    %ending freq of the scan
mass1=0.415/N;   %mass of the specimen-portion 1-kg
for n=1:N
        mass(n)=mass1;
end

line=fgetl(fin);
n=0;    %index of point number
while feof(fin)==0
    if line(1)=='T'
```

```
        n=n+1;
        q=0;    %index of current fft line
        for p=1:9   %continue to read and write 9 more lines
           line=fgetl(fin);
        end
        line=fgetl(fin);
        for p=1:(Nfft-1)/3  %Nfft-1: 2 readings at end of each frf,
3 fft lines per row
            line=fgetl(fin);
            q=q+1;
            h(n,q)=str2num(line(1:13))+i*str2num(line(14:26));
            q=q+1;
            h(n,q)=str2num(line(27:39))+i*str2num(line(40:52));
            q=q+1;
            h(n,q)=str2num(line(53:65))+i*str2num(line(66:78));
        end
        line=fgetl(fin);
        q=q+1;
        h(n,q)=str2num(line(1:13))+i*str2num(line(14:26));
    end
    line=fgetl(fin);
end
fclose(fin);

num=real(h(f,:));
s=0;    %summation
for n=1:N
    s=mass(n)*abs(h(n,:)).^2+s;
end
for n=1:Nfft
    freq(n)=f1+(n-1)*df;
end
for n=1:Nfft
    den(n)=2*pi*freq(n)*s(n);
end
eta=num./den;

fid = fopen('K20.100.pd31.epim.txt','w');
for n=1:Nfft
    fprintf(fid,'%12.8f %12.8f\n',freq(n),eta(n));
end
fclose(fid);
```

C. Algorithm of Analytical Power Input Method in MATLAB

```
clear;
fin=fopen('pcld17.f06');      %input from asc file
ff=1;  %reference point number in patran/Nastran 2005 r2
f1=30;  %starting freq
f2=5000;    %ending freq
Ndf=300+1; %number of frequency increments
df=(f2-f1)/(Ndf-1); %frequency resolution
n1=0;
n2=0;
n3=0;
line=fgetl(fin);
while feof(fin)==0
    temp=size(line);
    if temp(1,2)==31 & line(7:15)=='FREQUENCY'
        line=fgetl(fin);
```

```
        temp=size(line);
        if temp(1,2)==88 & line(44:88)=='C O M P L E X   V E L O C I
T Y   V E C T O R'
            n1=n1+1;
            line=fgetl(fin);
            line=fgetl(fin);
            line=fgetl(fin);
            liner=fgetl(fin);
            linei=fgetl(fin);
            h(ff,n1)=str2num(liner(57:69))+i*str2num(linei(57:69));
%read T3 column in f06 file
        end
        if temp(1,2)==101 & line(32:96)=='E L E M E N T   S T R A I
N   E N E R G I E S   ( A V E R A G E )'
            n2=n2+1;
            line=fgetl(fin);
            line=fgetl(fin);
            ese(n2)=str2num(line(101:113));
        end
        if temp(1,2)==102 & line(31:97)=='E L E M E N T   K I N E T
I C   E N E R G I E S   ( A V E R A G E )'
            n3=n3+1;
            line=fgetl(fin);
            line=fgetl(fin);
            eke(n3)=str2num(line(101:113));
        end
    end
    line=fgetl(fin);
end
fclose(fin);

for n=1:Ndf
    freq(n)=f1+(n-1)*df;
    num(n)=real(h(ff,n))/(2*2*pi*freq(n));
    den(n)=ese(n)+eke(n);
end
eta=num./den;
fout=fopen('pcld17.apim.txt','w');
for n=1:Ndf
    fprintf(fout,'%12.8f %12.8f\n',freq(n),eta(n));
end
fclose(fout);
```